

TIME DEPENDENT STUDY OF QUANTUM BISTABILITY

A THESIS

SUBMITTED TO THE DEPARTMENT OF PHYSICS
AND THE INSTITUTE OF ENGINEERING AND SCIENCE
OF BILKENT UNIVERSITY
IN PARTIAL FULFILLMENT OF THE REQUIREMENTS
FOR THE DEGREE OF
MASTER OF SCIENCE

By

Mustafa İhsan Boemig

July 1995

QC
20.7
.E24
1995

TIME DEPENDENT STUDY OF QUANTUM BISTABILITY

A THESIS

SUBMITTED TO THE DEPARTMENT OF PHYSICS
AND THE INSTITUTE OF ENGINEERING AND SCIENCE
OF BİLKENT UNIVERSITY
IN PARTIAL FULFILLMENT OF THE REQUIREMENTS
FOR THE DEGREE OF
MASTER OF SCIENCE

By

Mustafa İhsan Ecemiş


July 1995

Mustafa İhsan Ecemiş
Signature of the author

GC
20.7
E24
1995

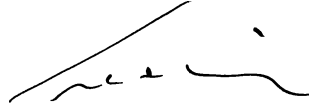
B 031418

I certify that I have read this thesis and that in my opinion it is fully adequate, in scope and in quality, as a dissertation for the degree of Master of Science.



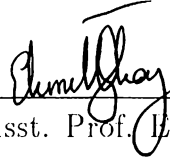
Prof. Cernal Yalabık (Supervisor)

I certify that I have read this thesis and that in my opinion it is fully adequate, in scope and in quality, as a dissertation for the degree of Master of Science.



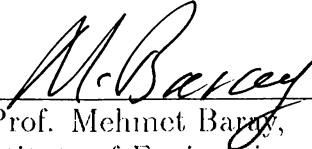
Prof. Atilla Ergelebi

I certify that I have read this thesis and that in my opinion it is fully adequate, in scope and in quality, as a dissertation for the degree of Master of Science.



Asst. Prof. Ekmel Özbay

Approved for the Institute of Engineering and Science:



Prof. Mehmet Baray,
Director of Institute of Engineering and Science

Abstract

TIME DEPENDENT STUDY OF QUANTUM BISTABILITY

Mustafa İhsan Ecemiş

M. S. in Physics

Supervisor: Prof. M. Cemal Yalabık

July 1995

The analysis of quantum transport phenomena in small systems is a prominent topic of condensed matter physics due to its numerous technological applications. The current analytical theories are not adequate for studying realistic problems. Computational methods provide the most convenient approaches. Numerical integration of the time-dependent Schrödinger equation is one of the most powerful tools albeit the implementation of the blackbody boundary conditions is problematic. In this work, a novel method which render possible this implementation is described. A number of sample calculations are presented. The method is applied to several one- and two-dimensional systems. A description of the time-dependent behavior of quantum bistable switching is given.

Keywords: one-dimensional systems, two-dimensional systems, transport theory, numerical solution, boundary conditions, Schrödinger equation, time dependence, crystal models, crystal lattices, Markov process, wave functions, quantum bistability.

Özet

KUVANTUM ÇİFT-KARARLILIĞIN ZAMANA BAĞLI ÇALIŞILMASI

Mustafa İhsan Ecemiş

Fizik Bölümü Yüksek Lisans

Tez Yöneticisi: Prof. Dr. M. Cemal Yalabık

Temmuz 1995

Küçük sistemlerdeki kuvantum taşınım olayı, çok sayıdaki teknolojik uygulamalarından dolayı yoğun madde fiziğinin önemli bir konusudur. Günümüzün analitik teorileri gerçek problemleri çalışmak için uygun değildir ve bu nedenle sayısal hesap metodları en elverişli yaklaşımları sağlamaktadırlar. Karacisim sınır şartlarını yerleştirmenin problemleri olmasına rağmen zamana bağlı Schrödinger denkleminin sayısal tamamlanması en güçlü araçlardan biridir. Bu çalışmada, bu yerleştirmeyi mümkün kılan yeni bir metod tanımlandı. Bazı örnek hesaplar sunulup, metod bir ve iki boyutlu sistemlere uygulandı. Kuvantum çift-kararlı anahtar davranışının tanımı verildi.

Anahtar

sözcükler: bir boyutlu sistemler, iki boyutlu sistemler, taşınım teorisi, sayısal çözüm, sınır şartları, Schrödinger denklemi, zamana bağlılık, kristal modelleri, kristal örgüleri, Markov işlemleri, dalga fonksiyonları, kuvantum çift-kararlılığı.

Acknowledgement

It gives me honor to express my deepest gratitude to Prof. M. Cemal Yalabık for his supervision to my graduate studies. This is not only due to his protective guidance and friendly discussions but also for his tolerance toward my inexhaustible requests concerning my social activities. In addition, he has delivered me the encouragement that I have often needed. My innermost thought is that he is the most suitable supervisor I could ever met.

I would like to thank E. Tekman for many fruitful discussions, a critical reading of the manuscript, and for his invaluable helps that he never grudged in various circumstances.

I acknowledge discussions and moral support by the faculty and research assistants of Department of Physics, Bilkent University during this study. In particular, I want to thank to my residence-mate K. Güven and office-mate H. Boyacı for their endurance toward any trouble that I caused in the course of our close interactions.

I appreciate moral support by many of my friends, especially O. Karadeniz and D. Kaynarođlu. I may also not skip my thanks to my friends within the staff of BCC for their unique hospitality, complimentary kindness, and conveniences they have shown to me during my research.

Finally, my intimate thanks are due to my whole family, in particular to my parents and my sister Zeynep, for their extreme interest, continuous moral support and distinct understanding. I owe a lot to them.

Contents

Abstract	i
Özet	ii
Acknowledgement	iii
Contents	iv
List of Figures	vii
List of Tables	ix
1 INTRODUCTION	1
1.1 Time-independent Schrödinger Equation	4
1.2 The Wigner Function	6
1.3 Hydrodynamic Aspects	8
1.4 Time-dependent Schrödinger Equation	10

2	BLACKBODY BOUNDARY CONDITIONS	16
2.1	The Method	16
2.1.1	Discretized Schrödinger Equation	17
2.1.2	Extension of the Boundary Region	20
2.1.3	The Update of the Wave Function	24
2.1.4	Injecting Boundary Condition	24
2.2	Sample Calculations	26
2.2.1	Absorption of a Wave Packet	27
2.2.2	Injection of Particles on a Tunneling Barrier	29
2.2.3	Injection of Particles to The Kink Structure	31
3	2-D APPLICATIONS	34
3.1	Exact Solutions of Two Particle Problem	34
3.1.1	The Problem of Bistability	35
3.1.2	n -Particle System Interacting via Pair Forces	36
3.1.3	Model Problem	37
3.1.4	Hartree Approximation	42
3.2	Kink Structure	44
3.2.1	The Structure	44
3.2.2	Negative Differential Resistance	47

3.2.3	Self Consistent Potential	50
4	1-D APPLICATIONS AND BISTABILITY	56
4.1	The Model	57
4.2	Results	62
4.3	A Time-Dependent Investigation of Bistable Switching	67
4.3.1	Determination of the Bistability Region	67
4.3.2	The Switching	71
4.3.3	The Waiting	78
4.4	Higher Dimensions	81
5	CONCLUSION	85
	APPENDIX: SOME LIMITATIONS	88
A.1	Wavelength Dependence	88
A.2	Choice of Boundary Conditions and Switching	91
A.3	Analytic Expression for the Full Update	92
A.4	Breaking-up of the Exponential Term	93

List of Figures

2.1	Schematic explanation of the extension of the boundary region	23
2.2	Schematic explanation of the update	25
2.3	Motion of a wave packet through an absorbing boundary	28
2.4	The relative error as a function of position l	29
2.5	Injection of particles to a tunneling barrier	30
2.6	Motion of a wave packet through the kink structure	32
3.1	Numerically exact solution of the two particle problem.	40
3.2	Function $\sin [(k - q)a]/(k - q)$.	41
3.3	Hartree approximation to two particle problem.	43
3.4	Kink structure potential profile	45
3.5	Model for electron transmission through the kink structure	46
3.6	Current through the kink structure as a function of energy	48
3.7	$I - V$ characteristics of the kink structure	49
3.8	Self consistent potential for the kink structure	54

4.1	Models of a resonant tunneling diode.	58
4.2	Transmission coefficients as a function of wave vector	61
4.3	$I - V$ characteristics of a double barrier for different β	64
4.4	Charge build-up between the barriers for different β	65
4.5	$I - V$ characteristics of a double barrier for different V_h	66
4.6	Bistability region of set #6.	68
4.7	Determination of V_r	70
4.8	Superposition of the switching regions.	72
4.9	The time derivative of the charge build-up.	73
4.10	Derivatives near V_r for different set of parameters.	75
4.11	Derivatives near V_l for different sets of parameters.	76
4.12	Maximum of the derivatives as a function of β	77
4.13	Lifetimes for different sets	79
4.14	Potential differences where the maximum of the derivatives occur	80
4.15	Double barrier in three dimensions.	81
4.16	Two-dimensional simulation of the double barrier structure.	83
A.1	The relative error as a function of wavelength	89

List of Tables

4.1	Parameters used in the simulation of the double barrier structure.	60
4.2	Sets of parameters for the simulation of the double barrier. . . .	62
4.3	Bistability regions for different sets.	69

Chapter 1

INTRODUCTION

The eagerness of micro-electronics technology is toward reducing the size of the electronic devices. Namely, smaller devices process faster, consume less power, are carried easier, and fit into smaller space. Remembering the progress this field achieved in the last few decades, who may claim that today's desktop computers will not be the solar powered pocket size diaries of tomorrow?

With the aid of the ion- and electron-beam lithography techniques, research laboratories of the nineties render possible the production of structures having dimensions on the order of few nanometers. In terms of condensed matter physics, these dimensions fall into the so-called regime of *mesoscopics* where the quantum effects become observable in device characteristics. Here, an important definition related to the dimensions is the phase coherence length l_ϕ , the distance an electron moves without losing the phase information of its wave function. The size of a mesoscopic structure is smaller than the phase coherence length and therefore the quantum interference effects become pronounced. Another definition is the electron mean free path l_e , the distance along which an electron moves without having any kind of scattering. If the size of a device is bigger than the Fermi wavelength λ_F and the electron mean free path, this is the so-called *diffusive regime*. On the other hand, sizes smaller

than both of these characteristic lengths correspond to the so-called *ballistic regime*. It is clear that as the dimensions are reduced, the investigation of this ballistic regime becomes more important.

In order to model new devices meeting a specific need or to investigate the operation of current ones, an approach which will take into account the quantum effects emerging out at these mesoscopic dimensions is required. Indeed, different theoretical formalisms on this scope have been carried out since 1950's [1]. Two mainstreams are the Kubo's linear response theory [2] and the Landauer (or so-called Landauer-Büttiker [5-7] afterwards) scattering approach [3,4].

One of the main problems in the theoretical modeling of the electronic devices lies in the definition of the "system of interest". Usually an electronic circuit consists of power supplies, resistors, capacitors, logical gates, etc. It is clear that a theory which treats all these macroscopic objects quantum mechanically, is far beyond our capabilities. In other words, one has to limit the *system of interest* to some smaller part of this complicated circuit. Hereby, the *system of interest* is frequently a device having mesoscopic dimensions and the theory must predict its response to the external effects such as the applied current or voltage. From this point of view, the system under analysis is "open" in the sense that it exchanges particles with its environment. This environment is designated by the term "reservoir". The particles may be "injected" from the *reservoir* to the *system of interest* or "absorbed" from the *system of interest* into the *reservoir*.

In practice, an electronic device is usually connected through at least two probes to the external world (circuitry) for measurement. Hence, the continuity equation is not satisfied for charge carriers in an *open system* due to the current flowing through these probes. It turns out that an *open system* does not admit a hermitian Hamiltonian and quantum mechanical treatment of non-hermitian operators is often problematic.

To overcome these difficulties of *open systems*, one may try to define some “boundary conditions” appropriate for the system under consideration [8]. Here the term *boundary*[†] describes the regions (for example, a 2-dimensional surface for a 3-dimensional structure) of the system through which the exchange of particles takes place. The aim in postulating these *boundary conditions* is to avoid the internal properties of the reservoirs. One of the main advantages of the Landauer approach lies in its simple implementation of the boundary conditions. It has successfully explained [9] some quantum phenomena such as Aharonov-Bohm oscillations [10,11], universal conductance fluctuations [12,13], etc. In these conductance calculations, the reservoirs are assumed to absorb all the incident particles, and inject others with the appropriate weights dictated by the corresponding thermal distribution function. These type of boundary conditions are called “blackbody conditions”[‡]. Albeit Kubo’s linear response theory is complicated for small systems and may result in different solutions, the equivalence of the two formalisms was proved in the last decade [9,14].

As noted earlier, there are many different approaches to the quantum transport phenomena in small systems. However, many of them, like the ones mentioned above, consider the *near-equilibrium* state of the device. In contrast, some electronic devices, such as a quantum-well resonant-tunneling diode, demonstrate important quantum effects while operating in the *far-from-equilibrium* mode. On the other hand, the elementary quantum theory does not provide an appropriate formalism for such non-equilibrium phenomena. In fact, special techniques to handle these situations using Green’s functions have been developed since early 1960’s by Kadanoff and Baym [15], and by Keldysh [16,17]. Some prominent recent efforts is towards a reformulation of steady state non-equilibrium quantum statistical mechanics [18]. The ultimate aim of that work is to obtain a nonperturbative theory for non-equilibrium quantum systems. To achieve this, a novel form of the conventional perturbation theory

[†]For the quantum transport problems concerning mesoscopic devices, the terms “contact” and “lead” are also used as a synonym for *boundary*.

[‡]We will often refer to these conditions by the term “absorbing and injecting boundary conditions”.

of non-equilibrium quantum mechanics similar to that of the equilibrium one is proposed, based on the so-called “maximum entropy approach”. Accordingly, a new approach to steady-state mesoscopic transport which is not limited to the linear response regime followed the previous work[19]. Nevertheless, current theories are not adequate for dealing with realistic problems.

At this stage, numerical simulations seem to be promising not only for the treatment of mesoscopic systems in the steady state regime but also for a detailed analysis of quantum transport phenomena in the non-equilibrium state. Namely, it is numerically possible to implement *ab initio* the elementary quantum mechanical laws. Hence, numerical methods are easily applicable to complicated geometries (some methods at *far-from-equilibrium* regime as well) whereas analytical approaches consider only systems having some sufficient symmetry, in the presence of small perturbations on the analytically solvable models. Another remarkable point is the rapid development of computer technology. Note that, numerical simulations can handle more complicated problems as faster processors are produced. Consequently, improving numerical models is significant for the analysis of quantum transport in small systems.

In the following sections, a number of numerical methods relevant for the investigation of quantum transport phenomena will be described [8,20].

1.1 Time-independent Schrödinger Equation

Based on the theory of scattering, time-independent Schrödinger equation is frequently used in the problems concerning *open systems*. The implementation of the *blackbody boundary conditions* on this equation is well known (see, for example, [8,21]). The particles are assumed to be incident from a contact with a given wave vector, further assumed to be absorbed completely by any contact if incident on it. Accordingly, the wave functions of this single particle scattering states are usually expanded in a set of traveling waves in the asymptotic region.

It is clear that at the contact regions, the forms of the solutions of these states are known due to the uniform potential therein. For example, for a one-dimensional system, the asymptotic wave functions of a particle injected from the left boundary with a wave vector k_i may be expressed as:

$$\begin{aligned}\psi(x) &= Ae^{ik_i x} + Re^{-ik_i x} && \text{at the left boundary} \\ \psi(x) &= Te^{ik_a x} && \text{at the right boundary}\end{aligned}\quad (1.1)$$

where k_a is the wave vector with which the particle is absorbed from the right boundary. These two wave vectors are connected to each other with the expression:

$$\hbar^2 \frac{(k_i^2 - k_a^2)}{2m} = e \Delta V. \quad (1.2)$$

Here ΔV is the potential difference between the left and right reservoirs, \hbar is the Planck constant, e and m are the charge and mass of the carriers respectively. The constants A, T and R^\dagger in Eq. (1.1) may be obtained by integrating the time-independent Schrödinger equation from the right to the left boundary, no matter how complicated the potential in the scattering region is. For two-dimensional systems, the calculations are more difficult but still numerically feasible[21]. Once the transmission probabilities $T_{i \rightarrow j}$ from the injected states i to the transmitted states j are computed, the total current flowing from the left to the right reservoir may be determined from the Landauer [3] formula:

$$I_{\rightarrow} = \sum_{i,j} f_i e \frac{\hbar k_i}{m} T_{i \rightarrow j} \quad (1.3)$$

where f_i is the distribution function (usually Fermi-Dirac for electrons) at the left reservoir, and $e\hbar k_i/m$ is the current carried by the state i . The total current transmitted through the system is given by:

$$I = I_{\rightarrow} - I_{\leftarrow}. \quad (1.4)$$

Applying this approach analytically to a narrow quantum channel the contribution of each mode (corresponding to the quantization in the perpendicular direction of the channel) to the transport, or the so-called universal

[†] ψ is usually normalized so that A is 1.

conductance, may easily be calculated as $2e^2/h$ [20].

More generally, all transport properties of the geometry may be determined from a superposition of the associated properties of the single particle solutions of the steady-state Schrödinger equation, weighed by the appropriate magnitudes of the injected waves dictated by the thermal properties of the contacts. Notwithstanding its extensive use, the method is not capable of describing the time-dependent dynamics of the system apart from some special cases (such as time-independent potential). On the other hand, the scope of this thesis is the time-dependent studies of quantum transport phenomena. Therefore, we will consult this approach only for testing the time-dependent method described in the next chapter.

1.2 The Wigner Function

The Wigner function approach [22,8,23] is an elegant method in which absorbing and injecting boundary conditions can be applied naturally. For a one-dimensional system, it may be defined through the expression:

$$f(x, p; t) = \frac{1}{2\pi\hbar} \int_{-\infty}^{+\infty} \Psi^* \left(x - \frac{R}{2}; t \right) \Psi \left(x + \frac{R}{2}; t \right) e^{-\frac{i}{\hbar} pR} dR \quad (1.5)$$

where x and t are the position and time variables respectively, p is the Fourier transform variable, and Ψ is the wave function. Generalization of the expression to higher dimensions is straightforward. Misleadingly, the variables x and R are often referred as “center of mass” and “relative” coordinates, respectively. Eq. (1.5) is basically a transformation from the density operator to the Wigner distribution function which is a function of both position and momentum. Hence, the computations concerning Wigner function method are realized in the classical-like phase space. Nevertheless one must be careful in its applications since this function may have negative values contrary to the usual distribution functions. Furthermore some distribution functions $f(x, p)$ constructed without the use of Eq. (1.5) may violate the uncertainty principle,

whereas some that satisfy may not be valid Wigner functions [24].

Some important properties of the Wigner function follow immediately from Eq. (1.5):

$$\int_{-\infty}^{+\infty} f(x, p) dp = \Psi^*(x)\Psi(x) \quad (1.6)$$

$$\int_{-\infty}^{+\infty} f(x, p) dx = \Phi^*(p)\Phi(p) \quad (1.7)$$

$$\int_{-\infty}^{+\infty} \int_{-\infty}^{+\infty} x f(x, p) dx dp = \int_{-\infty}^{+\infty} \Psi^*(x) x \Psi(x) dx = \langle x \rangle \quad (1.8)$$

$$\int_{-\infty}^{+\infty} \int_{-\infty}^{+\infty} p f(x, p) dx dp = \int_{-\infty}^{+\infty} \Phi^*(p) p \Phi(p) dp = \langle p \rangle \quad (1.9)$$

where

$$\Phi(p) = \int_{-\infty}^{+\infty} \Psi(x) e^{\frac{i}{\hbar} p x} dx. \quad (1.10)$$

By transforming the Liouville equation which states the equation of motion for the density operator, we obtain for the Wigner function:

$$\frac{\partial f}{\partial t} = -\frac{p}{m} \frac{\partial f}{\partial x} - \frac{1}{\hbar} \int_{-\infty}^{+\infty} \frac{1}{2\pi\hbar} V(x, p-p') f(x, p') dp'. \quad (1.11)$$

Here $V(x, p)$ is the kernel of the potential, expressed through the relation:

$$V(x, p) = 2 \int_0^{+\infty} \sin\left(\frac{pR}{\hbar}\right) \left[v\left(x + \frac{1}{2}R\right) - v\left(x - \frac{1}{2}R\right) \right] dR \quad (1.12)$$

where v is the potential energy. This kernel reflects the influence of the reservoirs on the *open system*. Note that in Eq. (1.11) we have a first order derivative with respect to x and no derivative with respect to p . This equation may be expanded in powers of \hbar in order to show the equivalence of f to collisionless Boltzmann distribution in the classical limit.

Implemented boundary conditions have the same characteristics as those discussed earlier in the Landauer approach, but are mathematically different. One has to specify only the distribution functions at the left and right reservoirs. Namely, for a simulation region of length L , these are $f(0, p)|_{p>0}$ and $f(L, p)|_{p<0}$ respectively. On the other hand, if $v(x)$ has a rapidly converging

series expansion which is valid for smooth potential functions, Eq. (1.11) further simplifies to

$$\frac{\partial f}{\partial t} = -\frac{p}{m} \frac{\partial f}{\partial x} - \frac{2}{\hbar} \sin \left[\frac{\hbar}{2} \frac{\partial}{\partial x} \frac{\partial}{\partial p} \right] v(x) f(x, p). \quad (1.13)$$

It is also possible to implement a phenomenological “collision term” into the equation of motion (1.11) due to its similarity to Boltzmann equation. The implementation of the dissipation processes through this intuitive term is one of the main advantages of this method. Nonetheless, the physicality of this concept is controversial. On the other hand, as pointed out earlier, the application is accomplished in the phase space. This means that a $2d$ -dimensional mesh is required for a d -dimensional system. Therefore at present, the method is not feasible for application to more than one-dimensional systems, (and even to one-dimensional systems at very large time scales). In addition to this, the algorithm is not straightforward and has serious stability problems [8,25]. The equivalence of the method to the density operator theory is not precise on a finite, and specially on a discrete space. As a final remark, note that the distribution function indicates the total charge density so that one is not able to examine different scattering states separately. This may be crucial for the investigation of some quantum effects such as bistability.

1.3 Hydrodynamic Aspects

The resemblance between the equations of motion of electronic wave functions and the waves in a fluid suggests that a hydrodynamic approach may be proposed for the quantum transport phenomena. As an example, the behavior of electrons in a ballistic field effect transistor is recently shown [26] to have similar characteristics as that of a fluid such as shallow water. In the high electron density limit, the study of the mechanics of the total electron concentration demonstrates interesting hydrodynamic peculiarities.

The hydrodynamic approach, expressed in terms of densities, assumes some form of distribution function with respect to momentum. In order to derive the hydrodynamic equations (see, for example, [27]), let us first define the particle (n) and mass (ρ) densities

$$\begin{aligned} n(x, t) &= \frac{\rho(x, t)}{m} \\ &= \int f(x, p; t) d^3p \end{aligned} \quad (1.14)$$

with a local velocity field

$$\vec{v}(x, t) = \int \frac{\vec{p}}{m n(x, t)} f(x, p; t) d^3p \quad (1.15)$$

where p is the Fourier transform variable. After integrating the equation of motion over d^3p , the continuity equation follows immediately:

$$\frac{\partial n}{\partial t} + \vec{\nabla} \cdot (n\vec{v}) = 0. \quad (1.16)$$

Besides, the Euler equation for irrotational flow also may be derived after a multiplication of the equation of motion by \vec{p} and integration over d^3p :

$$\rho \left[\frac{\partial v_i}{\partial t} + \vec{v} \cdot \vec{\nabla} v_i \right] = -\frac{\rho}{m} \vec{\nabla}_i V - \vec{\nabla}_j p_{ij}. \quad (1.17)$$

Here p_{ij} is the pressure tensor given by:

$$p_{ij} = \int (p_i - mv_i)(p_j - mv_j) f(x, p; t) d^3p. \quad (1.18)$$

The above hydrodynamic equations concerning the motion and the continuity of the fluid may describe a two-dimensional electron gas in a ballistic field effect transistor. This may be seen by substituting the fluid velocity $\vec{v}(x, t)$ and potential V by the local electron velocity and the electrostatic potential, respectively. Note that the same argument does not hold for a three-dimensional electron gas since the surface charge density in a two-dimensional channel is proportional to the electrostatic potential whereas it is dictated by Poisson's equation in three dimensions.

The hydrodynamic aspects is concluded by noting that it can not describe some quantum effects such as resonance phenomena. The reason, as mentioned above, is that the expressions are functions of densities, which are in turn, functions of position. Therefore, the information about the energy or the momentum of the particles, which are vital quantities in the quantum picture, are lost in this approach.

1.4 Time-dependent Schrödinger Equation

Numerical integration of the time-dependent Schrödinger equation is another promising approach for the study of quantum transport phenomena. As one can easily guess from its title, it has the advantage of describing the time-dependent dynamics of the system in comparison to the time-independent Schrödinger equation. Similarly, particles with different wave vectors are simulated separately, and the transport properties of the geometry is extracted from these single particle solutions as discussed earlier. On the numerical side, different equivalent schemes[†] exist for the “updating” procedure of the wave function. However the implementation of the blackbody boundary conditions is not straightforward.

Theoretically, the computation of the wave function of the next time step requires the “whole” wave function of the current time step. By the word *whole*, we mean all values of the wave function in an infinite space. On the other hand, the simulation region must allocate a finite space in the memory of the computer, hence it is physically impossible to retain the *whole* wave function. Unfortunately, for the case of *open systems*, the un-kept part of the wave function, to which we will often refer misleadingly as ‘*the wave function outside the boundary*’, has a crucial influence on the part of the wave function which is present in the simulation region.

[†]Some of these schemes are so elementary that even a physics sophomore can easily practice them without encountering any stability problems.

There exist two types of *natural* boundary conditions for the numerical integration procedure of the time-dependent Schrödinger equation. The first is the “reflecting boundary condition” which implies that the wave function is totally reflected back after hitting the boundary. The second is the “periodic boundary condition” in which, the wave function is perfectly absorbed from the boundary that it hits, and is injected back perfectly to the simulation region from the opposite boundary. It is clear that both types of boundary conditions are physically defective for the analysis of the open nature of the mesoscopic devices. Nevertheless, one may still use these conditions bypassing their handicaps. A very large simulation mesh, together with wave packets of finite extent, can overcome the problems associated with the boundaries [28,29]. But then, the simulation time is limited with the time scale during which the wave function hits the boundary and returns back to the simulation region. The dimensions of the mesh required for the investigation of the dynamics of some “slow” phenomena, such as a charge build-up process in a resonant tunneling diode, may be so large that the application will not be practically feasible within present computational capabilities.

Another approach for discarding the complications related to the boundaries is modeling the reservoirs together with the analyzed device. In this context, *the system of interest* is no longer *open*. The closure of the system renders possible the application of the *periodic* or *reflecting boundary condition*. Next, one starts with a large number of initial wave functions in each reservoir[†] and carries out the simulation until an unphysical situation is encountered due to the consideration of only a finite number of particles[‡]. Thus, this approach also is not adequate for the examination of most of the relevant quantum transport phenomena.

Now, let us return to the cause of the problem: the values of the wave function outside the boundary affect *the wave function within the boundary*. Thereupon, one may conjecture that the part of the the wave function which is

[†]Practically with bound states of the reservoirs.

[‡]In general, the particles at the reservoir at the higher potential are exhausted.

outside the boundary has left the simulation region at some earlier time. This description leads to an absorbing boundary condition which is based on the values of the wave function at previous times [8,30]. These type of boundary condition methods are called “non-Markovian”, in the sense that the boundary condition requires some knowledge of the system at previous times. In other words, the evolution of the system depends upon its “history”.

Implementation of non-Markovian boundary conditions is based on the linear prediction techniques [31]. The approach is supported by the following argument of irreversibility in quantum mechanics: if some degrees of freedom are removed in a system, the effects appear in the time domain [32]. Based on this statement, one may substitute the effects of ignorance of the values of the wave function outside the boundary by non-Markovian terms. However the application of the concept is not straightforward.

It is clear that a *Markovian blackbody boundary condition* method is necessary for an extensive usage of the powerful time-dependent Schrödinger equation in the field of quantum transport simulation. In fact this equation is a second order differential equation and similar equations rule over different fields of science, such as local weather prediction, geophysical calculations, applications with electromagnetic waves, etc. Hence, the theoretical efforts to implement perfect absorbing boundary conditions on these differential equations is not recent [33]. Nonetheless such a picture does not exist for the time-dependent Schrödinger equation.

On the other hand, the first numerical work on this scope was done recently by Mains and Haddad [34,35] for the case of a one-dimensional system. They suggested a curve-fitting approach for the wave function outside and near the boundary of the simulation region. By this means, some number of values of the wave function outside the mesh are guessed in order to update *the wave function within the simulation region* for the next time step. For a plane wave injected from the left boundary with a given wave vector k , they approximated

the boundary wave function as

$$\psi_{left}(x) \approx (b_l + c_l x) e^{-ikx} + a e^{ikx} \quad (1.19)$$

$$\psi_{right}(x) \approx (b_r + c_r x) e^{ik'x}. \quad (1.20)$$

Here k' is the wave vector which will be absorbed from the right boundary, and is related to k by the potential difference between the reservoirs with an equation similar to Eq. (1.2). The coefficients b and c are calculated by a linear fit to the values of the wave function at the boundaries of the simulation mesh. The time-dependent Schrödinger equation at the left boundary is written as

$$i\hbar \frac{\partial \psi}{\partial t} = \frac{\hbar^2 k^2}{2m} \psi + i \frac{\hbar^2 k}{m} c_l e^{-ikx} \quad (1.21)$$

where m is the mass of the electron. Note that the potential energy is taken to be zero at this boundary. Then, the time evolution of the wave function is computed applying the continuum Hamiltonian:

$$\psi(t = \Delta t) \approx \psi(t = 0) e^{-i(E/\hbar)\Delta t} + \frac{\hbar k}{m} c_l e^{-ikx} \Delta t \quad (1.22)$$

where Δt is the time increment, and E is the energy of the injected wave. This equation sets Dirichlet type boundary condition on the time update procedure. Moreover, the first term at the right hand side of Eq. (1.22) is for conventional evolution of the wave function as if the boundaries do not exist, and the second term expresses the local variation of the wave function due to the reflection from the scattering region. The coefficient c_l is given as a function of the coordinates of the first two mesh points Δx and $2\Delta x$ as:

$$c_l \approx \frac{f(2\Delta x) - f(\Delta x)}{\Delta x}, \quad (1.23)$$

where

$$f(\Delta x) = \left(\psi(\Delta x) - a_l e^{ik\Delta x} e^{-i(E/\hbar)t} \right) e^{ik\Delta x}. \quad (1.24)$$

The wave function is similarly updated at the other boundary.

In the same work, Mains and Haddad simulated a resonant tunneling diode with this method. In fact, another group [36] independently examined

a three-dimensional GaAs MESFET by implementing different boundary conditions to the time-dependent Schrödinger equation. Still another group [37] proposed a more robust blackbody boundary condition based on a tight-binding model.

In summary, the best way of investigating quantum transport properties of an actual physical mesoscopic structure is via numerical methods. They may handle not only steady state and small signal analysis of the geometries, but far-from-equilibrium situations as well. This point is prominent for device modeling, for explaining some experimental observations, as well as for predicting new quantum phenomena. Among a number of numerical approaches, the Wigner function and the time-dependent Schrödinger equation are the most promising ones due to their capability of describing time dependence of the system. Expressed in terms of a complex valued function, the Schrödinger equation has the advantages of being represented on a d -dimensional mesh for a d -dimensional system and of having more stable integration procedures. The handicap of the method lies in the implementation of the open system blackbody boundary conditions.

In the next chapter, we will introduce our method for curing this handicap and will present some sample calculations in order to exhibit its power. The following chapters are left to the applications of the method on two- and one-dimensional meshes respectively. In Chapter 3, we will see that the interacting two-particle problem in one-dimensional space may be solved numerically exactly considering only a single particle on a two-dimensional mesh. After that, a two-dimensional physical geometry will be considered and the installation of the self-consistent potential will be discussed. This recent structure exhibits a negative differential resistance and a bistability in the current-voltage characteristics [38]. A time-dependent study of it has been done for the first time. In Chapter 4, we will attack the problem of quantum bistability using a one-dimensional model structure. A time-dependent investigation of the switching phenomena will be presented for the first time.

The chapter will end up with the generalization of this model geometry to higher dimensions. Of course, such a novel and powerful method has a wide range of physical applications but the work which will be presented was limited with time and computation power that was available. Consequently, the open problems concerning the applications are enumerated in the concluding chapter, Chapter 5.

Chapter 2

BLACKBODY BOUNDARY CONDITIONS

The numerical integration of the time-dependent Schrödinger equation is a promising method for the analysis of quantum transport properties of mesoscopic structures. The main advantage of the procedure is its ability to describe the time-dependent dynamics of the system. Most of the practical applications suggest that there have to be some “contacts” to the system from which particles may be injected or absorbed. For cases which include such “open” boundaries, the theory requires the implementation of the appropriate blackbody boundary conditions which is not straightforward.

2.1 The Method

The principle idea of the method which is described below [41], is an extrapolation of the wave function outside the simulation region as an estimate of the wave that has already left the boundary at earlier times. Its novelty lies in the estimation process which is based on the values of the wave function in a

relatively large region near the boundary compared to the previous Markovian approaches [34–37,39,40]. The development of the wave function is calculated during a time step twice, once with reflecting or periodic boundary conditions throughout the full simulation space, second near the contact region, using an extrapolation of the wave function outside the contact region consistent with the absorption/injection condition. The full wave function is then updated using a mixture of the two time developments.

2.1.1 Discretized Schrödinger Equation

The time-dependent Schrödinger equation is expressed as:

$$\begin{aligned} i \hbar \frac{\partial \Psi(x, t)}{\partial t} &= H \Psi(x, t) \\ &= \left[-\frac{\hbar^2}{2m} \nabla^2 + V(x, t) \right] \Psi(x, t) \end{aligned} \quad (2.1)$$

where V is the potential, \hbar is the Planck constant, t is time in units of seconds, x is the spatial coordinate of the particle, and m is its mass. This equation may be discretized by replacing the continuum kinetic energy operator $-\frac{\hbar^2}{2m} \nabla^2$ by the discrete one $-\frac{\hbar^2}{2m} K$, through the relation:

$$\nabla^2 = -\frac{K}{(\Delta x)^2}. \quad (2.2)$$

Here Δx is the distance between two lattice points on the discrete space. For a one-dimensional system, this “difference” operator K , acting on the time-dependent value of the wave function Ψ at the l 'th lattice point gives us:

$$(K \Psi)_l = 2 \psi_l - \psi_{l-1} - \psi_{l+1}. \quad (2.3)$$

Generalization of K for higher dimensions is straightforward. Now, dividing Eq. (2.1) by an energy scale $\epsilon_0 = \hbar^2/2m (\Delta x)^2$, we have the unitless wave equation

$$i \frac{\partial \psi_l}{\partial \tau} = [K + v(l, \tau)] \psi_l, \quad (2.4)$$

where v is the unitless potential function ($v = V/\epsilon_0$) and τ is the unitless time variable which is scaled by \hbar/ϵ_0 .

The solution of the differential equation (2.4) is elementary and if $\hat{\Psi}(\tau)$ represents the vector of values of $\{\psi_l\}$ at time τ , it can be “updated” for the next time step through the relation:

$$\tilde{\Psi}(\tau + \Delta\tau) = \exp[-i \Delta\tau (K + v)] \tilde{\Psi}(\tau) . \quad (2.5)$$

The integration procedure used here, for the time development of the wave function, is to break up the exponential in Eq. (2.5) such that

$$\exp[-i\Delta\tau(K + v)] \approx \exp(-iv\Delta\tau/2) \exp(-i\Delta\tau K) \exp(-iv\Delta\tau/2) . \quad (2.6)$$

This approximation is correct to order $(\Delta\tau)^2$, and preserves the normalization and the time reversal symmetry of the wave function. The right hand side of the Eq. (2.6) can be re-expressed as:

$$(2.6) = \exp(-iv\Delta\tau/2) F^{-1} \underbrace{F \exp(-i\Delta\tau K) F^{-1}}_{\text{kinetic energy term}} F \exp(-iv\Delta\tau/2) \quad (2.7)$$

where F represents a discrete Fourier transformation operator and F^{-1} is its inverse. In order to update the wave function, the multiplication by the potential term in the position space is carried out first. Then, the wave function is transformed to the momentum space for the multiplication by the kinetic energy term which is diagonal in that space. After this multiplication, the wave function is Fourier transformed back to the position space and multiplied again by the potential term.

It is worthwhile to calculate the kinetic energy term indicated in Eq. (2.7) explicitly for a one-dimensional system. Let the value of the wave function after the multiplication by the rightmost potential energy term $\exp(-iv\Delta\tau/2)$, be denoted by ψ_l . The next operation is the discrete Fourier transformation which will yield the Fourier coefficients ξ as:

$$\xi_k = (F \Psi)_k = \frac{1}{\sqrt{N}} \sum_{l=0}^{N-1} \exp\left(i\frac{2\pi}{N}kl\right) \psi_l . \quad (2.8)$$

and the wave function may be expanded as:

$$\psi_l = (F^{-1} \Xi)_l = \frac{1}{\sqrt{N}} \sum_{k=0}^{N-1} \exp\left(-i\frac{2\pi}{N}kl\right) \xi_k. \quad (2.9)$$

Here, Ψ and Ξ denote the vector values of $\{\psi\}$ and $\{\xi\}$ respectively. Next, the action of the kinetic energy term $\exp(-i\Delta\tau K)$ on ψ_l has to be expressed. In order to achieve this, we begin with a simpler problem, the action of the operator K on ψ_l . The result is already given in Eq. (2.3), we expand the terms at the right hand side of this equation in terms of the Fourier coefficients ξ :

$$\begin{aligned} (K \Psi)_l = & \frac{2}{\sqrt{N}} \sum_{k=0}^{N-1} \exp\left(-i\frac{2\pi}{N}kl\right) \xi_k - \frac{1}{\sqrt{N}} \sum_{k=0}^{N-1} \exp\left(-i\frac{2\pi}{N}k(l-1)\right) \xi_k \\ & - \frac{1}{\sqrt{N}} \sum_{k=0}^{N-1} \exp\left(-i\frac{2\pi}{N}k(l+1)\right) \xi_k \end{aligned} \quad (2.10)$$

Grouping the common terms in the summation together:

$$(K \Psi)_l = \frac{1}{\sqrt{N}} \sum_{k=0}^{N-1} \exp\left(-i\frac{2\pi}{N}kl\right) \xi_k \left(2 - \exp(i\frac{2\pi}{N}k) - \exp(-i\frac{2\pi}{N}k)\right). \quad (2.11)$$

By using some simple trigonometric identities, we get the result:

$$(K \Psi)_l = \frac{1}{\sqrt{N}} \sum_{k=0}^{N-1} \exp\left(-i\frac{2\pi}{N}kl\right) \left(4 \sin^2\left(\frac{\pi}{N}k\right)\right) \xi_k. \quad (2.12)$$

The Fourier transformation of this expression gives:

$$(F K \Psi)_k = (F K F^{-1} \Xi)_k = 4 \sin^2\left(\frac{\pi}{N}k\right) \xi_k. \quad (2.13)$$

In order to obtain the final result, we will use here an identity which holds for any general operator functions V and W :

$$V e^W V^{-1} = e^{V W V^{-1}}. \quad (2.14)$$

Combining Eq. (2.13) with Eq. (2.14) yields for the kinetic energy:

$$\begin{aligned} (F \exp(-i\Delta\tau K) F^{-1} \Xi)_k &= \exp(-i\Delta\tau F K F^{-1}) \xi_k \\ &= \exp\left[-i\Delta\tau \left(4 \sin^2\left(\frac{\pi}{N}k\right)\right)\right] \xi_k \end{aligned} \quad (2.15)$$

which is diagonal in the momentum space.

The availability of fast Fourier transform algorithms make the transformation and inverse transformation of the wave function at each time step feasible. The discrete Fourier transformation implies periodic boundary conditions, however perfectly reflecting boundary conditions may also be implemented after an anti-symmetrization of the wave function through a doubling of the periodicity length.

As mentioned in Chapter 1, there exist different equivalent approaches for the numerical integration of the time-dependent Schrödinger equation (we will call “updating” of the wave function afterwards). In this work, we have used the procedure which is mentioned above. Nevertheless the method of implementing absorbing and injecting boundary conditions which is described below, is probably robust under a change of the integration procedure, this point has not been verified.

2.1.2 Extension of the Boundary Region

In order to implement an absorbing boundary condition, we try to make an estimation of the wave function which is outside of our simulation region and next to the boundary. First, we consider a number (say n) of points within the simulation region and next to the boundary where the potential may be assumed to be constant. And then, we extrapolate these n points to another n points outside the boundary with the understanding that this extrapolated part of the unknown wave function has left the boundary at some recent time. In order to define this estimate uniquely, we assume that these $2n$ points together have only outgoing momentum components, *i.e.* only outgoing waves exist in this region. This means that we choose these momentum components such that the discrete Fourier transform of the wave function composed of these $2n$ points corresponds to no incoming momentum components.

An analytic explanation would clarify this idea. We can consider, for example, the application of the procedure to the “left” (*i.e.* $-x$) boundary of a one-dimensional system. In this context, let ϕ_l denote the n leftmost values ψ_l (*i.e.* $1 \leq l \leq n$) of the wave function which are within the simulation region and next to the boundary. This is the part of the wave function which will be extrapolated to another n values outside the boundary (*i.e.* n unknown values of ϕ_l for $-n + 1 \leq l \leq 0$ will be determined). We can express any value of ϕ by its Fourier expansion as:

$$\phi_l = \frac{1}{\sqrt{2n}} \sum_{k=-n+1}^n c_k \exp\left(i \frac{2\pi}{2n} kl\right). \quad (2.16)$$

Here, c_k are the $2n$ Fourier coefficients with $-n + 1 \leq k \leq n$. The condition of having only outgoing momentum components (*i.e.* toward “left”) in this region can be stated analytically as:

$$c_k \begin{cases} = 0 & \text{for } k > 0 \\ \neq 0 & \text{for } k \leq 0. \end{cases} \quad (2.17)$$

Therefore only non-positive values remain in the summation of Eq. (2.16). Indeed there underlie $2n$ simultaneous linear equations which connect $2n$ values of ϕ to $2n$ values of c . In that total of $4n$ parameters, n values of ϕ which stay in the boundary are ‘given’ and n values of c are defined through the condition in Eq. (2.17). The problem is trivial now: there remain $2n$ unknown parameters to be determined from the solution of the $2n$ simultaneous linear equations in Eq. (2.16).

We can re-express Eq. (2.16) in a more simple form by replacing the term $\exp(-i\pi l/n)$ by a new parameter z_l :

$$\phi_l = \frac{1}{\sqrt{2n}} \sum_{k=0}^{n-1} c_{-k} z_l^k \quad (2.18)$$

The right hand side of Eq. (2.18) may be interpreted as a polynomial of order $n - 1$ in the variable z . At the n points z_l with $1 \leq l \leq n$, this polynomial

is specified to take the values ϕ_l . Its solution is unique, and we can use the Lagrange formula (see, for example, [42])

$$p(z) = \sum_{l=1}^n \phi_l \prod_{k \neq l} \frac{z - z_k}{z_l - z_k} \quad (2.19)$$

to determine it. The polynomial $p(z)$ then is the polynomial in Eq. (2.18) and may be used to obtain all $2n$ values of ϕ_l :

$$\phi_l = p \left[\exp \left(-i \frac{2\pi l}{2n} \right) \right]. \quad (2.20)$$

So the vector of n unknown values of ϕ are calculated by a matrix multiplication of an $n \times n$ square matrix by the vector of n known values of ϕ . Since this $n \times n$ square matrix is only a function of n , it may be calculated at the beginning of the computer code in order to optimize the program. The aim of the above procedure was to determine the boundary wave function ϕ . In this scope, we may also try to invert directly the Eq. (2.16). However, in the determination of coefficients in polynomials of a high degree, one may encounter numerical stability problems (see, for example, [43]). Because of this, the evaluation of the extrapolated values through the Lagrange formula is preferred over a direct inversion of Eq. (2.16). The method has been applied to polynomials of order up to 8 with no difficulty, using only single precision arithmetic.

The method of extending the boundary region is sketched schematically in Figure 2.1. Ψ is shown near the “left” boundary, with the boundary wave function Φ and the Fourier transform c . The dotted part of the wave function Φ may be calculated from Eq. (2.20).

The above choice of the momentum components to be specified is not unique. It is simple, and guarantees a “numerically exact” representation of outgoing wave functions nominally of a single wavelength and commensurate with the extended boundary region. Hence, the accuracy of the method would be expected to increase if the size of this boundary region could be increased, as this would allow longer and longer wavelengths to be commensurate with this region. However, as it stands, the method enables the absorption of

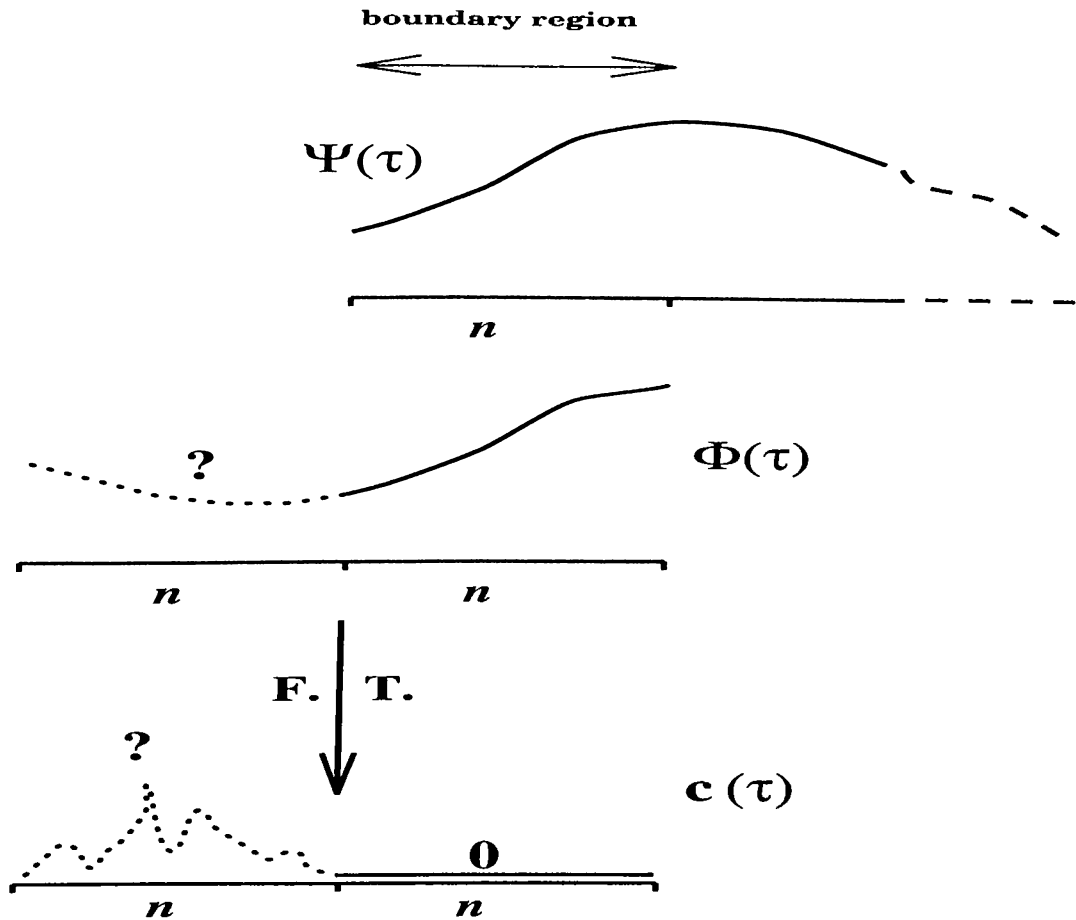


Figure 2.1: Schematic explanation of the extension of the boundary region (a) The full wave function Ψ to be absorbed at the “left” boundary. (b) the boundary wave function Φ to be extended outside the boundary region. (c) the Fourier transform c of the wave function Φ . The dotted lines with question marks are the “unknown” values of the wave functions Φ and c . There are a total of $2n$ such unknown parameters to be determined from the expression of the Fourier transform.

wavelengths much longer than the boundary region size, although its accuracy decreases for very long wavelengths. In applications where the dynamics of very long wavelengths dominate, one could modify the extrapolation procedure to include these wavelengths at the expense of others. On the other hand, for a numerically efficient implementation, the mesh length Δx should be chosen such that these large wavelengths are not generated, *i.e.* a smooth wave

function should not be represented by a needlessly large number of points.

2.1.3 The Update of the Wave Function

The boundary wave function ϕ composed of the $2n$ values may then be updated for the next time step (at the constant potential of the boundary), using periodic boundary conditions as described in Section 2.1.1. Although this type of boundary condition would not be appropriate for points near $l \approx n$ (rightmost end of the boundary), it is quite accurate near the boundary ($l \approx 1$). The full wave function ψ is also updated as described in Section 2.1.1, using perfectly reflecting or periodic boundary conditions. This type of update is obviously not appropriate near the boundary ($l \approx 1$), but is accurate sufficiently away from the boundary. So, at the boundary region, we have two different wave functions which are complementary in regions where they are accurate. For sufficiently small time-steps, there is a wide transition region in which both solutions are accurate and coincide. It is, then, a matter of switching from one wave function to the other one in the boundary region in order to obtain the full wave function ψ for that time step, consistent with an absorbing boundary condition.

The procedure of updating the full wave function is sketched schematically in Figure 2.2. Ψ and Φ are now updated for the next time step $\tau + \Delta\tau$. The two wave functions overlap at the central part of the boundary region.

2.1.4 Injecting Boundary Condition

So far, we have described the method to implement an absorbing boundary condition. If the particle is being injected from the same boundary with a

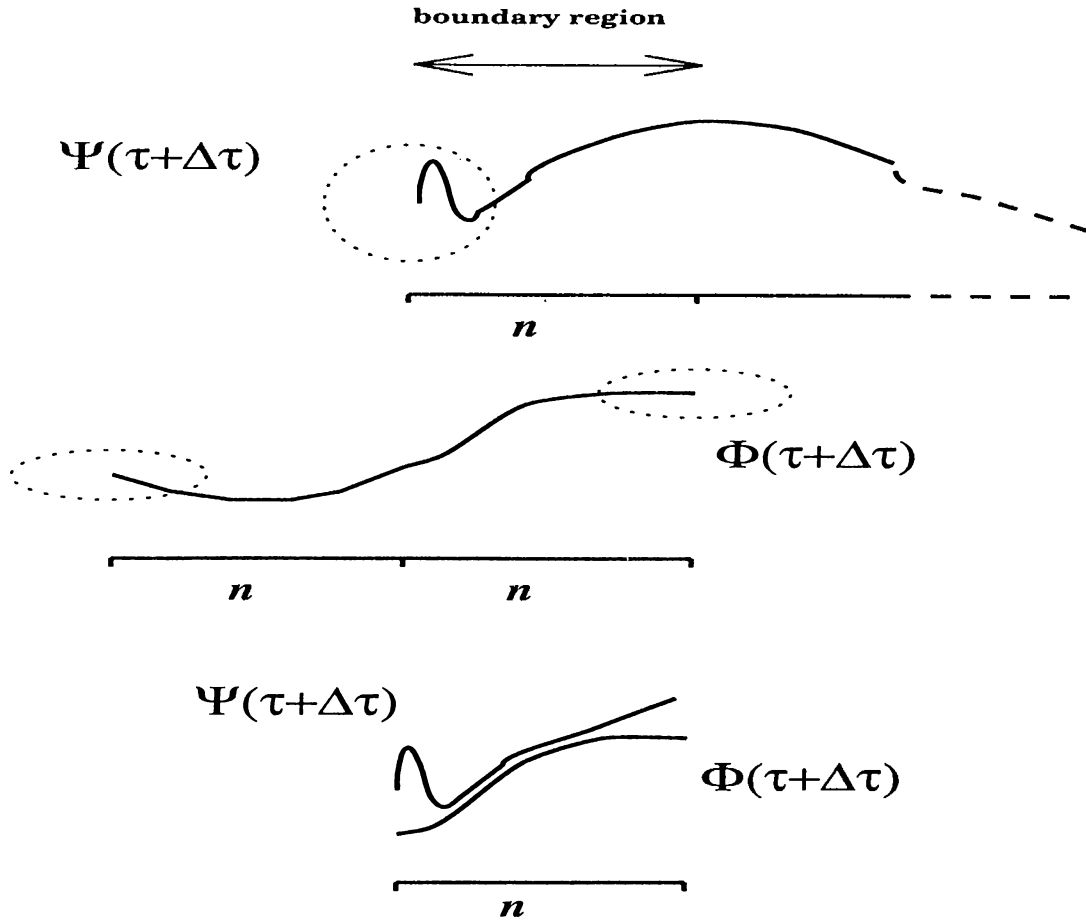


Figure 2.2: Schematic explanation of the update

(a) (b) The wave functions Ψ and Φ are shown at the time step $\tau + \Delta\tau$. They were updated using reflecting and periodic boundary conditions respectively. The dotted ellipses indicate the regions where the updates of the wave functions are not accurate. (c) The wave functions are superimposed in order to show the transition region where they are both accurate.

particular wave vector q , one then expects the wave function to have the form

$$\phi_l = A \exp(iql) + \frac{1}{\sqrt{2n}} \sum_{k=-n+1}^0 c_k \exp\left(i\frac{2\pi}{2n}kl\right) \quad (2.21)$$

where A is the coefficient of the incident wave. The additivity property of the wave functions that are injected and absorbed makes the implementation of the injecting boundary condition very simple once the absorbing one is realized. In this case, the wave function which has to be absorbed is $\phi_l - A \exp(iql)$ instead

of ϕ_l . Hence the updating procedure given above for the absorbing boundary conditions is applied to the set of values $\phi_l - A \exp(iql)$. Once that part of the wave function is updated for the next time step, the injected part of the wave function is also updated ($A \rightarrow A \exp(-iE_q \Delta\tau)$, with E_q the scaled energy of the incident wave). This second update is after the elementary quantum mechanics and does not necessitate the procedure described in Section 2.1.1. The sum of the two components then makes up the complete update of the wave function for ϕ in the boundary region. The full wave function ψ is also updated using perfectly reflecting or periodic boundary conditions, and the two updates are combined as before.

In implementing these types of boundary conditions in more than one dimensions with rectangular geometry, one again needs to know the analytic form of the solutions near the boundaries. Depending on the type of problem, a constant potential, or more typically, a “channel” (perpendicular to the boundary) with finite potential walls may be used, for which analytic form of the solutions near the boundary may be constructed. The form of the solution near the absorbing boundary will then be of the form

$$\phi(l_x, l_y, l_z) = A u(l_y, l_z) \exp(iql_x) + \frac{1}{\sqrt{2n}} \sum_{k=-n+1}^0 c_k(l_y, l_z) \exp\left(i\frac{2\pi}{2n}kl_x\right) \quad (2.22)$$

with a particle injected with wave vector q in the $+x$ direction and in the eigenmode $u(l_y, l_z)$ near the boundary. The integers l_x, l_y, l_z label the position coordinates on the three-dimensional mesh, and the expansion coefficients $c_k(l_y, l_z)$ may be determined as before for fixed l_y and l_z .

2.2 Sample Calculations

The implementation of blackbody boundary conditions was broadly tested on some one and two-dimensional systems with different challenging initial conditions. In these tests, we compared the method described above with

the “numerically exact” or “theoretically predicted” solutions. We observed that the wave functions approach to the equilibrium solutions even with very “unphysical” initial conditions. In this section, we will mention some of the sample calculations in order to indicate the accuracy of the method. First, example of a “simple” absorption is given, and is followed by a “simple” injection. After that, a two-dimensional application is presented. Most of the computations in this section have been carried out using single precision arithmetics. The procedure operated almost perfectly in these circumstances. Some details related to the limitations of the method are mentioned in the Appendix.

2.2.1 Absorption of a Wave Packet

The first application of the method is the motion of an initially Gaussian wave packet through an absorbing boundary. Since it is simple and the injection procedure does not take part, this is a typical test for the absorbing boundary condition.

The wave packet is initially a Gaussian with a momentum in the $+x$ direction. Its motion is displayed in Figure 2.3 for different scaled time values. The simulation region consists of 32 mesh points for which a perfectly reflecting boundary is implemented at $l_x = 1$ using the reflecting boundary condition, and a perfectly absorbing one at $l_x = 33$ according to the method described in Section 2.1.2 and 2.1.3. The size n of the boundary region is 8. The potential is zero throughout the simulation region. The accuracy of the wave packet leaving the boundary at the scaled time value of 15 has been checked against a simulation of the same wave packet on a mesh which extends to 128 points. At this value of the scaled time, one expects no errors on this larger mesh due to the reflecting boundary condition, as the wave packet is a safe distance away from the boundary on the right-hand side. Hereupon, this larger wave function is assumed “numerically exact”.

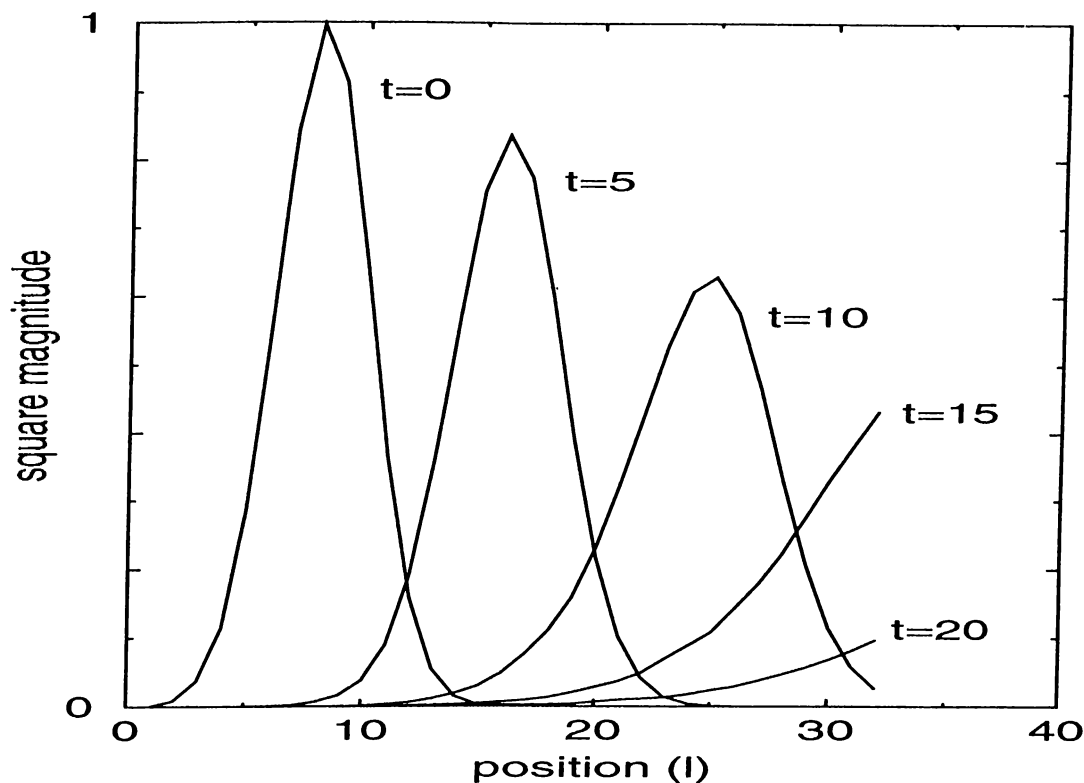


Figure 2.3: Motion of a wave packet through an absorbing boundary
 Motion of an initially Gaussian wave packet (corresponding to $\psi_l = \exp[(l-8)^2/16 + i0.982l]$ initially) under the effect of a perfectly reflecting boundary at the left, and a perfectly absorbing one at the right. The broken lines connect the discrete values of ψ_l at the indicated values of the unitless time variable.

The “relative error” in the wave packet on the smaller mesh in comparison to that on the larger mesh is displayed in Figure 2.4. It is defined as $|\psi_l/\Psi_l - 1|$ where ψ_l and Ψ_l are the values of the wave function on a simulation mesh of sizes 32 and 128 respectively. As apparent in this figure, there is a dramatic improvement in the approximation as the size n of the boundary region is increased, in fact at the scale of Figure 2.3, the wave function generated with $n = 8$ and $n = 16$ are indistinguishable from the one generated on the larger mesh. A boundary size corresponding to $n = 8$ seems to be optimal for a large class of problems in terms of accuracy/computational resource tradeoff.

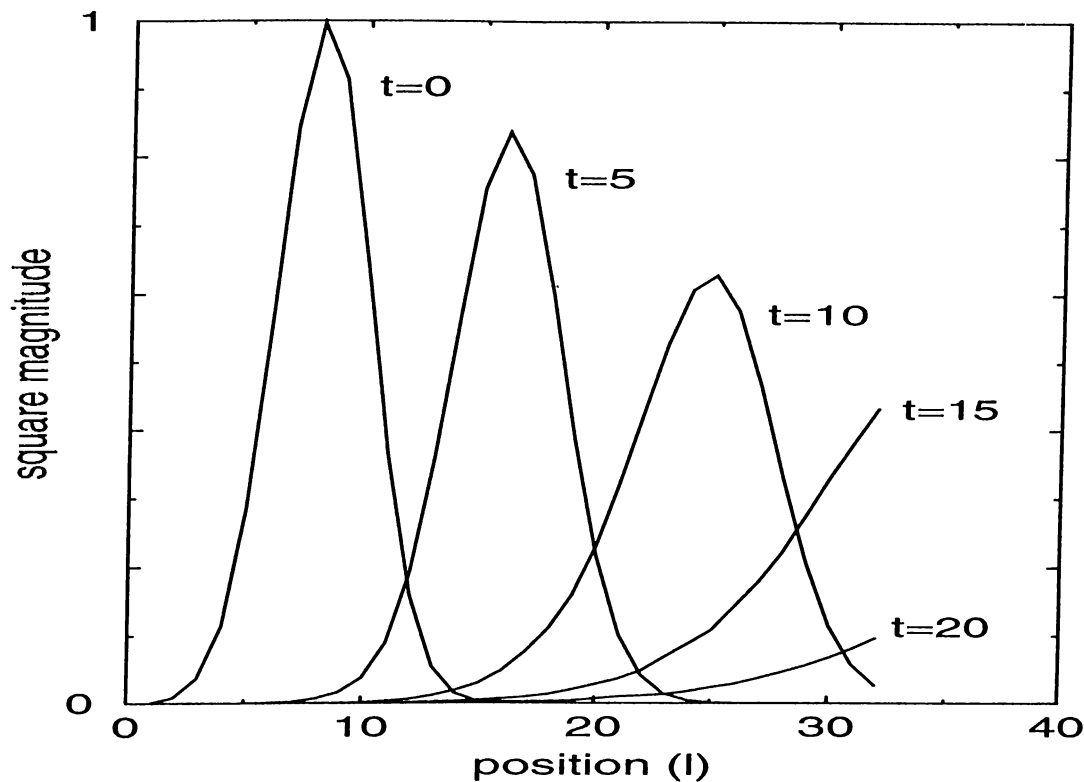


Figure 2.3: Motion of a wave packet through an absorbing boundary
 Motion of an initially Gaussian wave packet (corresponding to $\psi_l = \exp[(l-8)^2/16 + i0.982l]$ initially) under the effect of a perfectly reflecting boundary at the left, and a perfectly absorbing one at the right. The broken lines connect the discrete values of ψ_l at the indicated values of the unitless time variable.

The “relative error” in the wave packet on the smaller mesh in comparison to that on the larger mesh is displayed in Figure 2.4. It is defined as $|\psi_l/\Psi_l - 1|$ where ψ_l and Ψ_l are the values of the wave function on a simulation mesh of sizes 32 and 128 respectively. As apparent in this figure, there is a dramatic improvement in the approximation as the size n of the boundary region is increased, in fact at the scale of Figure 2.3, the wave function generated with $n = 8$ and $n = 16$ are indistinguishable from the one generated on the larger mesh. A boundary size corresponding to $n = 8$ seems to be optimal for a large class of problems in terms of accuracy/computational resource tradeoff.

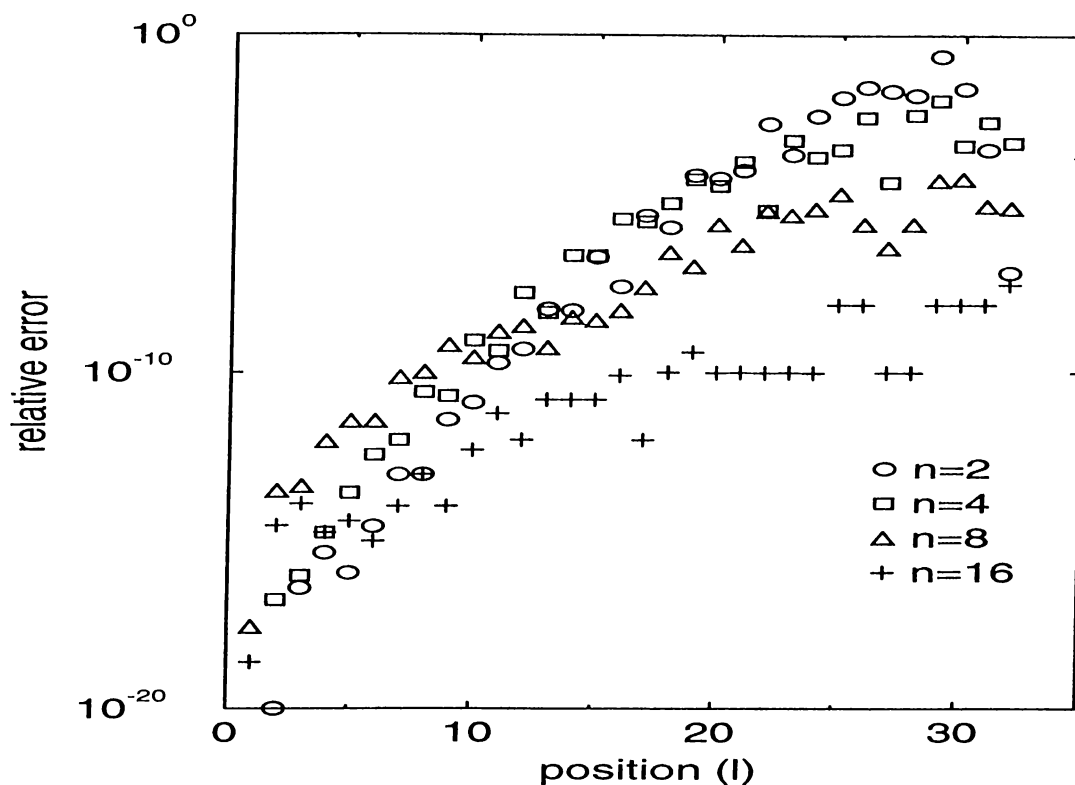


Figure 2.4: The relative error as a function of position l .

The relative error in the wave function at $t = 15$ of Figure 2.3 displayed for various values of the size n of the boundary region.

2.2.2 Injection of Particles on a Tunneling Barrier

Figure 2.5 shows the progress of a monochromatic wave injected into an initially empty space containing a tunneling barrier. A Gaussian wavefront having an analytical expression $\exp[-0.07(l - 22)^2]$ with $1 \leq l \leq 22$, has been imposed on the wave. The wave has a scaled unitless energy value of $\epsilon = 0.198$, corresponding to a wavelength of 14 mesh spacings. The time step $\Delta\tau$ is taken to be equal to 0.1. The potential is zero except between the vertical lines where it has a scaled value of 0.2. The results of the simulation implementing the method described above have been compared with the results of a simulation carried out on a periodic mesh of size 4096. Again, this large mesh avoids the problems associated with boundary conditions for the values

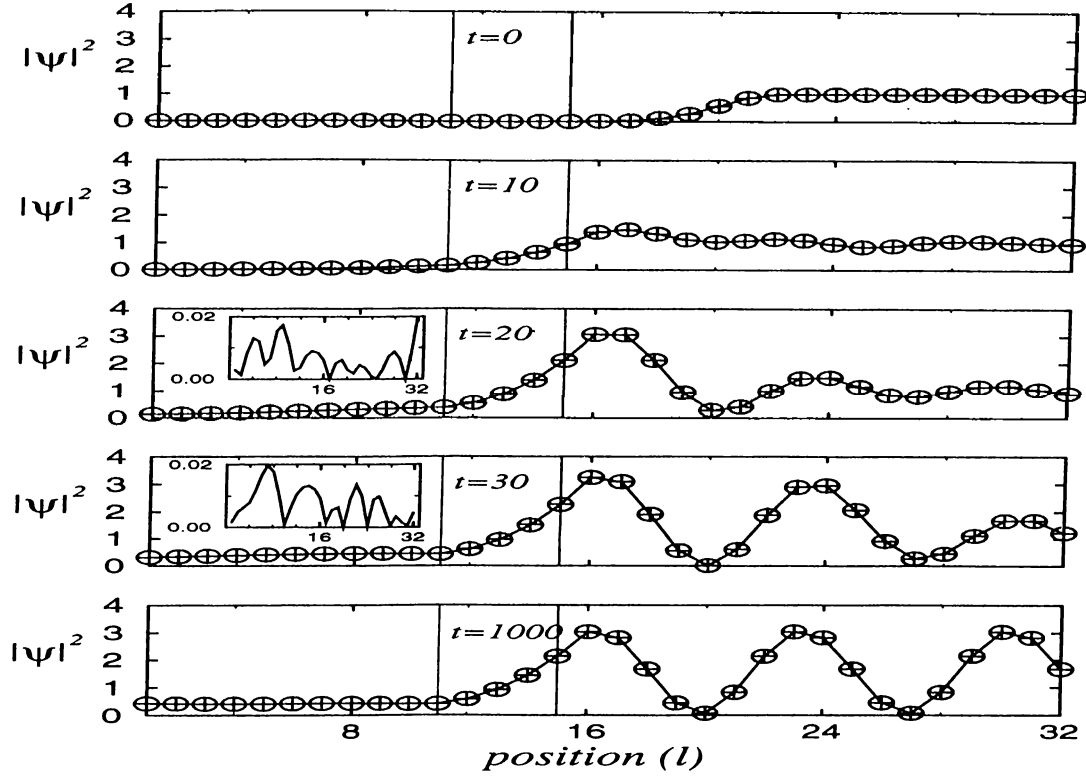


Figure 2.5: Injection of particles to a tunneling barrier

The progress of a wave with a Gaussian wavefront injected into initially empty space containing a tunneling barrier, at various values of the unitless time variable. The circles (connected by straight lines) correspond to the result of a simulation based on the method described in this work (with a boundary length of $n = 8$), the pluses correspond to the result of a computation on a mesh with 4096 points and with periodic boundary conditions. Two insets display the difference between the two magnitudes at an expanded scale.

of the time variable indicated in the figure. For our method, the situation is more challenging here in comparison to the example of the previous subsection, due to the fact that there is not only injection, but also absorption at both of the two boundaries. The part of the wave function which tunnels through the barrier is absorbed from the left boundary whereas the part that reflects back from the one at right. In addition to that, the simulation is run for large time scales as indicated on the figure. Accordingly, one expects that the errors grow up in time. In contrast, the difference between the results of the two simulations is not visible in the scale of the figure. As can be seen from

the insets, the errors in the magnitudes of the wave functions is less than one percent.

2.2.3 Injection of Particles to The Kink Structure

The boundary condition described in this work has also been tested on two-dimensional systems in which the wave function is incident (and absorbed) through channel like potentials. Figure 2.6 displays the progress of the wave function through a kink (or “double-bend”) shaped channel at different times. The boundary region has a length of $n = 8$, and the wavelength of the injected wave is approximately 13 mesh units. Even at large values of the scaled time, the method operated successfully while injecting and absorbing the wave function at both of the boundaries. As mentioned in Chapter 1, by carrying out an ensemble of single particle simulations (each corresponding to a different incident wave) in parallel, it is possible to study quantum transport through two-dimensional structures in the presence of time-dependent boundary conditions. Finally, it is recently reported that this kink structure has interesting nonlinear transport properties [38]. However, this topic is deferred until the next chapter where it is presented in detail.

In summary, a method which enables the absorption and injection of wave functions at the boundaries of a region is implemented to the numerical integration of time-dependent Schrödinger equation. The method is Markovian and is stable under a large range of conditions. Extension of the wave function to a relatively large number of points is the most important advantage of this method in comparison to other Markovian methods. The usage of the fast Fourier transform technique in the algorithm makes the method numerically efficient. Hence, the computer code may be parallelized very effectively. On the other hand, the idea of the method may be applicable to other types of wave equations, such as the Maxwell Equations, but this point is beyond the scope of this thesis. In the following chapters, the method is applied to some

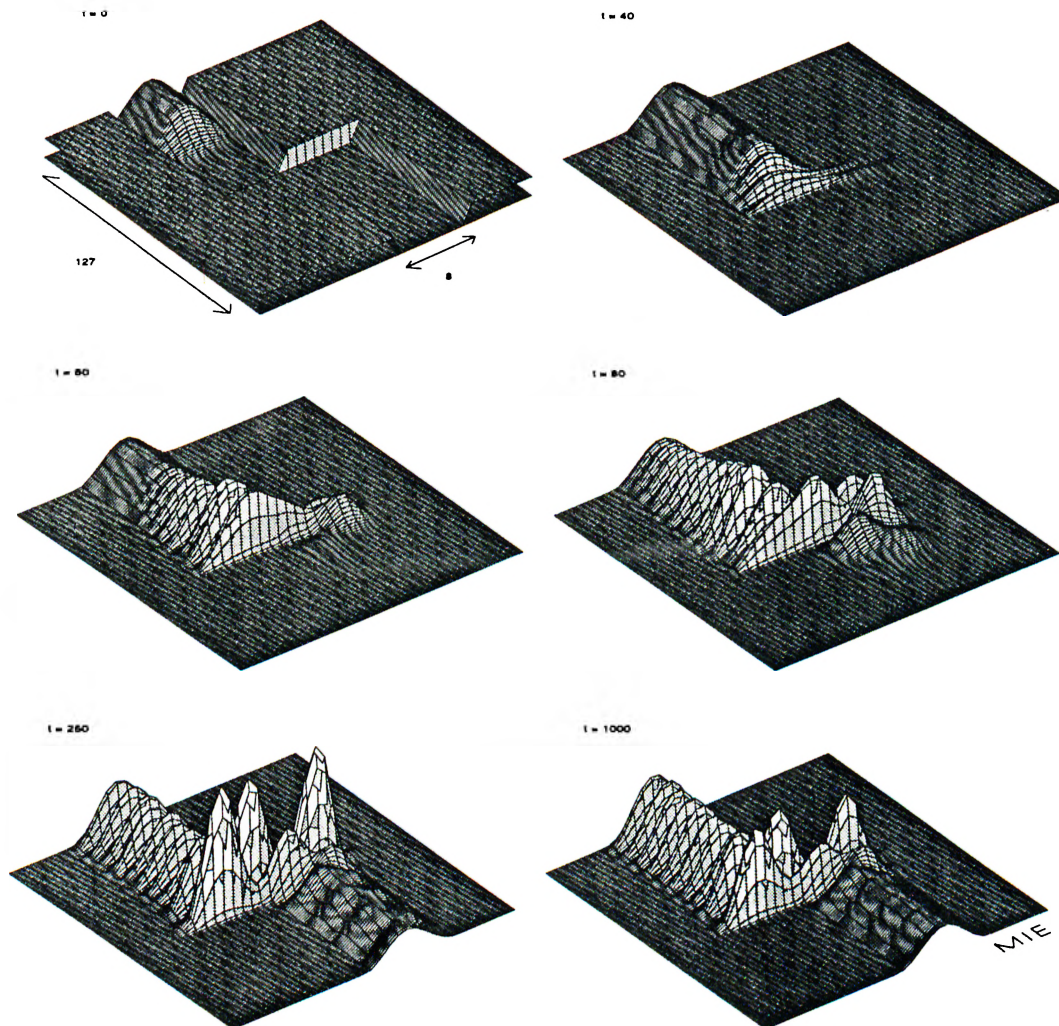


Figure 2.6: Motion of a wave packet through the kink structure

The development of the wave function in an electron waveguide with a kink. The figure shows the square-magnitude of the wave function on a 32×128 simulation mesh. The scaled values of time are indicated on the figure. The potential profile is superimposed on the wave function for $t = 0$.

number of two- and one-dimensional systems. Throughout the computations, the dissipation effects are always neglected. Indeed, implementation of these effects to time-dependent Schrödinger equation is also problematic [44]. The particles are assumed to be spinless, and this assumption has not any relevant

influence on the dynamics of the system even for the investigation of bistable switching mentioned in Chapter 4. The mass of the electron is calculated using the effective mass factor 0.0067 as in GaAs, and the mesh size and the temperature are taken as one nanometer and zero Kelvin respectively.

Chapter 3

2-D APPLICATIONS

The method of implementing blackbody boundary conditions has a wide range of applications in two-dimensional systems. Here, “two-dimensional system” is meant to be a system which requires a two-dimensional mesh for the solution of the time-dependent Schrödinger equation. In this context, a *two-dimensional system* may be any physical geometry composed of quantum channels and cavities (see, for example, [28,29,45]), as well as the solution to the problem of two particles in one-dimensional space, interacting via two-particle forces. In the two sections that follow, a numerically-exact solution of a two particle problem is given first, followed by an example of a laterally confining geometry, the “kink structure”.

3.1 Exact Solutions of Two Particle Problem

The two interacting particle problem in one dimension is equivalent to the problem of a single particle in two dimension. This equivalence may be used to solve numerically exactly a model of two particle problem. The investigation of the case is problematic with different approaches. On the theoretical side,

the system may be generalized to a n -particle system and be applied to the problem of bistability. However, these points are only introduced briefly.

3.1.1 The Problem of Bistability

The Schrödinger equation for an n -particle system is expressed in its most general form as:

$$H \Psi(x_1, x_2, \dots, x_n) = E \Psi(x_1, x_2, \dots, x_n) \quad (3.1)$$

where E is the energy of the system, x_k is the spatial and spin coordinate of the k 'th particle and H is the Hamiltonian given by the expression:

$$H = -\frac{\hbar^2}{2m} \{ \nabla_1^2 + \nabla_2^2 + \dots + \nabla_n^2 \} + V(x_1, x_2, \dots, x_n). \quad (3.2)$$

Here V is the potential energy of the system, including the external potential and all kinds of interactions between those n particles. The equation (3.1) then suggests a linear equation, and a linear equation results in a unique solution for a given set of scattering boundary conditions. So for a given potential profile, one has a unique wave function Ψ , and energy E which satisfy the exact Schrödinger equation. The physical properties of the system, such as charge build-up and current, are derived from the n -particle wave function Ψ . We may conclude that for a given potential difference, the current transmitted through an electronic device corresponding to a given set of incident states is unique. The experimental observations of bistability seem to oppose this statement (see, for example, [46,47]).

To give the exact answer to the open question of this paradox is beyond the scope of this thesis. But it is worthwhile to denote its analogy with the bistability seen in phase transitions. The non-analyticity in the theory of phase transitions may be analyzed with a mean field approximation approach, but a rigorous treatment results in a much more complicated picture.

An explanation of quantum bistability may be similar to the phase transition analogy: the solution of the time-independent Schrödinger equation is unique, but probably unstable. There may be other, very slowly decaying metastable states. The system started from any initial state will develop into one of the bistable solutions with a little perturbation. These bistable solutions must have very long, practically infinite lifetimes. Switching phenomena of the system, from one of these bistable solutions to the other one, is another interesting problem. A study of this effect is given in the next chapter.

3.1.2 n -Particle System Interacting via Pair Forces

As noted earlier, the potential energy term V in Eq. (3.2) is written in its most general form. It follows that Eq. (3.1) is very complex to solve. Hence, we shall assume hereafter that the interaction between electrons is determined by pair forces. Our main goal is to postulate that an n -particle system interacting via pair forces may be treated in terms of a two particle system. In this way, it is very helpful to rewrite the Hamiltonian in Eq. (3.2), in the second quantization scheme as:

$$\hat{H} = \sum_k \epsilon_k c_k^\dagger c_k + \frac{1}{2} \sum_{k,l,m,n} \hat{V}_{klmn} c_k^\dagger c_l^\dagger c_l c_m \quad (3.3)$$

where ϵ_k is the energy of the single particle state k , c_k^\dagger and c_k are the creation and annihilation operators of fermion system respectively, satisfying the commutation relations $[c_k, c_l^\dagger]_+ = \delta_{kl}$, and $[c_k, c_l]_+ = [c_k^\dagger, c_l^\dagger]_+ = 0$. Note that, these single particle states are the eigenstates of an individual electron in the field of particles other than electrons, such as nuclei in atoms and molecules. \hat{V}_{klmn} is the interaction matrix element given by:

$$\hat{V}_{klmn} = \iint \psi_k^*(x) \psi_l^*(x') \hat{V}(x, x') \psi_m(x') \psi_n(x) dx dx' . \quad (3.4)$$

Here, ψ_k is the wave function of the single particle state k . Furthermore, we may expand the two particle wave function $\hat{\Psi}$ in terms of complete orthonormal

set of single particle eigenfunctions ψ_k as:

$$\hat{\Psi}(x, x') = \sum_{kl} a_{kl} \psi_k(x) \psi_l(x'). \quad (3.5)$$

As a result, the determination of the expansion coefficients a_{kl} in Eq. (3.5) (*i.e.* the scattering solutions of two particle problem) may yield the transport properties of the n -particle system, such as current density and charge build-up.

Two particle system in a one-dimensional space, and a single particle in a two-dimensional space are equivalent problems, with the appropriate potential energy functions. Exploiting this analogy, the method of blackbody boundary conditions permits the computation of “numerically exact” solutions of a two-particle system[†] in one-dimension in an easy way. Generalization of these two particle solutions to an n -particle system interacting via pair forces, is not straightforward and requires some further work. Accordingly, it is not included in this thesis. The last point to notice is that the *numerically exact* solutions of this two particle problem (or forms generalized to n particles) may be compared with the well-known mean field approximation results in order to understand the phenomena of bistability.

3.1.3 Model Problem

As mentioned above, it turns out that the exact solutions of a two particle problem may play an important role in the field of quantum transport. In general, a two particle system is expressed with the Hamiltonian:

$$H = -\frac{\hbar^2}{2m} \{ \nabla_1^2 + \nabla_2^2 \} + V(x_1, x_2) \quad (3.6)$$

where x_1 and x_2 are the spatial coordinates of the first and second particles respectively and V is the potential energy. The spin states of the particles will be neglected throughout the calculations.

[†]This method provides opportunity for solving the problem of n interacting particles directly, but the algorithm would be very complex.

We propose a simple model form where the potential V is expressed as:

$$\begin{aligned} V(x_1, x_2) &= V(x_1) + V(x_2) + V_{int}(x_1, x_2) \\ V(x) &= \alpha [\delta(x - a) + \delta(x + a)]. \end{aligned} \quad (3.7)$$

The external potential is a double delta function, one at $x = -a$ and the other at $x = a$. V_{int} is the interaction energy of the particles. Recalling that our aim is to propose a simple system for the observation of bistability, this term has to be expressed with special care.

Heretofore, we did not describe the occurrence of bistability. In experiments, bistability occurs in systems having strong resonant characteristics, such as a tunneling double barrier structure. In addition to that, theoretical work indicates that the charge accumulation of the resonant state blocks other states via the Coulomb interaction, and thus a bistability arises [48]. A detailed description of the event is given in the next section for the case of kink structure. Based on the above explanation, we notice that V_{int} must be chosen with the condition that the electrons would feel each other's charge accumulation between the delta function barriers. On the other hand, the interaction may vanish outside of these. For simplicity, we propose:

$$V_{int}(x_1, x_2) = \begin{cases} V_0 & -a < x_1, x_2 < a \\ 0 & \text{otherwise.} \end{cases} \quad (3.8)$$

Note that the electrons would feel a constant potential V_0 if they are between the barriers simultaneously, and no extra potential if at least one of them is outside the delta functions.

As discussed in the previous section, it is possible to treat the problem of two particles in one-dimensional space, as a problem of single particle in a two-dimensional space. It is clear that the indexes 1 and 2, in Eq. (3.6) and Eq. (3.7), may be supposed to label the coordinate axes of a two-dimensional plane, where x_n stands for the value of the particle's coordinate with respect to the axis n . It follows that the first term of the Hamiltonian in Eq. (3.6)

is the kinetic energy of a distinct particle, while the second term is the potential energy function on this two-dimensional mesh, originating only from the external field. As seen, this system of an individual electron can easily be analyzed numerically by using time-dependent Schrödinger equation, with the aid of the blackbody boundary conditions for large time scales. Finally, the wave function $\Psi(x_1, x_2)$ on the two-dimensional mesh has to be symmetrized or anti-symmetrized in order to get the solutions of two-particle problem. Recalling that the total wave function of a system of electrons must be anti-symmetric, the wave function $\Psi(x_1, x_2)$ of the two-dimensional mesh should be symmetrized (*i.e.* $\{\Psi(x_1, x_2) + \Psi(x_2, x_1)\}/\sqrt{2}$) if the electrons have the same spin, or anti-symmetrized (*i.e.* $\{\Psi(x_1, x_2) - \Psi(x_2, x_1)\}/\sqrt{2}$) if they have opposite spins.

Sample results of the simulation of this two particle problem are indicated on Figure 3.1. The external potential is taken to be a double barrier structure for which the resonant wave vector is equal to 0.628. The positions of the barriers are shown on the figure. At left, one of the particles is injected with this resonant energy and the other has the energy of the shifted resonant state due to the interaction potential. It is clear that this particle is transmitted through the barriers accumulating a large amount of charge while the other particle is reflected back. The probability of finding both particles between the barriers is also considerable. Another remarkable point on the figure is that the latter may be transmitted if the former is between the barriers. Two small peaks at the right-bottom of the mesh manifest this fact. At the right part, both particles are injected with the resonant energy of the double barrier. Having one of the particles between the barriers and the other reflected back, or both between the barrier, is highly probable. On the other hand, one of the particles may be transmitted while the other is not. Even though they have both the resonant energy, it is not possible to detect them beyond the barriers simultaneously. This system is simulated for different pairs of particles with different energies and interaction constants, starting from different initial conditions. However, a bistable nature is never detected. The system developed

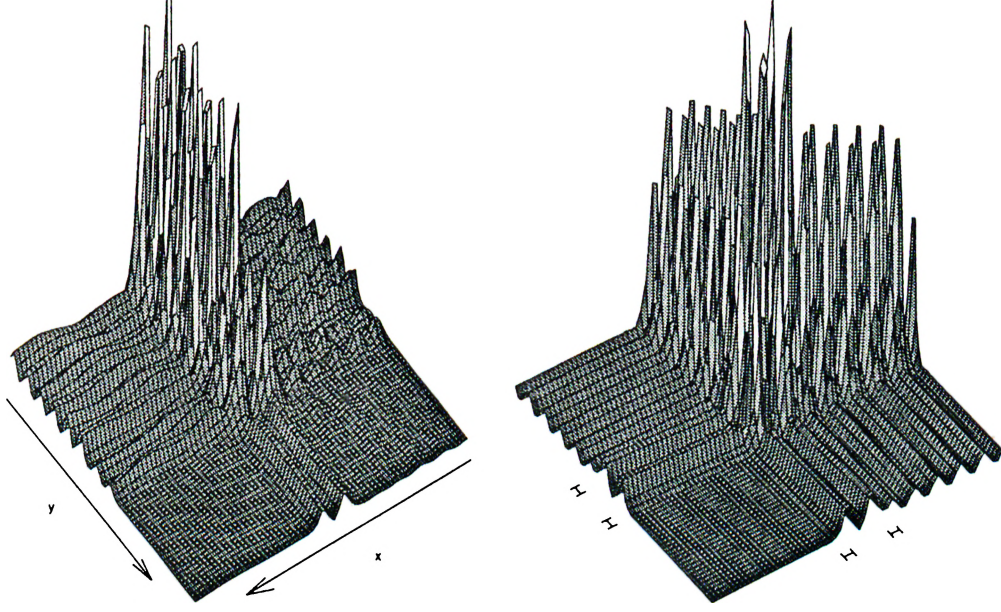


Figure 3.1: Numerically exact solution of the two particle problem.

The two particle problem is simulated on a two-dimensional mesh. The barriers have a thickness of 3 mesh points, a height of $0.6\epsilon_0$, and separated with a distance of 7 mesh points. At the left part of the figure, the particles have wave vectors 0.693 and 0.628, at right each has 0.628. The interaction constants V_0 are 0.1 and 0.06 respectively.

rapidly into unique solutions.

Finally, this subsection will be concluded by the calculation of the interaction matrix element \hat{V}_{klmn} defined in Eq. (3.4), for the case of our model Hamiltonian given in Eq. (3.6) and Eq. (3.7). Having the solution of the wave function between the barriers as $[b \exp(ikx) + c \exp(-ikx)]$, the matrix element becomes:

$$\hat{V}_{klmn} = V_0 \int_{-a}^a \int_{-a}^a dx_1 dx_2 (b_1 e^{ik_k x_1} + c_1 e^{-ik_k x_1})^* (b_2 e^{ik_l x_2} + c_2 e^{-ik_l x_2})^* (b_2 e^{ik_m x_2} + c_2 e^{-ik_m x_2}) (b_1 e^{ik_n x_1} + c_1 e^{-ik_n x_1}). \quad (3.9)$$

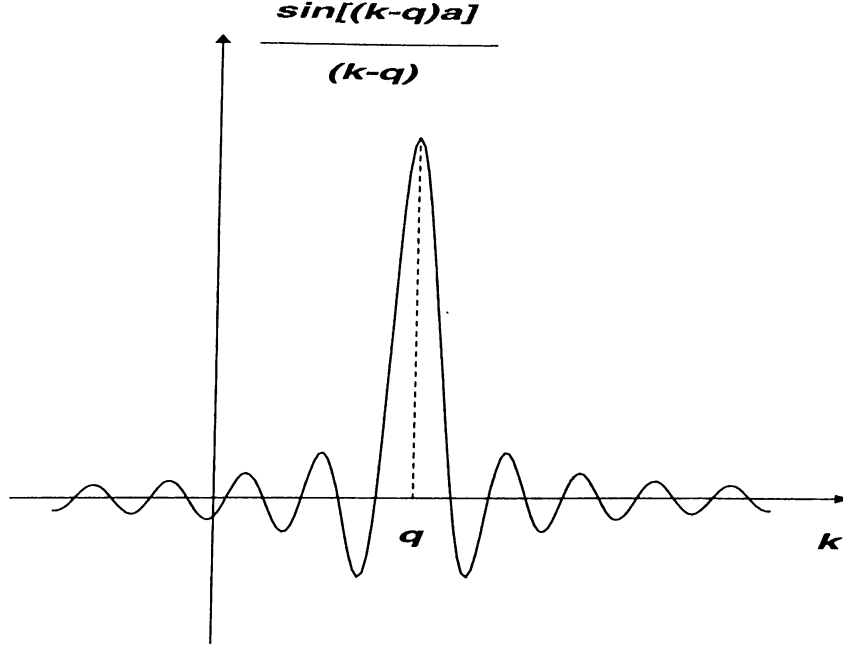


Figure 3.2: Function $\sin [(k-q)a]/(k-q)$.

The function $\sin [(k-q)a]/(k-q)$ is shown in the figure as a function of k . The function has a peak at $k = q$, which is sharper if a is bigger.

The integrals are elementary and it follows immediately:

$$\begin{aligned} \hat{V}_{klmn} = 4 V_0 & \left[\left\{ |b_1|^2 + |c_1|^2 \right\} \frac{\sin [(k_n - k_k)a]}{k_n - k_k} + \{ b_1^* c_1 + c_1^* b_1 \} \frac{\sin [(k_n + k_k)a]}{k_n + k_k} \right] \\ & \times \left[\left\{ |b_2|^2 + |c_2|^2 \right\} \frac{\sin [(k_m - k_l)a]}{k_m - k_l} + \{ b_2^* c_2 + c_2^* b_2 \} \frac{\sin [(k_m + k_l)a]}{k_m + k_l} \right]. \end{aligned} \quad (3.10)$$

Inasmuch as the most important terms in Eq. (3.10) are the sine terms, $\sin [(k-q)a]/(k-q)$ is sketched qualitatively in Figure 3.2. The peak at $k = q$ means that the matrix element is bigger if the electrons conserve their momentum after the interaction. The important point to remember here is that the total momentum of the electrons need not to be conserved. On the theoretical side, one may go through the calculation with the matrix element in Eq. (3.10), by using some approximations to it (such as the replacement of the sinusoidal terms with Gaussians or delta functions). Nevertheless, the procedure is not straightforward.

3.1.4 Hartree Approximation

In the last subsection, we described a model of a two particle problem, and tried to solve it *numerically exactly* using time-dependent Schrödinger equation. Hereafter in this subsection, we will attack the same problem by using Hartree approximation in the time-independent Schrödinger equation picture. With this approximation, the potential energy term in Eq. (3.6) decouples, and the problem reduces to a set of two equations as:

$$\begin{aligned} -\frac{\hbar^2}{2m}\nabla_1^2\Psi_1 + \left[V(x_1) + \int_{-a}^a dx_2 V_0\Psi_2^*\Psi_2 \right] \Psi_1 &= E_1\Psi_1 \\ -\frac{\hbar^2}{2m}\nabla_2^2\Psi_2 + \left[V(x_2) + \int_{-a}^a dx_1 V_0\Psi_1^*\Psi_1 \right] \Psi_2 &= E_2\Psi_2. \end{aligned} \quad (3.11)$$

The model may be further simplified in order to get rid of the integral terms. We may assume as an interaction potential

$$V_{int}(x_1, x_2) = \beta \delta(x_1) \delta(x_2) \quad (3.12)$$

which yields us in the Hartree approximation, the set of equations:

$$\begin{aligned} -\frac{\hbar^2}{2m}\nabla_1^2\Psi_1 + [V(x_1) + \beta \Psi_2^*\Psi_2|_{x_2=0}] \Psi_1 &= E_1\Psi_1 \\ -\frac{\hbar^2}{2m}\nabla_2^2\Psi_2 + [V(x_2) + \beta \Psi_1^*\Psi_1|_{x_1=0}] \Psi_2 &= E_2\Psi_2. \end{aligned} \quad (3.13)$$

The interaction term in Eq. (3.12) means that the electrons feel one another by a constant potential β while they are simultaneously at the origin, and do not feel anything otherwise. The set of nonlinear equations (3.13) may be solved self consistently using a recursive relation method. The number of stable solutions depends on the momentum of the particles, and the interaction parameter β . The Figure 3.3 shows the solution for a given momentum of the second particle and a given interaction parameter β as a function of the momentum of the first particle. It is interesting to note that the system results in more than one solution for some range of parameters. It follows that a system of n particles in the mean field approximation may yield bistability

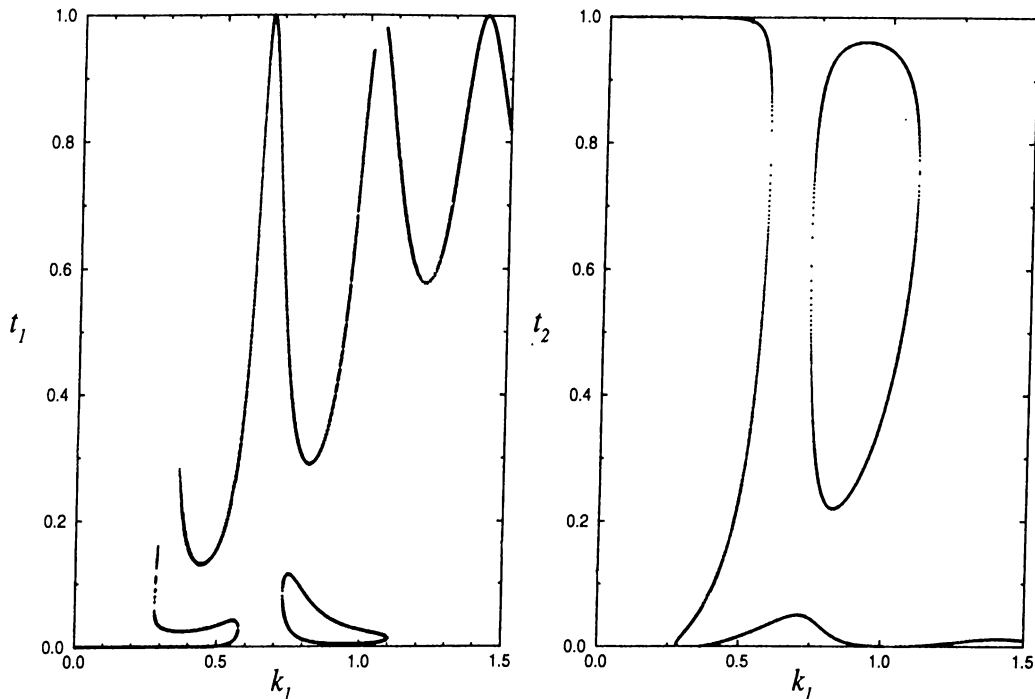


Figure 3.3: Hartree approximation to two particle problem.

The transmission probabilities t_1 and t_2 of the particles are sketched as a function of the momentum of the first particle k_1 . The second particle has a momentum of 0.321 and the interaction constant β is 1.

in the quantum transport properties. The investigation of such a phenomena using time-dependent Schrödinger equation is deferred until the next chapter.

As a final remark, note that the above problem in the Hartree approximation exhibits some chaotic behavior as a function of the interaction parameter β . Accordingly, the bifurcation in the number of solutions becomes infinite for some interaction constant bigger than a critical value. Nonetheless, this observation is not surprising for a nonlinear system and its investigation is beyond the scope of this thesis.

3.2 Kink Structure

The kink structure, or the so-called “double-bend”, is a geometry with non-linear transport properties. It has been shown [38] that it exhibits negative differential resistance at low voltages and has bistability as well, which may survive to room temperature for sufficiently small feature sizes. As described below, a broad wavelength selection process in electron transport through the geometry causes a “window” in the energy of electrons, which in turn gives rise to the negative differential resistance. Due to the absence of the effects of a sharp resonance in this process, one expects that this geometry has much smaller charging effects and response time, with respect to the systems showing “cavity” type resonances. Recently, the geometry is produced experimentally and a negative differential resistance is observed in the current-voltage characteristics [49]. Here, the structure will be presented first, followed by a time-dependent analysis of the geometry. Thereinafter, the process of installing a self consistent potential is discussed.

3.2.1 The Structure

The potential profile of the kink structure was given earlier in Figure 2.6, superimposed on the wave function progressing through the kink. It is simply a deformation of a straight, narrow electron path as shown in Figure 3.4.

In order to understand the transmission process of electrons through the kink structure, one may conjecture the following one-dimensional model: From the view point of the cross section in the y direction, the electrons injected from one of the reservoirs are initially in one of the energy levels of the quantum wire. When the electrons reach the cavity part of the geometry, the event, from the view point of the same cross section, is a “sudden” doubling of the distance between the walls of the quantum well. As elementary quantum mechanics dictates, the behavior of an eigenfunction of a quantum well, under a *sudden*

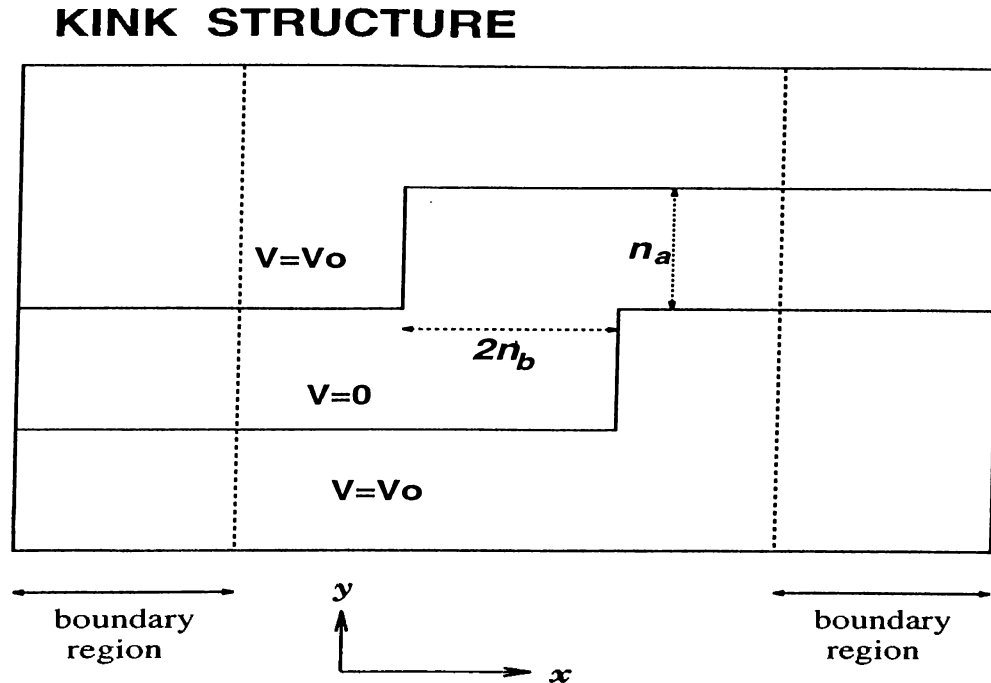


Figure 3.4: Kink structure potential profile

The qualitative shape of the potential profile of the kink structure is shown with different important parameters. V_0 is the potential of the “walls” of the channels, n_a is the width of the quantum wells and $2n_b$ is the extent of the cavity region of the structure. The quantum wells may also be shifted laterally in opposite directions in order to enlarge the cavity.

doubling of the well separation, is to move between the walls repeatedly. As a result, the electrons are expected to shift laterally during their longitudinal motion through the central part of the kink structure. Finally, the distance between the walls may be thought as halved when the electrons are at the other end of the cavity. According to this simple explanation, the transmission coefficients of the electrons depend on the percentage of their wave functions which enter other quantum wire at the halvening of the well.

The situation is illustrated schematically in Figure 3.5. The shift of an electron wave function in the y direction depends on the amount of time it traverses the cavity, which is, in turn, related to the momentum of the electron. In parts (a) and (b), the momentum of the electron is so low that it *bounces* from

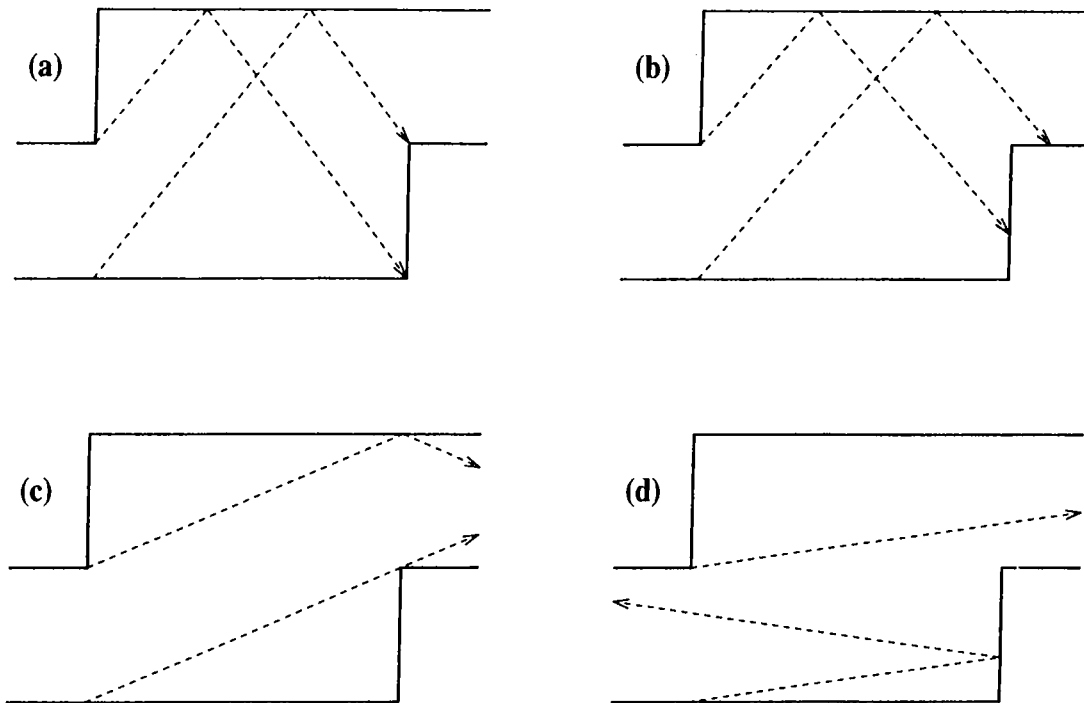


Figure 3.5: Model for electron transmission through the kink structure. For small kinetic energies, the behavior of an electronic wave function injected to a kink structure may be thought of as a wave shifting laterally while traversing the geometry. (a) The particle is reflected back. (b) The particle is partially transmitted. (c) The particle is injected with the “proper” wavelength, and transmitted with a unit probability. (d) At some larger energy, the particle hits the opposite wall and is partially transmitted.

the side walls of the cavity and does not carry an appreciable amount of current. At some larger energies, the time spent by the electron in traversing the cavity may be equal to the amount of time required for the wave function to shift into the other quantum wire. This means that the transmission probability for electrons injected with that “proper” (or “correct”) momentum is very high. This case is shown in part (c) of Figure 3.5. However, an electron with a momentum larger than this amount will be reflected back from the opposite wall due to the insufficient amount of time it spends in the kink region for shifting to the other quantum wire. This case, as shown in part (d), will yield a smaller transmission probability. It may be concluded that, this “window” of energies for the transport may result in a negative differential resistance in

the current-voltage characteristics of the structure.

Of course, the situation is much more complicated in a real kink structure. The simplified picture discussed above does not hold for electrons having higher energies. These exhibit sharper resonances in the same characteristics as the Fano resonances. These resonant wave functions loosely couple to the incoming and outgoing electron waves, and manifest cavity type oscillations. It is known that, the amount of time required for such a resonance to build up is large compared to the traversal time. Hence, a considerable amount of charge may be accumulated by those resonant states. Therewith, a self consistent treatment of the transport phenomena would end up with a bistability in the current-voltage characteristics.

For the simulation of the structure, it will be assumed that the electrons are sufficiently confined to the plane of the Figure 3.4 so that quantized energy levels in the z direction are well separated in energy. Hereby, the expected form of solution near the absorbing boundary, mentioned in Eq. (2.22), reduces to:

$$\phi(l_x, l_y) = A u(l_y) \exp(iql_x) + \frac{1}{\sqrt{2n}} \sum_{k=-n+1}^0 c_k(l_y) \exp\left(i\frac{2\pi}{2n}kl_x\right) \quad (3.14)$$

where $u(l_y)$ is the eigenstate of the injected particle in the quantum wire (or *channel*) with the integers l_x and l_y labeling the position coordinates on the two-dimensional mesh. The expansion coefficients $c_k(l_y)$ corresponding to blackbody boundary conditions may be determined for fixed l_y as explained in Chapter 2.

3.2.2 Negative Differential Resistance

The characteristics of the kink structure depends considerably on the parameters of the geometry. Based on the one-dimensional model of the previous section, one may deduce that among these the ratio b/a is the most crucial one. It mainly determines the place and the width of the window

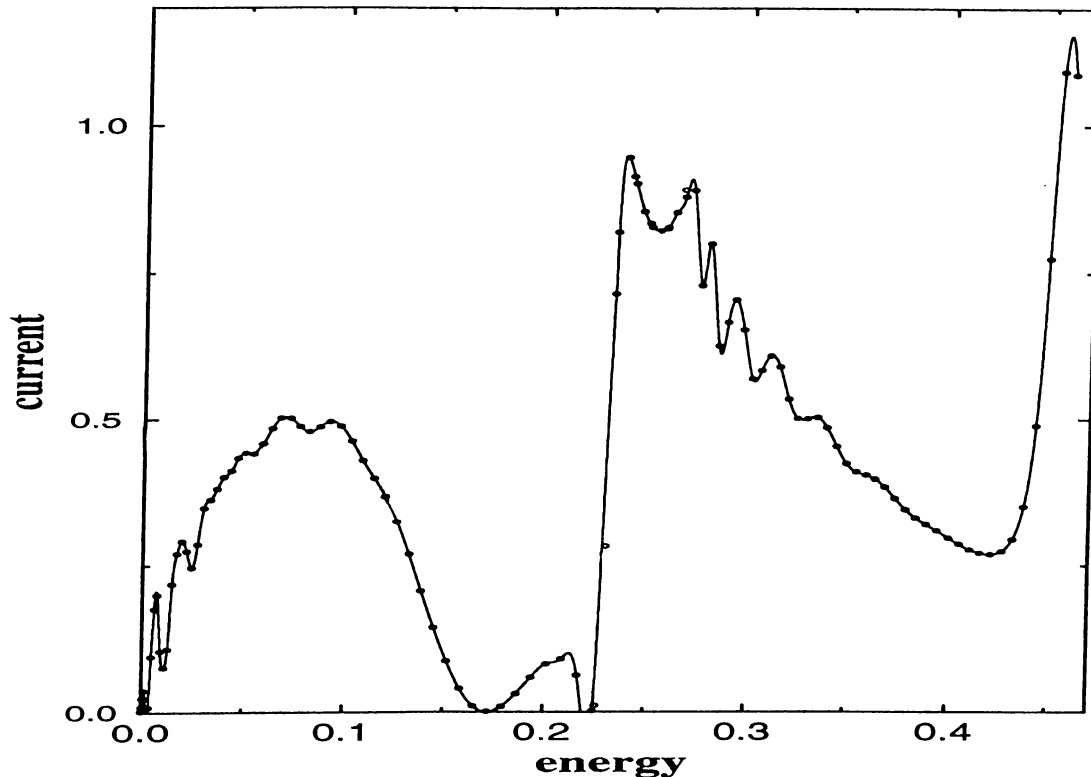


Figure 3.6: Current through the kink structure as a function of energy. The current transmitted through the kink structure is shown as a function of energy of injected particles. The ratio b/a is 0.5. The system is simulated for different injected wave vectors indicated by small circles. The curve is a spline fitted to these points.

in the momentum. Figure 3.6 indicates the current transmitted through the structure as a function of energy of incident electrons in the y direction in the absence of any potential difference. Note that electrons are injected only in the first subband of the quantum wire and transmitted to the other channel in any mode. The curve is obtained via a time-dependent simulation and qualitatively consistent with time-independent solutions [38]. For energies near 0.2 the transmission probability is very low and even vanishes. This is the *window* in the energy which will give rise to the negative differential resistance. On the other hand, the peaks at the right of the *window* corresponds to Fano type resonances as discussed earlier.

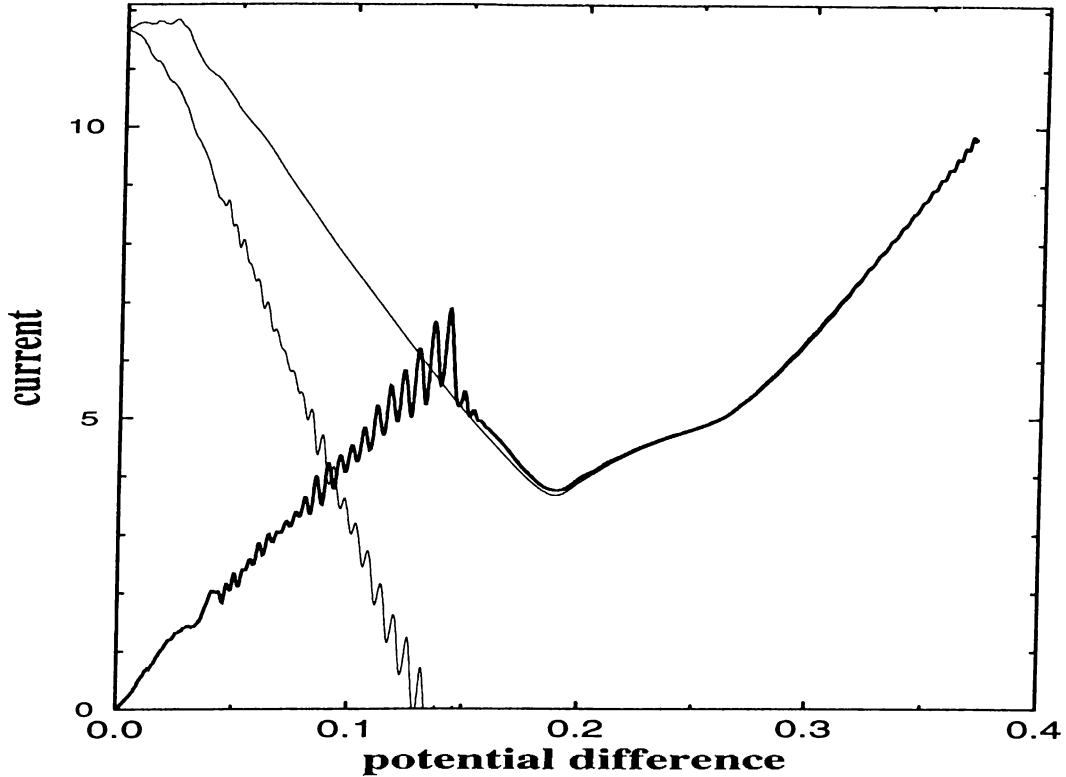


Figure 3.7: $I - V$ characteristics of the kink structure

Current-voltage characteristics of the kink structure is indicated with the thick curve. The currents transmitted by the particles of each reservoirs are shown with two thin curves.

The time-dependent simulation of the kink structure in the presence of an adiabatic potential difference is shown in Figure 3.7. The negative differential resistance region is apparent on the figure. The width of this region and the valley-peak ratio of the current may be tuned by changing the ratio b/a . In the simulation, 40 electrons at each reservoir are taken into account. This number is large enough for describing the quantum transport properties of such a system smoothly. The Fermi energy is 0.225 times the energy scale ϵ_0 , and this corresponds to approximately $0.128eV$. With this energy, the electrons can only occupy the first subband of the channel which has the energy level at $0.093\epsilon_0$. Hence, the kinetic energy in the direction of propagation has a maximum value of $0.225 - 0.093 = 0.132\epsilon_0$ for the electrons at the constant

potential of the contacts [†]. It is concluded that the current carried by the particles of the reservoir at lower potential must vanish at that energy. The figure is consistent with this prediction. On the other hand, the oscillations in the current are remarkable. Namely, these are due to the reflection of the electrons of the reservoir at lower potential from the potential ramp. The effect resembles to the water waves hitting a beach. It turns out that the time-dependent increase of the slope of the ramp stimulate these oscillations.

3.2.3 Self Consistent Potential

In the previous subsection, we have dealt with particles of different wave vectors separately. We have then determined the transport properties of the geometry from a superposition of these single particle solutions, weighed by the magnitudes calculated from the thermal properties of the reservoirs. For a more realistic simulation, one has to take into account relevant interactions among particles.

For structures which exhibit charging effects, the electron-electron interaction is certainly the most important interaction. On the other hand, Fano type resonances encountered at the cavity of the kink structure, may also build up a considerable amount of charge in this region. This charge build-up will effect the electron-electron interaction significantly if the cavity dimensions are sufficiently small. While electrons with high energies are trapped at this part of the geometry, electrons with low energies may not be transmitted because of the Coulomb interaction. We expect in this case a much lower current passing through the geometry compared to the case of non-interacting electrons. Given some larger potential difference between the reservoirs, the electrons accelerated through the potential ramp may kick the electrons in the resonant state out of the central region, causing an abrupt drop in the current. Albeit the same phenomena is observed in most of the resonant tunneling

[†]This energy correspond to a Fermi wavelength of 17.2 mesh units.

structures, one should expect smaller time scales for the current drop in the kink structure due to the absence of tunneling. Note that, decreasing potential difference may yield a bistability effect in the current which is an important characteristics in terms of technological applications.

One has different approaches available for the simulation of the electron-electron interaction. One of these is to assume a smooth potential profile across the channel. Expectation of low particle densities for an electron in the resonant state at the corners of the geometry may support this assumption. Therefore, a constant potential plateau may be added to the external potential of the structure as the interaction potential. Note that, the height of the plateau must be proportional to the total charge accumulated at the cavity part of the kink in order to yield a bistability in the current. This simplified model has the advantage that it does not introduce any complicated potentials to the boundary region.

On the other hand, a better and more sophisticated approximation to the problem of electron-electron interaction is to solve the Poisson equation numerically and to superimpose the potential calculated to the potential of the geometry. This process has not to be done at each time step, because the self consistent field of a group of electrons varies slowly in time compared to the motion of the electrons. The Poisson equation may be solved by taking into account the thickness of the two-dimensional electron gas, but it is more convenient to deal with the electron gas confined to an infinitesimally thin surface. With this assumption, Poisson equation can be written as:

$$\nabla^2 V(x, y, z) = - \frac{\rho(x, y, z)}{\epsilon} = - \frac{\sigma(x, y)\delta(z)}{\epsilon} \quad (3.15)$$

where V is the electric potential in three-dimensional space due to the electrons confined in the x - y plane with surface charge density σ , and ϵ is the permittivity constant of the medium. We may expand the potential in our quasi-discrete

space as:

$$V(x, y, z) = \frac{1}{\sqrt{2\pi N_x N_y}} \sum_{k_x=1}^{N_x} \sum_{k_y=1}^{N_y} \int_{-\infty}^{+\infty} dk_z \tilde{V}(k_x, k_y, k_z) \exp\left(i\frac{2\pi}{N_x}k_x x\right) \exp\left(i\frac{2\pi}{N_y}k_y y\right) \exp(ik_z z) \quad (3.16)$$

where \tilde{V} is the Fourier transform of the potential V , N_x and N_y are the dimensions of our simulation region in the x and y directions respectively. If we operate on this expression by the Laplacian ∇^2 we get:

$$\nabla^2 V(x, y, z) = \frac{1}{\sqrt{2\pi N_x N_y}} \sum_{k_x=1}^{N_x} \sum_{k_y=1}^{N_y} \int_{-\infty}^{+\infty} dk_z \tilde{V}(k_x, k_y, k_z) \exp\left(i\frac{2\pi}{N_x}k_x x\right) \exp\left(i\frac{2\pi}{N_y}k_y y\right) \exp(ik_z z) \left[-\frac{4}{(\Delta x)^2} \sin^2\left(\frac{\pi k_x}{N_x}\right) - \frac{4}{(\Delta y)^2} \sin^2\left(\frac{\pi k_y}{N_y}\right) - k_z^2 \right]. \quad (3.17)$$

Expanding the surface charge density σ in terms of its Fourier transform $\tilde{\sigma}$, and denoting the delta function in its integral representation, we have the equality in Eq. (3.15) restated as:

$$\tilde{V}(k_x, k_y, k_z) = \frac{\tilde{\sigma}(k_x, k_y)}{\sqrt{2\pi} \epsilon \left[\frac{4}{(\Delta x)^2} \left\{ \sin^2\left(\frac{\pi k_x}{N_x}\right) + \sin^2\left(\frac{\pi k_y}{N_y}\right) \right\} + k_z^2 \right]}. \quad (3.18)$$

Next, we have to substitute this expression in Eq. (3.16). We may now evaluate the k_z integral and look at its limit as z tends to zero:

$$\lim_{z \rightarrow 0} \int_{-\infty}^{+\infty} \frac{dk_z \exp(ik_z z)}{\left[\frac{4}{(\Delta x)^2} \left\{ \sin^2\left(\frac{\pi k_x}{N_x}\right) + \sin^2\left(\frac{\pi k_y}{N_y}\right) \right\} + k_z^2 \right]} = \frac{(\Delta x) \pi}{2 \sqrt{\sin^2\left(\frac{\pi k_x}{N_x}\right) + \sin^2\left(\frac{\pi k_y}{N_y}\right)}}. \quad (3.19)$$

Finally, electrostatic potential energy on the $x-y$ plane is given by:

$$V(x, y, z=0) = \frac{\Delta x}{4\epsilon \sqrt{N_x N_y}} \sum_{k_x=1}^{N_x} \sum_{k_y=1}^{N_y} \frac{\tilde{\sigma}(k_x, k_y)}{\sqrt{\sin^2\left(\frac{\pi k_x}{N_x}\right) + \sin^2\left(\frac{\pi k_y}{N_y}\right)}} \exp\left(i\frac{2\pi}{N_x}k_x x\right) \exp\left(i\frac{2\pi}{N_y}k_y y\right) \quad (3.20)$$

Thus, the calculation of the potential reduces just to the evaluation of the discrete Fourier transform of the charge density, multiplication by a diagonal term, and a Fourier transformation back to the position space. The availability of fast Fourier transform algorithms makes this process feasible, even once each time step. In the simulation, it must be remembered that an electron feels the potential generated by other electrons, and not by itself, especially in the simulation of resonant structures. It is recommended to compute the potential that every electron sees separately by taking charge contributions of other electrons only, as the charge density σ .

Another remarkable point about the calculation of the electrostatic potential is the choice of boundary conditions. For the kink structure discussed above, it is clear that anti-symmetric boundary conditions are more realistic at the y boundaries. This anti-symmetrization will result in zero potential along these boundaries. In the x direction, the dimension of our simulation region is very small so that taking anti-symmetric or periodic boundary conditions would result a higher potential than expected. Since for this case, our computation will contain the potential of other nearby kink structures. One can overcome this problem, by extending the charge density discretization in the x direction (say from 32 to 127) with the assumption that there is no charge in this newly added region. Again anti-symmetric boundary conditions can be preferred for having zero slope in potential at the boundary.

A typical self consistent potential profile is shown in Figure 3.8 together with the charge accumulated. The method of absorbing and injecting boundary conditions described in Chapter 2 assumes that we have a constant potential at the boundary that may absorb or inject particles. So at the boundary region, the potential must be constant in the x direction. To fulfill this condition, some kind of averaging must be done in this region. Here, we preferred to average the potential in all the boundary region and set it to a constant. Then, the transition from the average potential to the exact one must be carefully smoothed out.

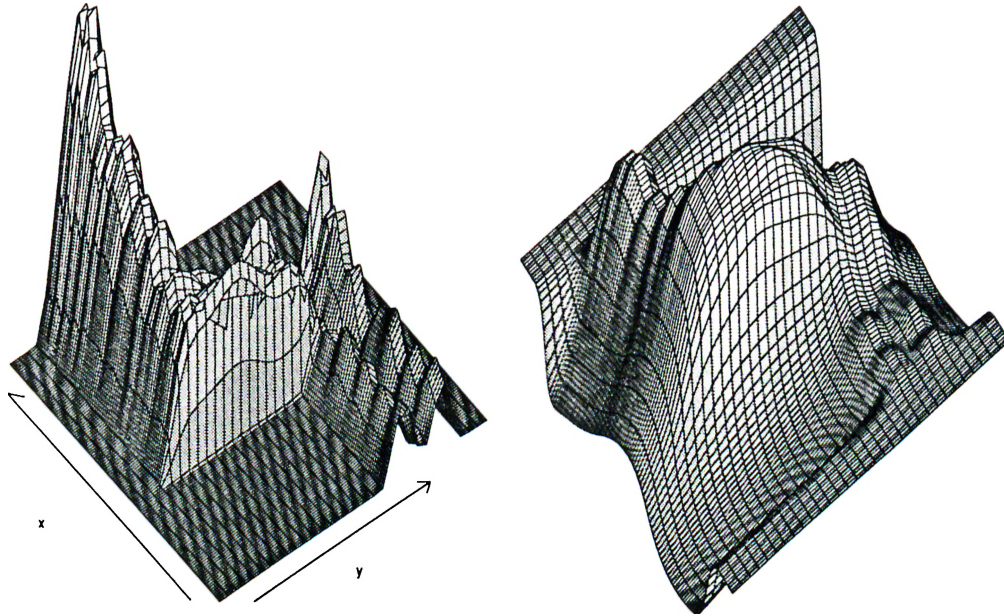


Figure 3.8: Self consistent potential for the kink structure

The total charge and the self consistent potential it generates are shown in a simulation. In comparison to Figure 3.4, the channels are shifted laterally here, in order to enlarge the cavity region of the structure, and thus accumulate more charge.

Examination of the effects of the Coulomb interaction on the transport properties of the kink structure would be interesting work. For this purpose, we have developed the computer code which have passed all the test runs successfully. Unfortunately, we realized that obtaining a current-voltage characteristics will last very long time with the available computational resources. On the other hand, we were interested in the study of bistability instead of the detailed current-voltage characteristics which may more easily be obtained by solving the time-independent Schrödinger equation. Even though the method of blackbody boundary conditions makes possible the simulation of a two-dimensional system on a simple workstation instead of a supercomputer, the examination of the mechanism underlying the bistability requires more powerful hardware than a workstation. Besides, the problem of bistability in a time-dependent context is a recent and complicated subject. The examination

of the problem in a simple one-dimensional model structure, instead of a complex two-dimensional one, will be more effective for the understanding of the phenomena. This work is presented in the next chapter.

Chapter 4

1-D APPLICATIONS AND BISTABILITY

One of the most interesting, while simple one-dimensional quantum system is the double barrier structure. It not only has many applications as an electronic device, but retains the interest of the scientific community as well [50,34,51–54]. In the first section, a model for this physical geometry is proposed, followed by the mean field approximation results of the quantum transport through the model device. In a logical order, this chapter should precede Chapter 3 which concerns two-dimensional applications, but it deserves to be the last chapter before the conclusion, because of the interesting time-dependent properties of bistability –investigated in the third section. It may also be recalled that results related to higher dimensional structures may be obtained from a one-dimensional analysis, by weighing the wave function amplitudes by appropriate density of states. Finally, the chapter will be concluded with that topic.

4.1 The Model

The potential energy function of a double barrier structure is given by

$$V(x) = \begin{cases} V_h & a < |x| < a + b \\ 0 & \text{otherwise.} \end{cases} \quad (4.1)$$

Here b and V_h are the thickness and height of the barriers respectively, and $2a$ is the distance between the barriers. Apart from this external potential function, a particle should feel the potential generated by the other particles. Hereafter, this interaction potential will be treated in the mean field approximation context and will only be limited to the space between the barriers. This assumption does not contradict the actual physical situation, inasmuch as the screening effects prevent the electrons from strongly feeling others' potential. On the other hand, if the distance between the barriers is very small, the screening effects in this region would be negligible and a strong confinement of electronic charge at the resonant state will increase the potential an appreciable amount. Let us consider an interaction potential

$$V_k(x) = \begin{cases} \beta \sum_{s \neq k} \int_{-a}^a dx' |\Psi_s(x')|^2 & -a < x < a \\ 0 & \text{otherwise.} \end{cases} \quad (4.2)$$

where V_k is the interaction potential perceived by the k 'th particle, and β is an arbitrary interaction constant. The charge accumulation is integrated between the barriers, and summed over all states except the k 'th state. Hence, an electron would not feel its own potential.

Notwithstanding the simplicity of a double barrier structure, one may encounter some numerical problems in the modeling of the system. An intuitive model, in the presence of a potential difference ΔV between the reservoirs, is sketched qualitatively in Figure 4.1-(a). First, note that the discontinuities of the potential energy at the ends of the potential ramps must be avoided. These

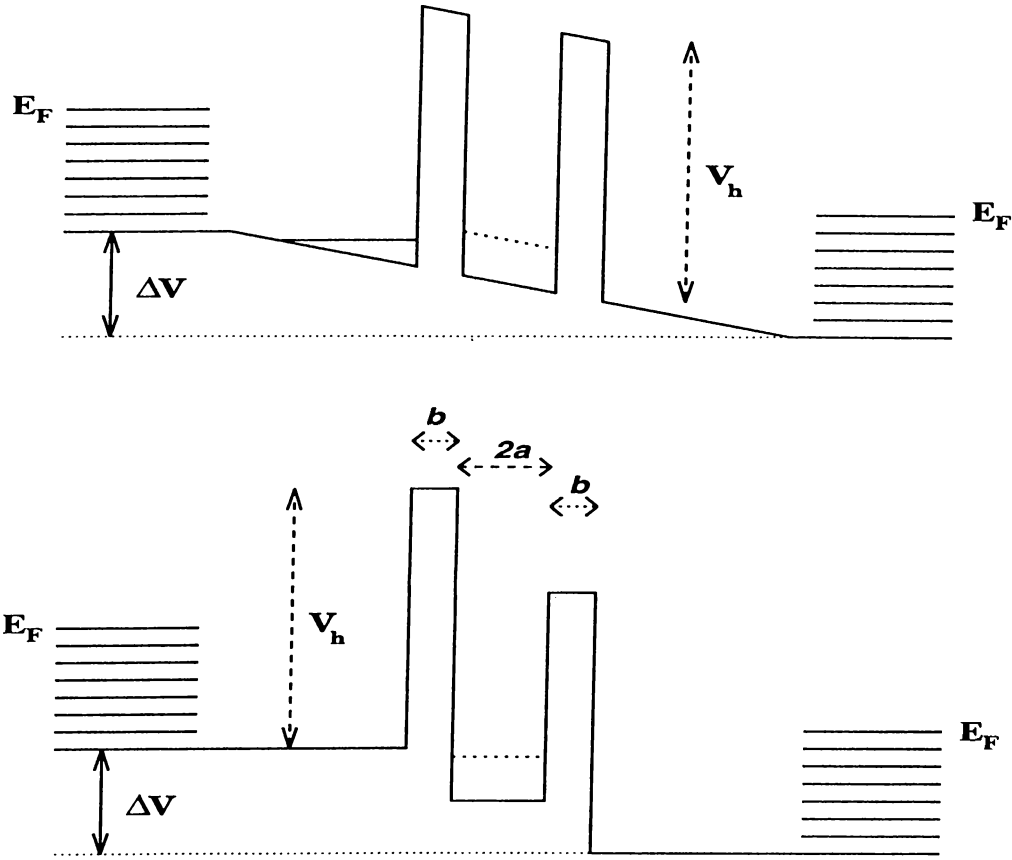


Figure 4.1: Models of a resonant tunneling diode.

(a) The conventional model for a resonant double barrier structure. The energy state at the left hand side of the barrier at higher potential is indicated by a horizontal line. (b) The model used throughout in this work. Note that there is no resonant energy state outside the barriers. Dashed lines show the interaction potential due to the charge accumulation for both models.

“corners” may produce some unphysical wave vectors in the Fourier space, and as a result disturb the simulation. However, they can be easily smoothed out.

In addition to this, the model exhibits resonant states which accumulate charge not only between the barriers but also outside. Namely, there exist some unphysical quasi-bound states of the system, near the higher potential side of the barriers. The charge build-up associated with these unphysical states seems to be more critical for the electrons which try to go up to the potential ramp, as a result of the fact that each electron may come in resonance with

that energy level while the potential difference across the geometry is increased adiabatically. The time-independent solutions of the Schrödinger equation also runs into similar problems for this model. Nonetheless, in an actual resonant tunneling device, the derivative of the potential ramp with respect to distance is much smaller than the one in our simulation mesh. This implies that, only very long wavelengths may form such a resonant state outside the barriers. On the other hand, the resonance of such long wavelengths is prohibited by phase breaking mechanisms.

In order to overcome the difficulties discussed above, we propose the model sketched in Figure 4.1-(b). It is clear that there will be no resonant states outside the barriers for this model. Except the barriers, no discontinuity occurs in the potential energy function neither unphysical wave vectors. Still, the interaction potential on the k 'th particle is calculated similarly, as expressed in Eq. (4.2).

Another important point in the simulation is the dimensions of the structure. The higher and thicker the barriers are, the sharper is the resonance. Obviously one requires a relatively sharp resonance to observe bistability. Accordingly, we will show later that a very smooth resonance does not exhibit a considerable bistability region. On the other hand, to calculate a physical property of the structure, one has to sum over the effects of electrons with different wave vectors. Because of this, the number of wave vectors required for the simulation increases as the width of the resonance peaks decreases. This unfavorable situation is accompanied by the large time scales of resonance formation which imply long computation times. Consequently, one has to fine tune the width of the resonance by adjusting these parameters.

Our aim is to observe the passage of the particles from the resonant state[†], while a potential difference is applied adiabatically. A particle moving from the reservoir at higher potential to the one at lower potential is accelerated due to the electric field generated by the potential ramp. As a result, its velocity (*i.e.*

[†]For simplicity, one had better chose the first resonant state for this investigation.

Parameter	Value	Unit
Length of the simulation region	127	mesh point
Extent of the boundary region (n)	8	mesh point
Width of the barriers (b)	1	mesh point
Distance between the barriers ($2a$)	5	mesh point
Mesh size (Δx)	10^{-9}	m.
Time step ($\Delta \tau$)	0.05	$\hbar/\epsilon_0 \approx 1.157$ fs.
Fermi energy of the contacts (E_F)	0.14	$\epsilon_0 \approx 0.57$ eV.

Table 4.1: Parameters used in the simulation of the double barrier structure.

its wave vector) is increased. In other words, when it encounters the barriers, its wavelength decreases. This requires that our Fermi wavelength to be close to the wavelength of the resonant state[†]. According to quantum mechanics, the wavelength of the resonant state is determined mainly by the distance between the barriers[‡]. On the other hand, as pointed out in Section 2.1.2, the method of absorbing and injecting boundary conditions favors small wavelengths for simulation, and this determines a maximum for the Fermi wavelength. In summary, one is constrained to have a small distance between the barriers in order to have reliable computation. Unfortunately, a resonant state wave function needs more than a certain number of points to be represented smoothly between the barriers, and that favors large distances between the barriers. The choice of this dimension is therefore strictly restricted between the limits of these two conflicting arguments.

The dimensions of the structure chosen to comply with the computational limitations are given in Table 4.1, alongwith other important parameters. The same parameters are used in all of the computations in the remainder of this chapter. For convenience, the height of the barriers is chosen to be a

[†]Otherwise the particle having Fermi energy is never in the resonant state during the simulation.

[‡]Recall that for a quantum well structure with infinitely high walls, the wavelength of the first energy level is twice larger than the well width. As the height or the thickness of the walls decreases, this wavelength shifts to higher values due to the tunneling phenomena.

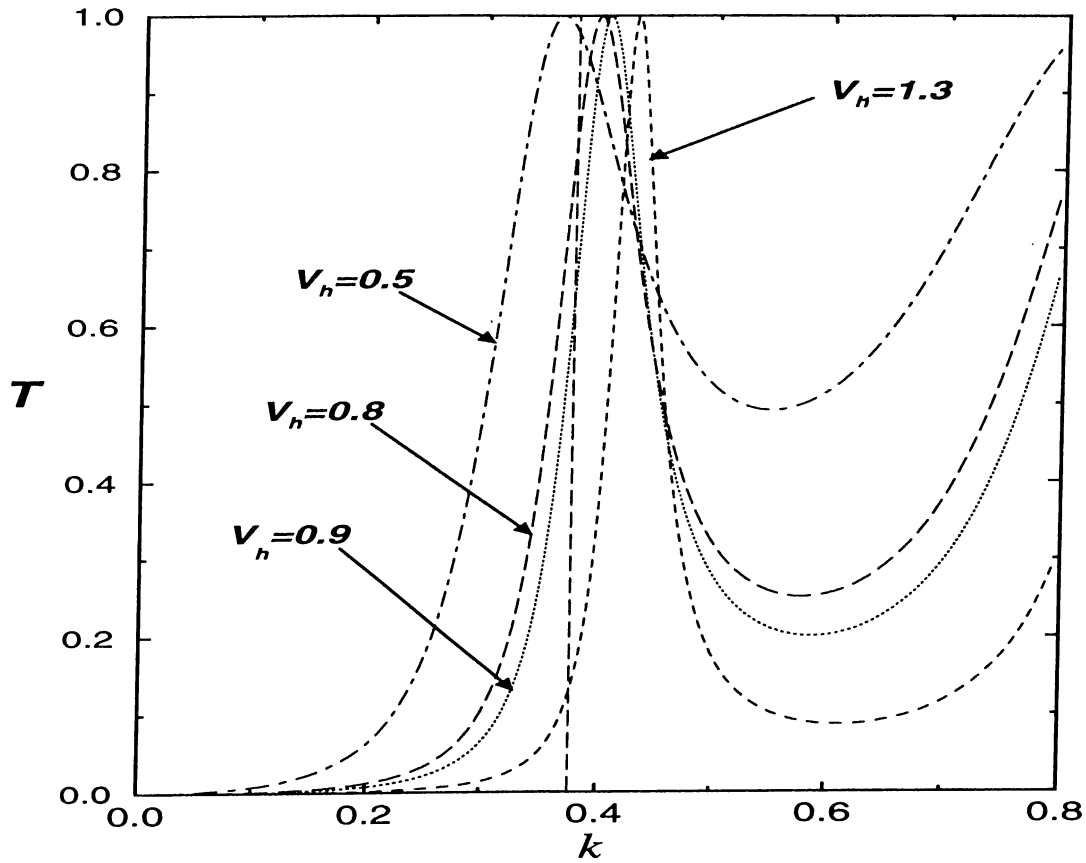


Figure 4.2: Transmission coefficients as a function of wave vector. Transmissions coefficients T through a double barrier structure is sketched as a function of wave vector k for different barrier heights V_h . The other dimension of the geometry are as in Table 4.1. The Fermi wave vector is indicated by a vertical dashed line. This graph was obtained by solving time-independent Schrödinger equation.

variable in order to change the resonance width of the structure. For the sake of completeness, transmission coefficients of particles as a function of their injected wave vectors k are shown in Figure 4.2 for different barrier heights. These values of heights will be used in the following sections.

Set #	Barrier height (V_h)	Interaction constant (β)	Number of particles
1	0.5	0.002	40
2	0.8	0.002	40
3	0.9	0	40
4	0.9	0.0002	40
5	0.9	0.0009	40
6	0.9	0.002	40
7	0.9	0.004	40
8	0.9	0.004	80
9	0.9	0.002	60
10	1.3	0.002	40

Table 4.2: Sets of parameters for the simulation of the double barrier.

4.2 Results

The double barrier structure is simulated for different sets of parameters in order to obtain its transport properties. In those sets, we changed the height of the barrier V_h , the total number of particles in the reservoirs[†] and the interaction constant β . The sets are given in Table 4.2. Our main goal is to observe the bistability for a double barrier structure, examine the characteristics of it for different parameters, and explain how it develops if possible.

One of the most important characteristics of a device is certainly its current-voltage characteristics corresponding to electronic transport. In our simulation, we firstly let the system reach its equilibrium state in the absence of any potential difference between the contacts. After that, the current transmitted through the structure is calculated while changing the potential difference between contacts very slowly, *i.e.* adiabatically. This time-dependent potential difference, in units of the energy scale ϵ_0 introduced in Chapter 2, is chosen to

[†]Note that, the number of particles in one of the reservoirs is half of this number.

be

$$\Delta V(\tau') - \Delta V(\tau) = 3.5 \times 10^{-5} (\tau' - \tau), \quad (4.3)$$

and its adiabaticity is checked against time-independent solutions in the absence of the interaction potential. Here, τ denotes the time, scaled by \hbar/ϵ_0 . Finally, reaching some large potential difference, we started to decrease the potential at the same rate in order to observe a bistability.

Figure 4.3 shows the current-voltage characteristics of the model double barrier structure for the parameter set numbers 3 to 8. The main difference among these sets is the interaction parameter. As expected, a bistability region for the current appears with increasing interaction parameter β . It is seen that the maximum current transmitted through the structure is approximately same for all sets, but it shifts to higher potential differences with increasing β . This result is not surprising, since a high potential difference is needed for particles to go over the interaction potential which is higher for large β . Note that, in spite of the fact that the same current is transmitted for different β , the charge accumulation between the barriers is appreciably smaller for large β as seen in Figure 4.4. Again, the main difference among these sets is the interaction parameter. Note that, at zero potential difference between the contacts, the charge accumulation between the barriers is lower for a higher interaction constant, as expected. Another remark about the current-voltage characteristics is that, for different values of the interaction constant, approximately the same current is transmitted through the structure at large potential differences. Note that at this region, the charge accumulation also is independent of β as apparently manifested in Figure 4.4.

It was intended to superimpose on Figure 4.3, current-voltage characteristics obtained by solving the time-independent Schrödinger equation for the same dimensions, with account taken of the 40 particles. Nevertheless, the difference between this curve and the curve of set #3 is invisible in the scale of the figure. It turns out that the time dependence of the potential difference is sufficiently adiabatic for these sets of parameters. In relation to this observation, it is

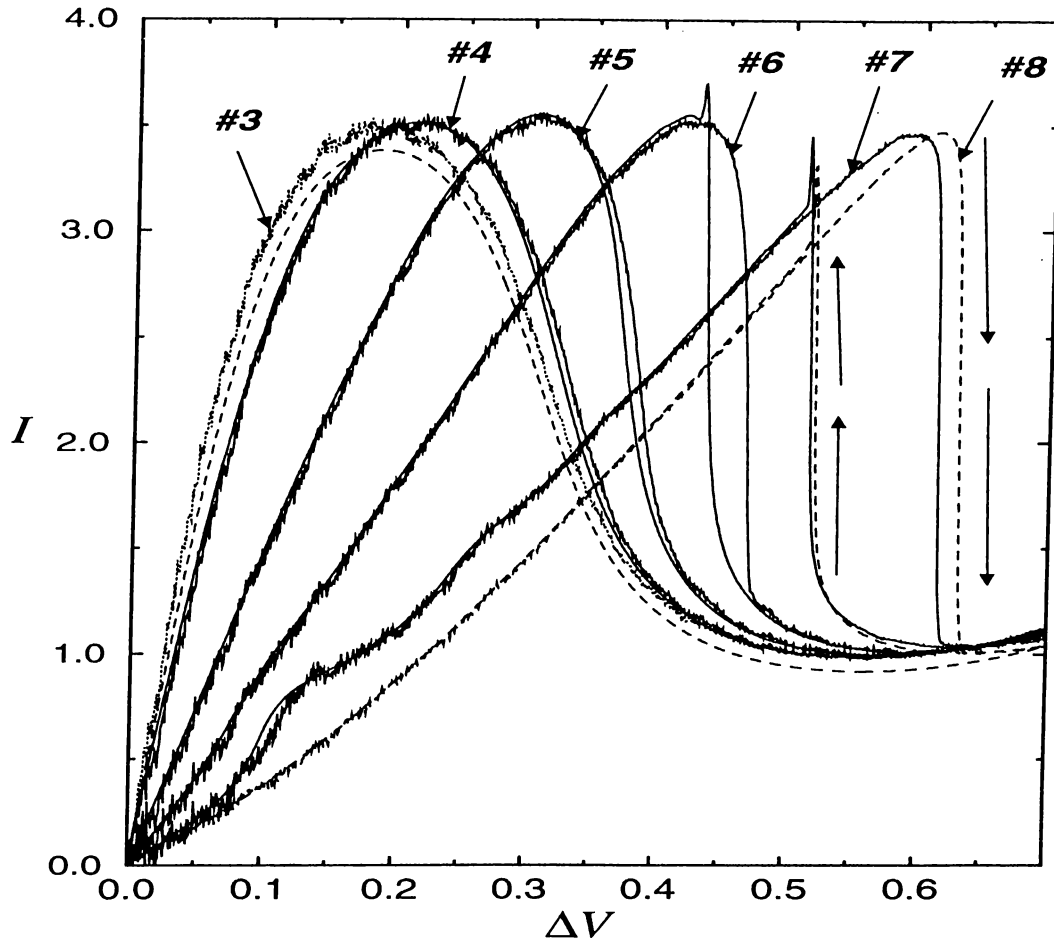


Figure 4.3: $I - V$ characteristics of a double barrier for different β .

The current-voltage characteristics of the double barrier structure is shown for parameter sets 3-8. With a total of 400 particles, the time-independent solutions for the same barrier dimensions, in the absence of the interaction, yielded the dashed curve under the curve of set #3. The direction of the hysteresis in current is shown by the arrows for the set #8. The same directions hold also for other sets.

important to notice that the method of absorbing and injecting boundary conditions operates very well in these simulations.

Another remark about Figure 4.3 is that the transmitted current is slightly overestimated due to a finite number of particles in the computations. Notice that, the time-independent current-voltage characteristics obtained using 400 particles without interaction is very close to set #3. In the presence of the

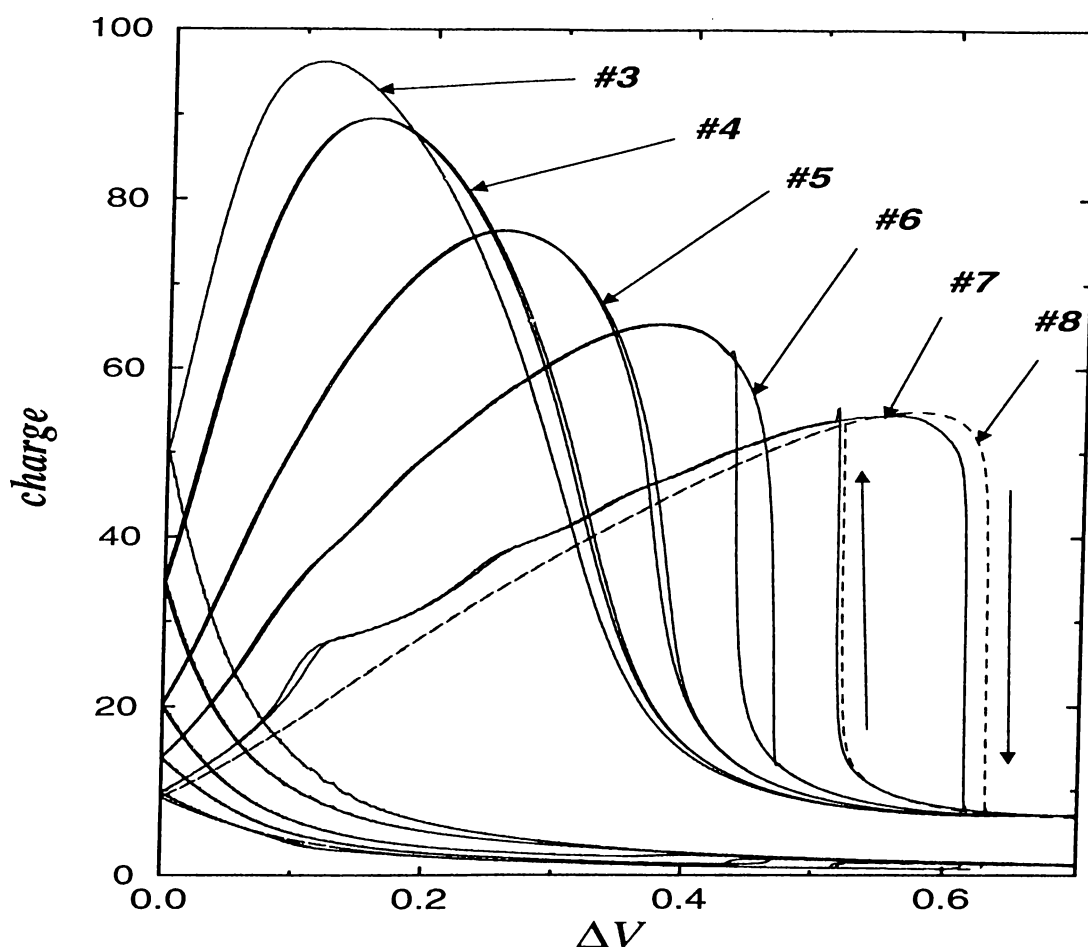


Figure 4.4: Charge build-up between the barriers for different β . The charge accumulation between the barriers is shown for set of parameters 3-8. The charges accumulated by the particles of different reservoirs are shown separately for all sets. As expected, they are equal for a zero potential difference. The arrows indicates the direction of the hysteresis in current for the #8. The same directions are also valid for other sets.

interaction potential, a simulation with a large number of particles seems to exhibit a larger bistability region slightly shifted to higher potential differences. This may be seen by comparing the results for sets #7 and #8.

The current-voltage characteristics of the model double barrier structure is indicated in Figure 4.5 for various barrier heights, with the superposition of the time-independent characteristics obtained for noninteracting particles. Note that the dashed curves are the solutions of the time-independent Schrödinger

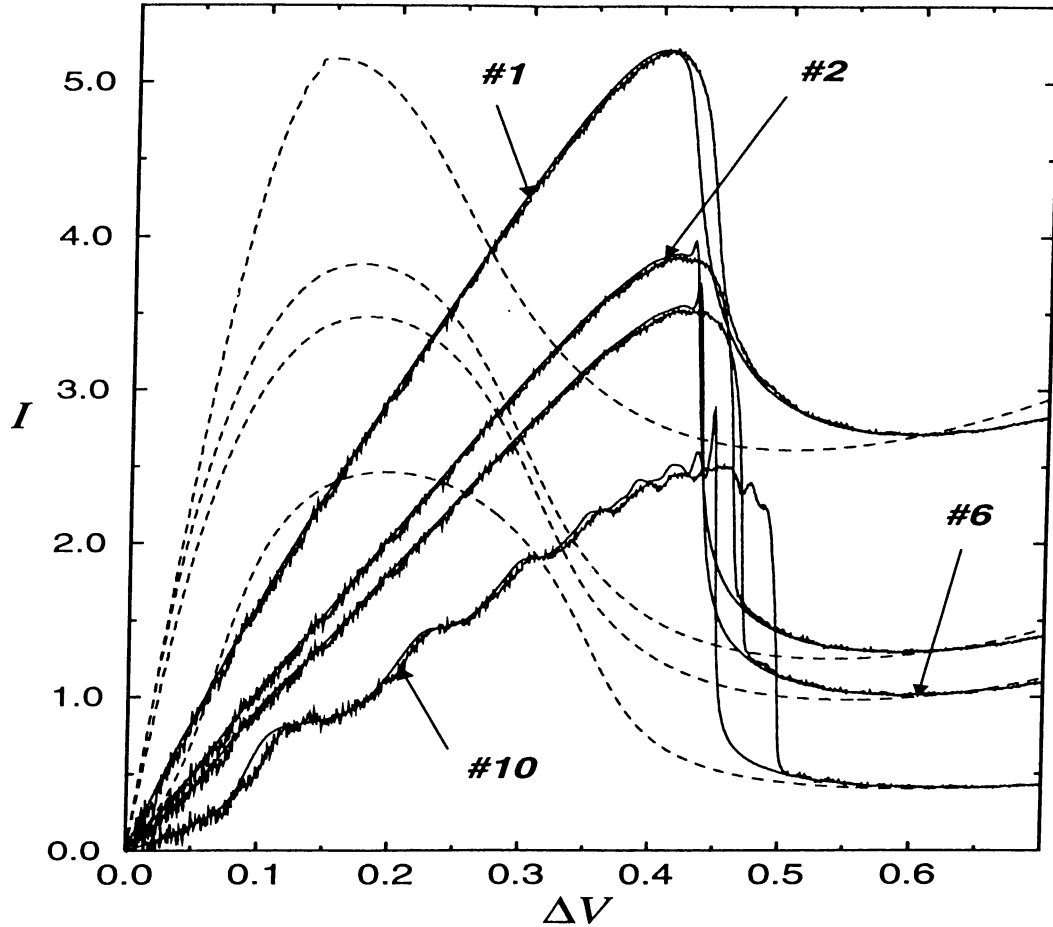


Figure 4.5: $I - V$ characteristics of a double barrier for different V_h . The current-voltage characteristics of the double barrier is shown for parameter sets 1, 2, 6, and 10. Notice that the interaction constant β is the same for those sets, while the barrier heights differ. The dashed curves indicate the current-voltage characteristics of the same structures without the interaction potential. Note that the dashed curves are the solutions of the time-independent Schrödinger equation with 40 particles.

equation with 40 non-interacting particles. It is clear that the maximum of current transmission does not depend on the interaction constant β but is sensitive to a change in the barrier height. As mentioned above, it is shifted to higher potential differences as the interaction constant is increased. The important point is that even though it occurs approximately at the same potential difference, the bistability is stronger for sharper resonances. Hence a

slower escape rate implies a stronger bistability. Indeed, for set #1 bistability exists only due to the time dependence of the potential difference. One expects that it will not show up in a time-independent study. Finally, the oscillations in set #10 suggests that the number of particles in the simulation is less than required. The effects of separate transits of energetic particles through the resonant state may be observed clearly.

4.3 A Time-Dependent Investigation of Bistable Switching

It has been argued in this thesis that the numerical solution of the time-dependent Schrödinger equation is a powerful method to determine quantum transport characteristics of a mesoscopic structure. In addition, different applications of the method have been presented, and some of them have been proposed as open problems. Nevertheless, the results given so far could also have been obtained by using a time-independent analysis. In this section, the significance of the method is justified in the time-dependent examination of bistable switching.

4.3.1 Determination of the Bistability Region

In the previous section, the current-voltage characteristics of the model double barrier structure were determined by using an adiabatic time-dependent potential. To check the adiabaticity assumption, the potential was changed ten and hundred times slower than the rate stated in Eq. (4.3). Figure 4.6 shows this situation for set #6. It can be seen that the current does not differ from the former one, but in the bistability region. It is clearly observed that, as the increase of the potential difference is more adiabatic, the switching in the current becomes more abrupt. More generally, one predicts that in principle,

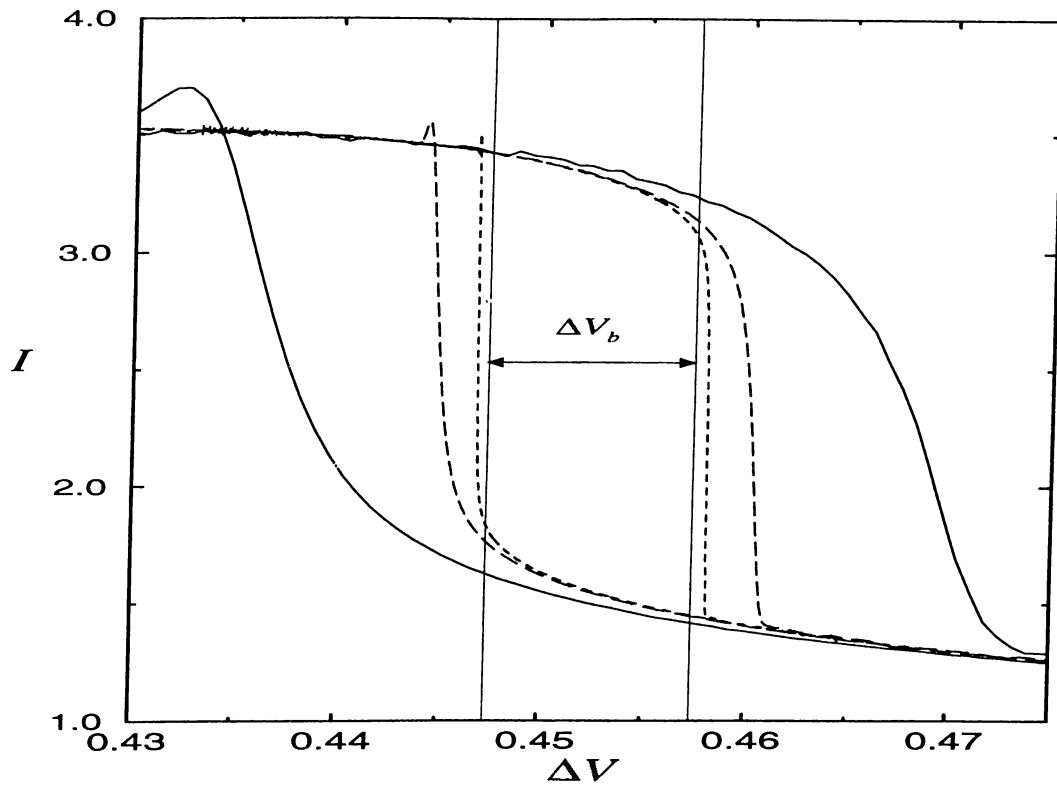


Figure 4.6: Bistability region of set #6.

Bistability region in the $I - V$ characteristics of set #6 is shown with three different adiabaticity. The solid curves are for the potential difference applied after the Eq. (4.3), the long dashed curves are ten times more “adiabatic” than this, and the dashed ones are hundred times. The vertical solid lines indicates the “real” limits of the bistability region ΔV_b .

a current drop should have an infinite slope in the time-independent case. These infinite slopes, one for the increase of the potential difference and the other for its decrease, are indicated with two vertical lines in the same figure. Their determination will be explained later. Theoretically, given a potential difference at the left (right) of these lines, the system at equilibrium is definitely on the “high current” (“low current”) state. On the other hand, between the vertical lines, the system may be in one of these two states. What makes the situation more interesting is that the state of the system is dictated by its “history”. Accordingly, a system initially at the *high current* (*low current*) state prepared at the left (right) of the vertical lines remains at this state

Set #	V_l	V_r	ΔV_b
1	—	—	—
2	0.444130(6-7)	0.449368(4-5)	0.0052378
3	—	—	—
4	—	—	—
5	—	—	—
6	0.447388(8-9)	0.457379(2-3)	0.0099904
7	0.524300(7-8)	0.605513(6-7)	0.0812129
8	nd	nd	nd
9	0.450444(6-7)	0.461829(6-7)	0.0113850
10	0.459833(7-8)	nd	nd

Table 4.3: Bistability regions for different sets.

while the potential difference is increased as much as the right (left) line. However, exceeding this limit would end up with a switching to the *low current* (*high current*) state. We will refer to the potential difference of the right and left vertical lines as V_r and V_l , and the region between them will be called “bistability region”. Its expression is defined as $\Delta V_b = V_r - V_l$.

In order to calculate the bistability region, one has to determine V_l and V_r . First, the potential difference is increased from zero to a certain value, with the time dependence of Eq. (4.3). After that, the system is simulated holding the potential difference at that constant value. If the system switches to the *low current* state, it will be concluded that this potential difference is larger than V_l . Hence, next time, a smaller potential difference must be tried. If the system does not switch after a long simulation time, one may conclude that the given potential difference was smaller than V_l , and try a larger potential difference for the next time. Repeating this procedure, the region where V_l may exist is narrowed. V_r also may be determined similarly, starting from a very large potential difference instead of zero.

The calculated values of V_l and V_r are given in Table 4.3, along with their difference ΔV_b . The dashes denote that the bistability region does not exist for

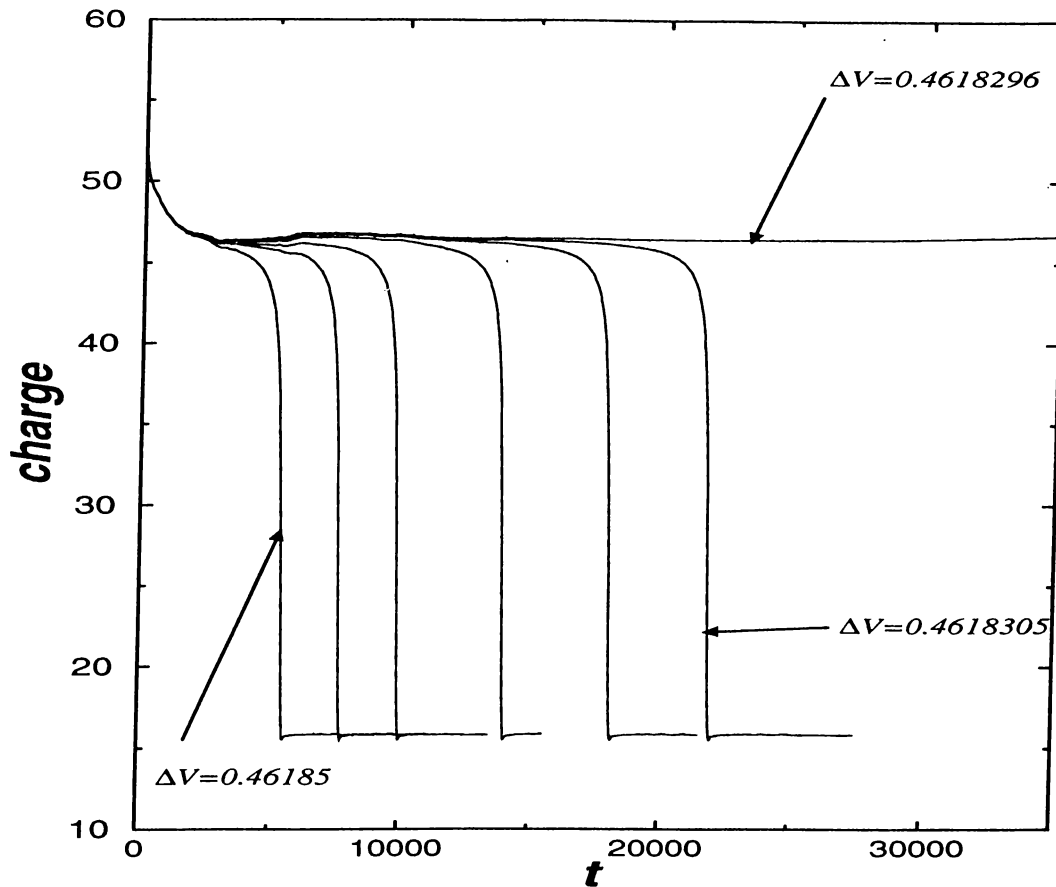


Figure 4.7: Determination of V_r .

The time-dependent simulations of the double barrier structure for parameter set #9. The potential differences which are not denoted on the figure are 0.4618400, 0.4618370, 0.4618337, and 0.4618315 from left to right respectively.

these sets. Even though they may appear in Figures 4.3, 4.4, and 4.5 for some sets, they do not exist in the real sense. As briefly noted earlier, the reason why they appear is the time dependency of the system. The effect would vanish with a “more adiabatic” change of the potential difference in this region. The letters ‘nd’ stand for “not determined”.

It is worthwhile to have a closer look at the determination process of V_r . Figure 4.7 shows the charge build-up between the barriers in several simulations realized at different potential differences near this limit. An analysis of the charge build-up is preferred over that of the current, because

the latter exhibits some small oscillations in time. It is clear that the systems are initially in the *high current* state. It is possible to separate this figure into three different regions. In the first region, a small and rapid decrease in the current is observed. This drop is not surprising since the *non-perfect adiabaticity* in the preparation of the system already suggests that the current transmitted through the structure in the bistability region is higher than the time-independent solutions predict. Therefore, the system settles down to that solution[†]. This region is not of much interest because it depends on how adiabatic the system is carried to this potential difference. In the second region, the system seems to “wait” for switching. The charge build-up between the barriers and the current transmitted through the structure are almost constant in this region. It is apparent that the “waiting” time depends on the potential difference. It increases as the applied potential difference approaches V_r . Finally, the third region contains the “switching” of the system and it occurs only for potential differences smaller than V_r , as mentioned above: the system switches for $\Delta V = 0.4618305$ but remains in the *high current* state for $\Delta V = 0.4618296$. Note that, three similar regions appear in the determination process of V_l where other type of switching occurs (*i.e.*, from *low current* to the *high current* state). In the following subsections, the *switching* and *waiting* regions are investigated.

4.3.2 The Switching

Let us focus on the switching region. Our argument is that the switching phenomena occur independent of the potential difference but depend only on the structure parameters. This means, after the waiting time the system switches with the same time dependence for all potential differences. To demonstrate this, we have to shift the curves of Figure 4.7 so that the switching regions corresponding to different potential differences are superimposed.

[†]As discussed above, the time-independent solution is unique for potential differences higher than V_r . In this case, the system seems to “wait” in the metastable state for switching.

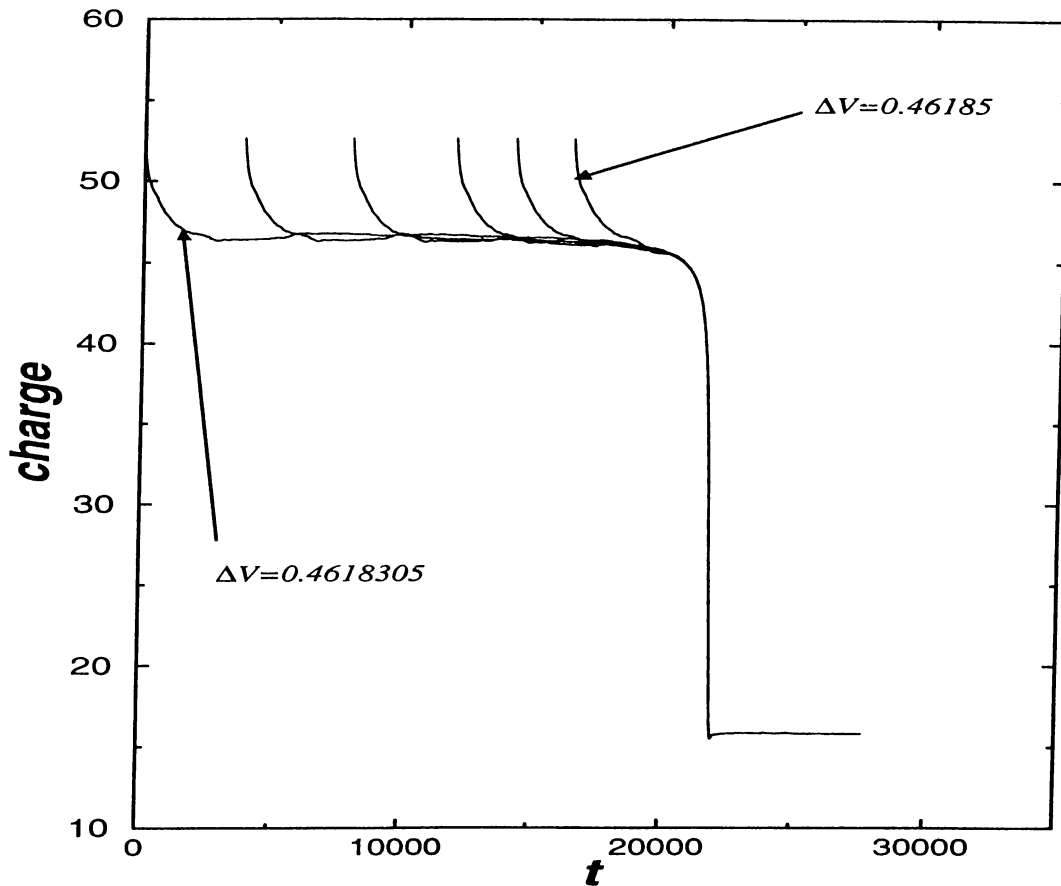


Figure 4.8: Superposition of the switching regions.

The potential differences not denoted on the figure are the same as the ones in Figure 4.7. Note that a small change in the potential difference mainly affect the *waiting* time. The parameter set is again #9.

Figure 4.8 indicates this shifted time dependencies. It is clear that any possible small difference in switching is not visible in the scale of this figure. The potential differences in these simulations are so close to each other that the system switches approximately to the same charge (current). On the other hand, the *waiting* region dramatically increases with a very small decrease in the potential difference. For a closer look at the phenomena, the derivatives of the charge with respect to time are sketched in Figure 4.9. The tails at the left side of the curves demonstrate the rapid drop of the charge (current) in the first region. The derivatives are zero in the waiting region where the

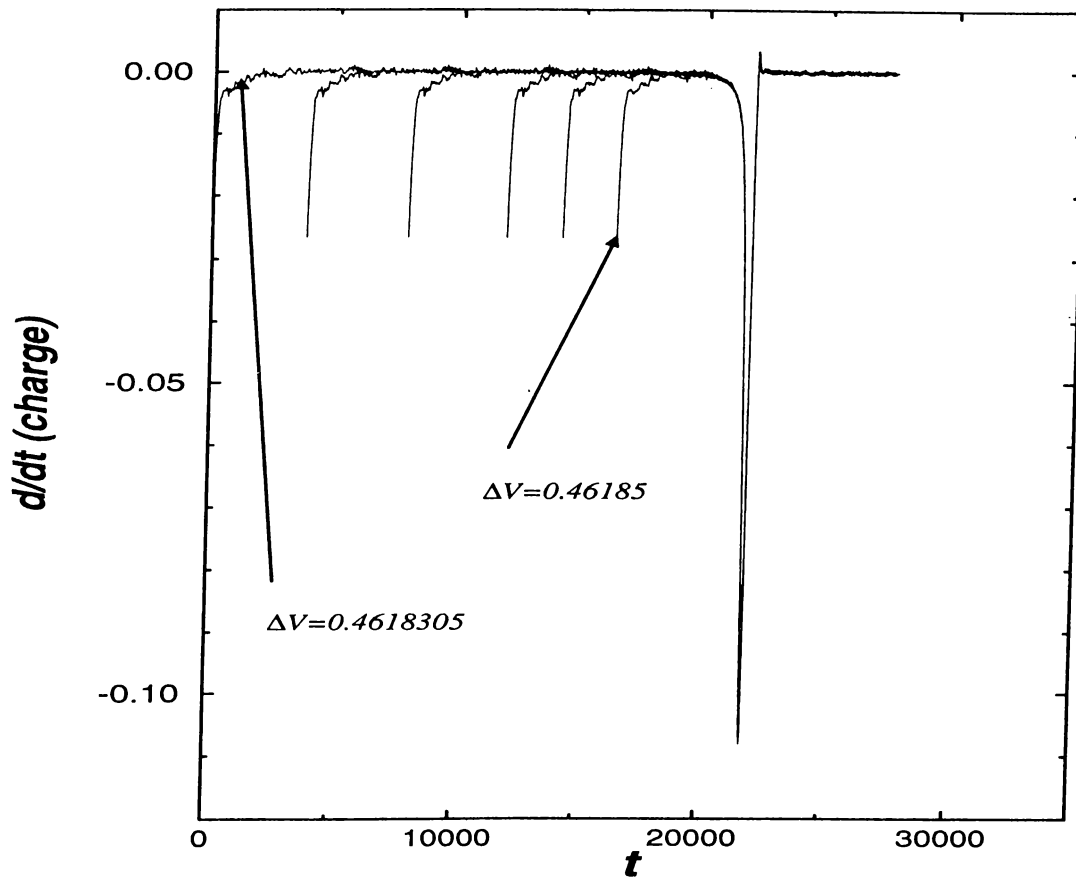


Figure 4.9: The time derivative of the charge build-up. The curves in Figure 4.8 are differentiated with respect to time. Notice the interesting peak in the switching region. The parameter set is again #9.

observables of the system do not change. Besides, there is a large peak in the switching region which implies the abrupt drop in the charge accumulated between the barriers (current transmitted through the structure). It turns out that even the derivatives are the same for all the curves in this region. This observation supports the above argument about the generality of the switching phenomena.

Let us return to the original case where the potential difference was increasing adiabatically, starting from zero. During this process the energy of the resonant state shifted to lower energies for electrons injected from the reservoir at higher potential. At first, the electrons with energies near the Fermi

energy enter to the resonant state in the presence of the interaction potential due to the charge accumulated by the electrons having nearby energies. Then, at some higher potential difference, electrons with lower energies correspond to the resonant state. However, the charge accumulated by the electrons with higher energies is crucial for their resonance. At this time, some of the electrons with higher energies, under the effect of the shift of the resonant level due to the charge of the electrons at lower energies, may still correspond to the resonant state. Hence, the system is in the high current state. On the other hand, with a further shift of the resonant level due to an increase in the potential difference, electrons with higher energies correspond to the non-resonant states. Hence their charge is released and the resonant level shifts also for the electrons with lower energies so that the current transmitted through the system drops abruptly.

Based on the similar arguments, an explanation for switching in the other direction may also be explained. When the potential difference is decreased from a higher value, the electrons with lower energies correspond to the resonant state first. But now, the electrons with higher energies do not correspond to the resonance so that the current remains low.

The effects of different parameters on the switching mechanism may be seen from the derivative of the charge build-up with respect to the scaled time. Indeed the qualitative nature is similar for all parameter sets. Figures 4.10 and 4.11 indicate these derivative curves for different structure parameters. Observe that larger peaks correspond to smaller widths. A higher peak means a more abrupt drop in the charge between the barriers, so a bigger charge release. The peaks are observed to become higher if the interaction constant β , the barrier height V_h , or the number of particles are increased. These kind of fast and powerful responses to small changes in input may be technologically important. Note that the time scale of the signal may be as small as approximately 300 femtosecond. Obviously, in order to be significant, these effect must not be washed out by the parasitic effects of the contacts,

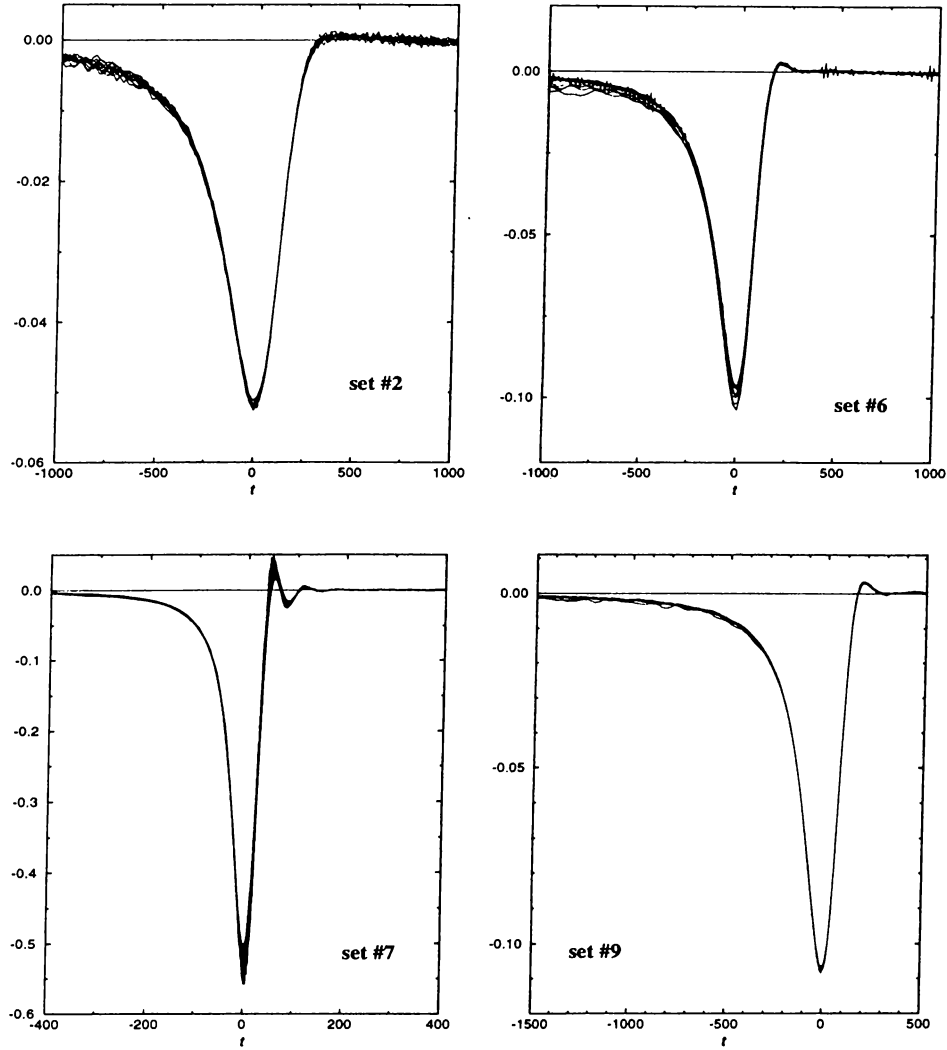


Figure 4.10: Derivatives near V_r for different set of parameters.

The peak region of the time derivatives of the charge build-up between the barriers are shown for different set of parameters. The switching is from the *high current* to the *low current* state. A large number of curves (12 for set #2, 14 for set #6, 17 for set #7, and 14 for set #9) at different potential differences are superimposed on the figure.

etc.

Finally, let us investigate the characteristic time of these signals as a function of the interaction parameter β . We will assume that this time, say

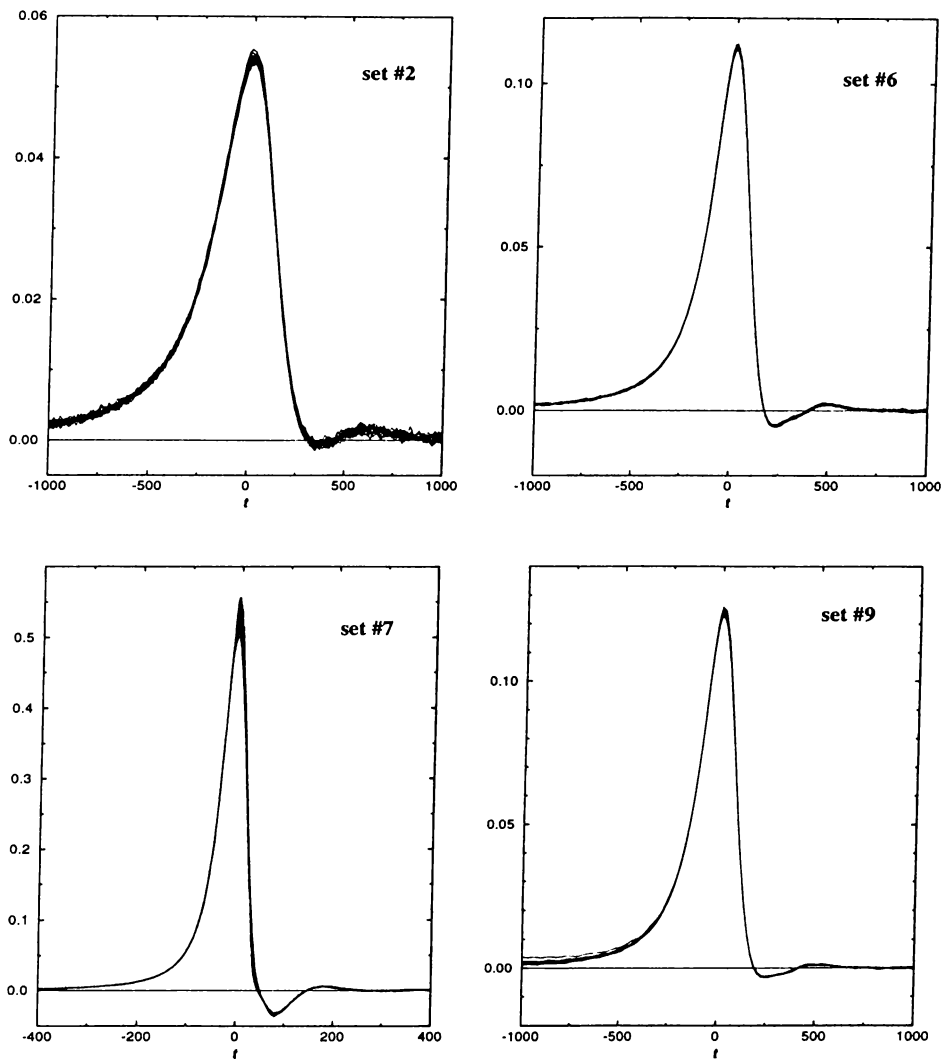


Figure 4.11: Derivatives near V_l for different sets of parameters.

The peak region of the time derivatives of the charge build-up between the barriers are shown for different sets of parameters. The switching is from the *low current* to the *high current* state. A large number of curves (19 for set #2, 20 for set #6, 17 for set #7, and 12 for set #9) at different potential differences are superimposed on the figure.

τ , is inversely proportional to the maximum of the derivatives. Figure 4.12 indicates these maximum values as a function of β . Note that the data points

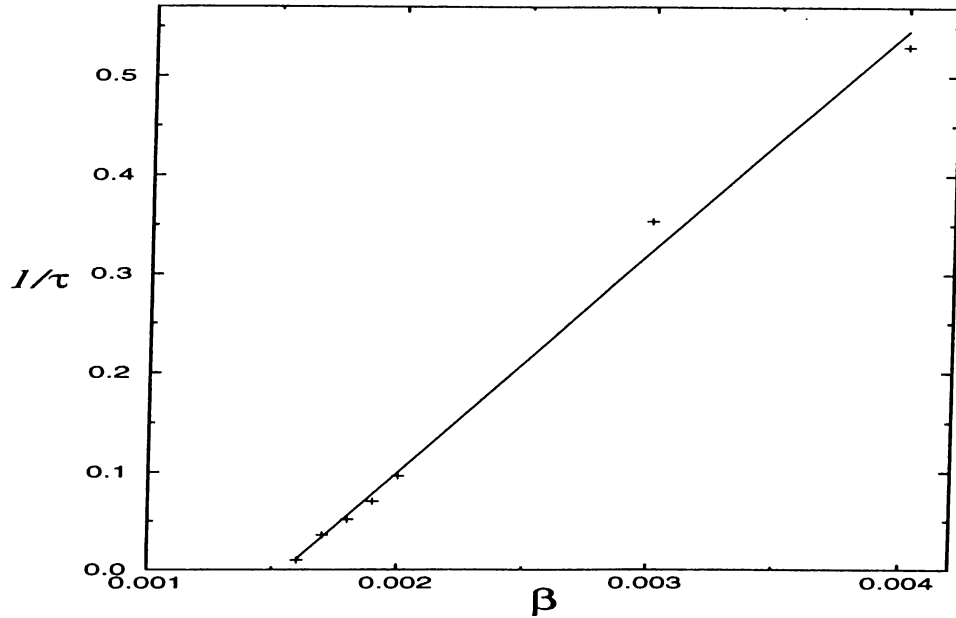


Figure 4.12: Maximum of the derivatives as a function of β

The inverse of the “relaxation time” has a linear dependence to the interaction constant β . The data points are indicated with pluses and the solid line is the curve fitted to these points.

fit to a straight line. Therefore, we may express analytically

$$\frac{1}{\tau} \propto (\beta - \beta_0) \quad (4.4)$$

where β_0 is the interaction constant where bistability starts to occur. Here $\beta_0 \approx 0.00155$. Exploiting the analogy with the phase transition phenomena, we may postulate that this formula resembles to $\tau \approx (T - T_c)^{-z}$ where T and T_c are the measured and critical temperatures respectively, τ is the relaxation time, and z is the universal critical exponent. In our case z is obviously equal to 1. Note that the value of this term for the case of phase transitions is also 1 within the mean field approximation.

4.3.3 The Waiting

As mentioned above, the other important region in Figure 4.7 is the *waiting* region. It is clear that the system waits longer if the potential difference is closer to the switching potential (V_r or V_l). The term “lifetime” may be the best word to designate the event. While one goes away from the switching potential V_r (V_l), the lifetime of the system at the high current state (low current state) decreases. This *lifetime* is expected to be related to the tunneling time of the particles. In fact, for the current case, one may argue that the system has an infinite lifetime at the bistable solutions. Even though it will not be proved here, it is known that the time-independent solutions of this system results in three solutions (*i.e.* tri-stability) at the bistability region. Here we postulate that the unique solution of the *exact*[†] time-independent Schrödinger equation lies between these bistable solutions of the time-dependent picture. It appears that this solution is unstable. On the other hand, although the mean-field theoretical bistable solutions are not the solutions of the *exact* equation, these metastable states have practically an infinite *lifetime* for decaying. Randomly initiated, the system will develop into one of these bistable states.

In order to fortify the above argument we may examine the *lifetime* of the system as a function of the potential difference for different parameter sets and for both kinds of switching (*i.e.* near V_l and V_r). Indeed, it is difficult to make an absolute definition of *lifetime*. However, some relative time scales would be enough in order to show how it is related to the potential difference. At first, the derivative curves are shifted so that their maximum would be at time $t = 0$. After that, the *lifetime* is taken as the time where the derivative is roughly zero. As mentioned above, the “tail” at the beginning of the curve does not attract any interest because it depends on how the system is prepared initially for this potential difference. The abrupt change in the state of the system at this region is simply to reach the more stable bistable solution.

[†]This means without mean-field approximation. Remember the discussion in Section 3.1.1.

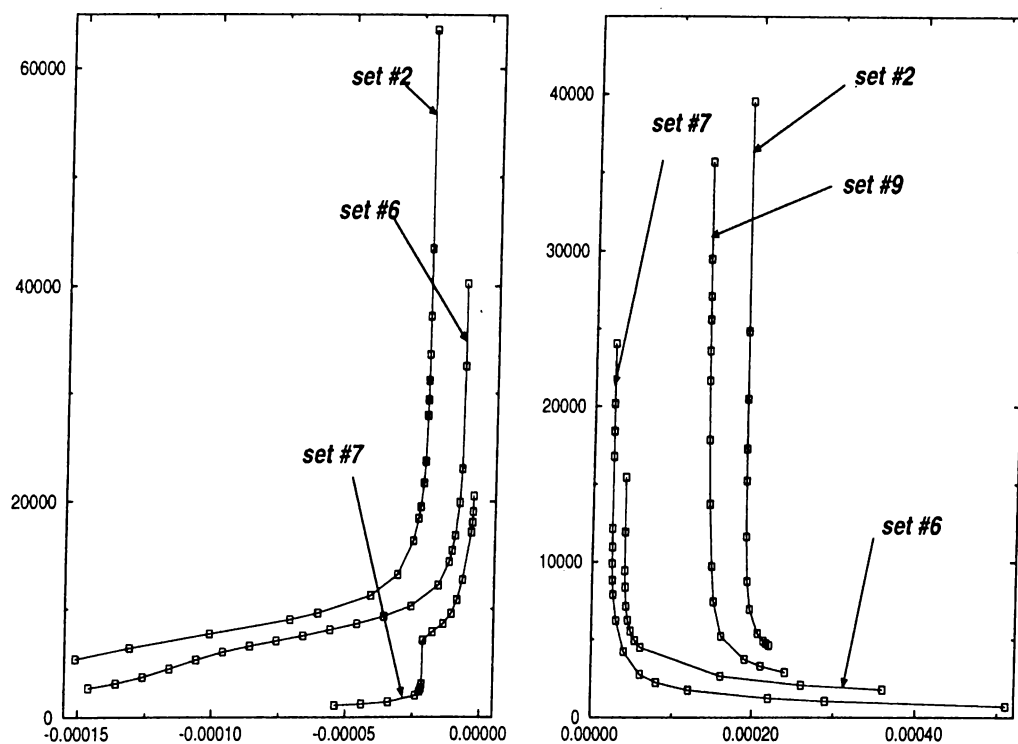


Figure 4.13: Lifetimes for different sets

Lifetimes for different sets of parameters are superimposed on two graphs. At left, the switching is from the low current to the high current at right from the high current to the low current state. The vertical and horizontal axes indicate the lifetimes and the relative potential differences respectively.

The *lifetimes* calculated as discussed above are displayed in Figure 4.13. As apparent on this figure, the *lifetime* of the systems is a fast growing function of the potential difference. Near the limits of the bistability region it diverges so that our proposition about the infinite lifetime of the bistable solutions is supported.

We will conclude this section with an interesting artifact of these simulations. Figure 4.14 displays the values of the potential differences where the maximums of the derivative curves take place for different interaction constants β . The derivatives are obtained in a simulation where the potential were changing adiabatically, hundred times slower than the rate expressed in

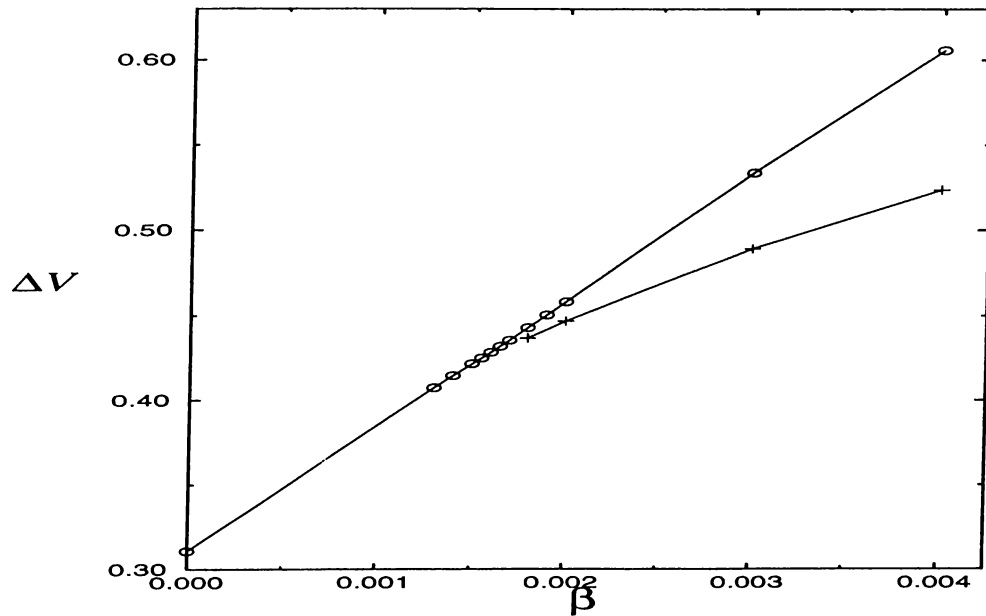


Figure 4.14: Potential differences where the maximum of the derivatives occur. The potential differences where the maximum of the derivatives occur are shown as a function of β . The circles correspond to the increase of potential difference, and the pluses to its decrease. These symbols are connected by broken lines.

Eq. (4.3). We notice that the broken lines connecting the circles result in a straight line. This argument holds for a very large range of β^\dagger including also $\beta = 0$ case where we have dealt only with non-interacting particles. The values of the potential differences on this line correspond to V_r after the bistability region opens. For the decrease of the potential difference, the maximum of the derivatives occurs at V_l and are indicated by the plus signs on the same figure. They differ from V_r after the bistability region appears, or equivalently when the interaction constant β is larger than β_0 . The value of β_0 determined from this figure is consistent with the one estimated in the previous subsection.

[†] $\beta = 0.004$ may be a small number but its effect is large.

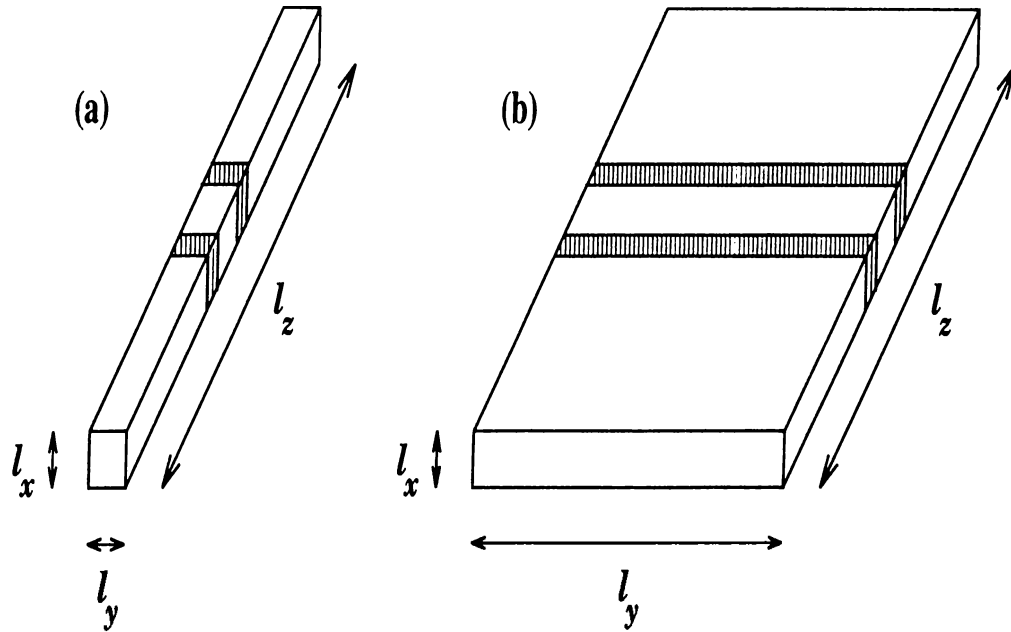


Figure 4.15: Double barrier in three dimensions.

(a)- “One-dimensional” model for a resonant double barrier structure. Electrons are sufficiently confined in the z direction so that quantized energy levels in the $x - y$ plane are well separated in energy. (b)- “Two-dimensional” model for a resonant double barrier structure. Electrons are confined in the $y - z$ plane so that quantized energy levels in the x direction are well separated in energy. The location of the barriers is indicated by the shaded areas.

4.4 Higher Dimensions

The examination of the one-dimensional double barrier model is a prominent step toward the investigation of quantum bistable systems. However, physical structures are produced in three dimensions. The main assumption in the above calculations is that in the directions perpendicular to our one-dimensional model, the dimensions of the structure is so small that electrons can only propagate in the first subband in these directions. This situation is sketched in Figure 4.15-(a). On the other hand, often these structures in practice have a width in one of these directions, where one speaks about a two-dimensional electron gas. In this sense, the model of Figure 4.15-(b) is more realistic for the simulation. Notwithstanding its two-dimensional characteristics, this system

may be simulated on a one-dimensional mesh with a generalization of the previous model.

Let us denote with K_F the Fermi wave vector in the reservoirs connected to our structures. After the first model, we may define

$$k_F^2 = K_F^2 - \left(\frac{\pi}{l_y}\right)^2 - \left(\frac{\pi}{l_x}\right)^2 \quad (4.5)$$

as the Fermi wave vector injected to our structure. The electrons in the simulation, having wave vectors up to this limit, are weighted only after the thermal distribution function of the contacts. On the other hand, after the second model, they may occupy different energy levels in the other directions so that

$$k^2 = K_F^2 - \left(\frac{n\pi}{l_y}\right)^2 - \left(\frac{\pi}{l_x}\right)^2 \quad (4.6)$$

where n is the number corresponding to the energy level in the y direction and k is the wave vector of the particle injected to the structure corresponding to the Fermi wave vector in the reservoirs. In this case, particles having the same energy in the reservoirs may have different wave vectors in the y direction, hence a different wave vector in the z direction. This implies that another distribution function may be used to study the effects of a widening of a channel. The first thing one may expect in such a model is that the charge in the system will be appreciably larger than the one in the former model. On the other hand, the charge is now confined in a larger volume. Consequently, a different interaction will show up between the barriers. This suggests that the interaction potential constant β must be scaled. Here we have made a rough approximation originated from elementary electrostatics: The potential at the surface of a two-dimensional charged disc is proportional to its radius. Hence, the interaction constant β is scaled proportional to $1/l_y$.

The results of several simulations for different l_y are shown in Figure 4.16. This distance l_y was not defined in the previous section. In order to compare the currents, it is taken as $l_y = L = \lambda_F\sqrt{3}/2$ where λ_F is the Fermi wavelength of the reservoirs as is used in the previous calculations ($\lambda_F \approx 16.7$ mesh units).

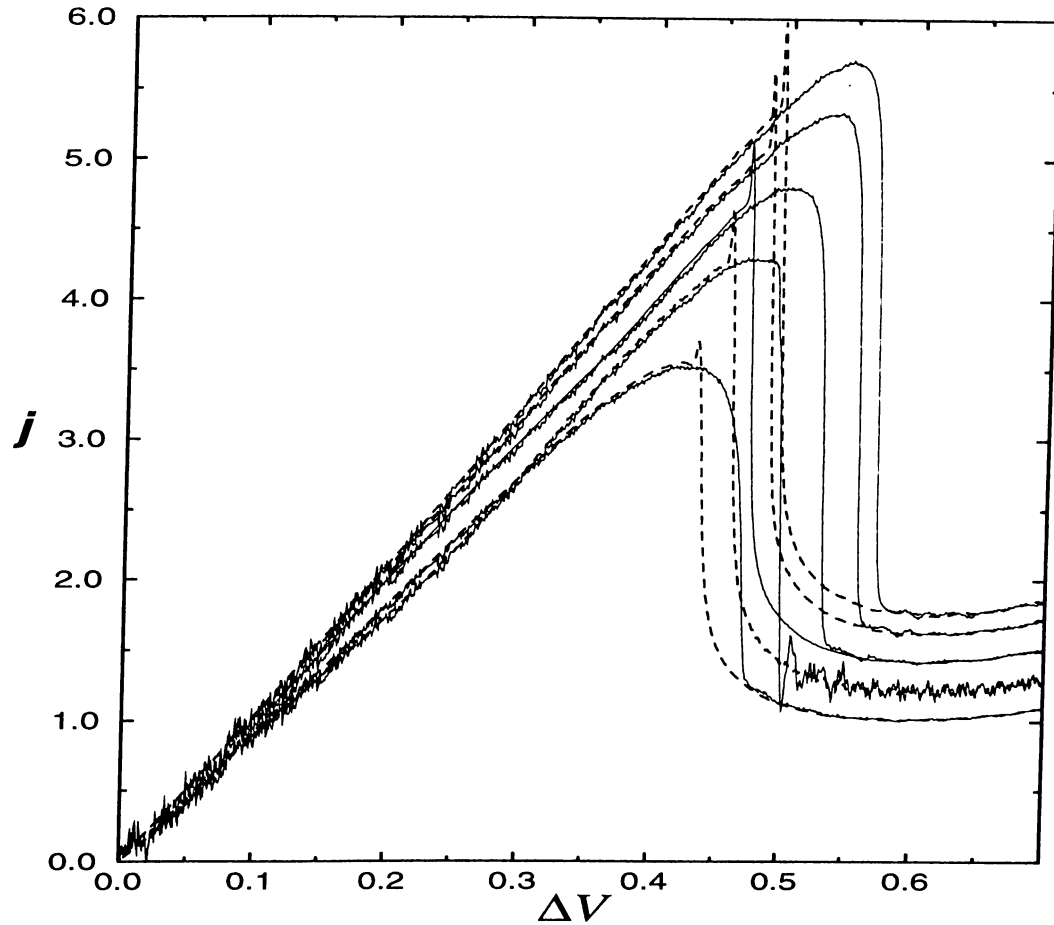


Figure 4.16: Two-dimensional simulation of the double barrier structure. The current densities j for different l_y are shown as a function of the potential difference ΔV . The parameters of the structure are that of set #6.

The current densities on the figure are calculated through $j = L/l_y \times I$ where I is the current. The currents transmitted while ΔV is decreasing are sketched with dashed lines in order to simplify the graph. The dimensions of l_y are 1, 1.5, 2, 5, and $100L$ from left to right respectively.

The current transmitted through the system is higher and the bistability region is larger for a wider structure. In fact, our expectation was toward a decrease in the bistability region since the experiments suggest that this characteristics of the resonant tunneling diode vanish in higher dimensions. We conjecture that the approximation in scaling of the interaction parameter

β lead us into these results. As pointed out earlier, even a small change in this parameter have a great influence on the bistable nature of the system. A much better approximation may be via three-dimensional solution of the Poisson equation. This was not done here. On the other hand, one may easily treat the double barrier problem in a most general form where l_x is also large enough to permit the electrons to propagate in the higher energy levels quantized in this direction. The simulation of this three-dimensional version of the double barrier model is straightforward, but is not included in this thesis.

Chapter 5

CONCLUSION

In this thesis, a novel numerical method for studying the quantum transport phenomena in small systems is proposed and applied to several one- and two-dimensional systems. The method is based on the numerical integration of the time-dependent Schrödinger equation. This approach may describe the time-dependent dynamics of a d -dimensional system on a d -dimensional mesh. Despite these advantages over other approaches, the implementation of the blackbody boundary conditions was so far problematic. At this point, our method described in Chapter 2 puts the Schrödinger equation on a par with the other approaches by successfully enabling the absorption and injection of the wave function at the boundaries of a simulation region. This makes it feasible to study most of the realistic open systems for large time scales in their far-from-equilibrium states. The accuracy of the method is tested in numerous different problems. Chapter 2 states some of the simple examples in order to convince the reader on the extensive power of the method.

The applications of the method to two-dimensional systems are presented in Chapter 3. The exact solution of the two particle problem in a one-dimensional space is given first. A limited study resulted in no bistability for the numerically exact case. In contrast, a Hartree approximation to the same problem ends up

with bistable (and chaotic) solutions.

The kink structure is introduced as an application of the method to a two-dimensional actual physical geometry. The transmission probabilities of the particles incident to the system are calculated as a function of their kinetic energies, using our time-dependent approach. The prominent current-voltage characteristics which include a negative differential resistance region are reported for the first time in a time-dependent context. This structure is promising in terms of the future technological applications.

In Chapter 4, the method is applied to several one-dimensional systems. First, a model geometry for resonant tunneling structure is introduced. This structure has well-known nonlinear current-voltage characteristics and exhibits a bistability region within the mean field approximation approach. These properties are reported for different sets of structure parameters and interaction constants. As an original result of this thesis, a time-dependent investigation of bistable switching is presented. The behavior of the system in the interesting “waiting” and “switching” regions are reported. It is concluded that even though they are not the “exact” solutions of the time-independent Schrödinger equation, these bistable solutions have practically infinite “lifetimes”. On the other hand, the switching mechanism is independent of the potential difference, and is dictated only by the parameters of the system. This problem was challenging for the time-dependent Schrödinger approach due to the requirement of very large time scales of simulation and the consideration of far-from-equilibrium states. However, the method successfully handled these systems. Finally, this model is generalized to higher dimensions by appropriately weighing the amplitudes of the wave functions of different wave vectors.

It has been said that “an author never finishes a book, he merely abandons it.” At present, this is exactly true for this thesis. The topics may be presented in a different and better way, as well as extended in order to deal with more realistic cases. We may call the latter one “open problems”. First, one may

examine the method with a more profound analytical approach in comparison to the one that is mentioned in this thesis. The method may still be improved. However, in this work, we were content with its accuracy.

Solving the two interacting particle problem numerically exactly is interesting and only an introduction is presented here. Its extensive investigation may reveal important characteristics of the n -particle system, but the generalization procedure is not straightforward. Next step may be the application of a potential difference and the examination of the solutions. On the other hand, the kink structure may be simulated in the presence of a self consistent potential in order to study its bistability in a time-dependent picture. Furthermore, the switching mechanism may be investigated, but note that, this study would require more powerful hardware than a simple workstation.

Since it is a novel subject, the open problems concerning the bistable switching are numerous. The study presented here may be repeated for a larger number of parameter sets. We may only postulate that bistability observed in quantum transport has some similar characteristics to the well-known phase transition phenomena. Using this analogy, one may go further and results in interesting peculiarities in the investigation of bistable switching.

Appendix

SOME LIMITATIONS

So far, the method of absorbing and injecting boundary conditions described in Chapter 2 is successfully applied to numerous different systems. In this appendix, certain practical points about the application of the method will be presented. These points are based on experience gained through the simulations carried out to produce all the computational work included in this thesis. One is strongly recommended to read this appendix if she/he intends to use the method in her/his own research.

A.1 Wavelength Dependence

The accuracy of the method of blackbody boundary conditions depends primarily on the wavelength of the particle being injected or absorbed. One expects that the method would not handle the absorption of particles with a wavelength larger than the boundary region. The reason is that these waves may not be fully expressed in the boundary region due to the insufficient number of mesh points. Nonetheless, as briefly mentioned in Section 2.1.2, in the applications the method enables the absorption of wavelengths much

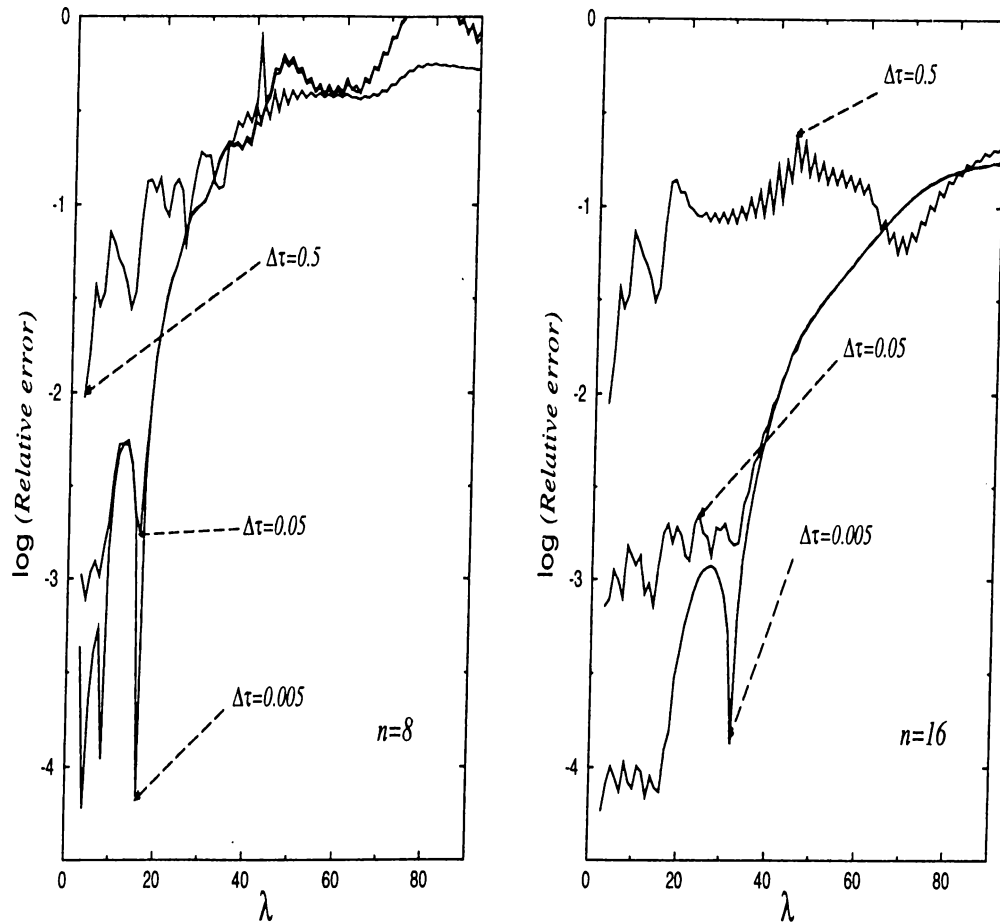


Figure A.1: The relative error as a function of wavelength

The logarithm of the relative error is indicated as a function of wavelength λ for two different values of the boundary region size, $n = 8$ and $n = 16$. For each size of the boundary region, three different time steps $\Delta\tau = 0.5, 0.05$, and 0.005 are considered.

larger than the boundary region size.

Figure A.1 indicates the average relative error of the wave function as a function of the incident wavelength. The particles are injected to a double barrier having the structure parameters same as the parameter set #3 of Table 4.2, in the absence of any potential difference. This kind of resonant structures are the most challenging geometries for testing the blackbody boundary conditions. The relative error is defined as $|\psi_l/\Psi_l - 1|$ and it is

averaged throughout all the simulation region. Here ψ is the time-dependent wave function updated after the blackbody boundary condition method and Ψ is the solution of the time-independent Schrödinger equation. As the initial condition, the two wave functions are taken to be identical. The numerically exact wave function Ψ is evaluated by a multiplication with the term $\exp(-iE\Delta\tau)$ where E is the energy of the injected wave and $\Delta\tau$ is the time step. The relative errors are calculated after the system is simulated for very large time scales.

It is clear on the figure that the accuracy of the method decreases as the wavelength is increased. Namely, the relative errors are quit small for $\lambda < 2n$. In addition to that, for the wavelengths which are commensurate with the boundary region size the method is highly reliable. For example, notice the dips at $\lambda = 4, 8$, and 16 for $n = 8$ and at $\lambda = 32$ for $n = 16$. On the other hand, the time step $\Delta\tau$ has an appreciable influence on the errors, especially for small wavelengths. $\Delta\tau = 0.05$ appears to be an optimum time step for a one-dimensional system both in terms of accuracy and use of computational time.

It is interesting to note that the errors are fixed for a given set of parameters whatever be the initial condition. Accordingly, very unphysical initial conditions (for example, no wave function at all in the simulation region) also tend to the time-independent solutions yielding the above figure for errors. Hence, there is no loss of generality in taking the time-independent solution as the initial condition. Furthermore, this argument demonstrates the reliable power of the method. As a final remark, note that the errors are much smaller if one does not care about the phase of the wave function and defines the relative error as $|\psi_l/\Psi_l| - 1$. Thus, the current and charge build-up are computed with insignificant errors. On the other hand, a slight difference between the phase of the time-dependent wave function and that of the numerically exact solution is not surprising after such large time scales.

A.2 Choice of Boundary Conditions and Switching

As discussed earlier, the boundary wave function ϕ is updated for the next time step using periodic boundary conditions. Although this is not a strict restriction, it is preferred over reflecting boundary conditions. An update using reflecting boundary conditions will also yield an accurate result near the boundary ($l \approx 1$). But, boundary wave function ϕ , at the constant potential of the boundary, is assumed to move in only one direction, and periodic boundary conditions fit better to this assumption. The errors in the update of ϕ , occurring at points near $l \approx n$, would be greater in the case of reflecting boundary conditions and these could “diffuse” into the full wave function.

The choice for the means of updating the full wave function seems to be less problematic. However, in spite of its lower computation speed, a reflecting boundary condition is more favorable in the case of a large potential difference between the reservoirs. The wave functions injected from the reservoir with the higher potential gain considerable amount of kinetic energy while moving “downhill” the potential ramp. With periodic boundary conditions, when they reach the other reservoir’s boundary, they have a chance to “diffuse” the reservoir from which they had initiated. This situation may affect the time-dependent behavior of the system much more than predicted.

On the other hand, the wave functions injected from the reservoir with lower potential reflect from the potential ramp and are absorbed from the boundary they were injected. Again, the use of periodic boundary conditions for the update of these full wave functions may cause the same *diffusion* problem, but now the diffusion occurs into the reservoir which is at the higher potential. These waves will gain some potential energy, and disturb the system if it has some strong resonance structure. Use of reflecting boundary conditions prevent these sources of errors.

Switching from the full wave function ψ to the boundary wave function ϕ is another important criterion that can affect the performance of the method to some small extent. A very smooth transition means to give considerable amount of weight to one of the functions where it is not appropriate. In every time step, some error may grow up in (or *creep* into) the full wave function. On the other hand, a step like transition may cause a discontinuity in the full wave function. This effect generates some unwanted Fourier components. To determine the transition function which operates best for a special geometry, a trial-and-error approach is recommended.

A.3 Analytic Expression for the Full Update

If $\Psi(\tau)$ represents the vector of values of $\{\psi\}$ at time τ , its full update for the next time can be expressed through the relation:

$$\Psi(\tau + \Delta\tau) = A \Psi(\tau) + I e^{-i E_q \tau} \quad (\text{A.1})$$

where A and I (I for *injection*) are a matrix and a vector respectively, which depend on the potential function, the wavelength of the injected wave, and the switching method. At some constant potential function[†], these matrices are constant. In such a case, after n consecutive updates, the wave function is related to its initial value by the expression:

$$\Psi(n\tau) = A^n \Psi(0) + (1 - A e^{i E_q \tau})^{-1} (1 - A^n e^{i E_q n\tau}) I e^{-i E_q (n-1) \tau}. \quad (\text{A.2})$$

which is a simplified form of a geometric series. At equilibrium, the time-dependent wave function must yield the time independent solution, so the right hand side of Eq. (A.2) must converge to some constant vector times $e^{-i E_q \tau}$ as n goes to infinity. This condition is satisfied if all the magnitudes of the eigenvalues of the matrix A are smaller than 1. These eigenvalues

[†]For a quantum transport simulation, this statement requires constant potential difference between the reservoirs and absence of any self consistent potential.

were checked for different potential functions and realized that some of them have magnitudes very close (or perhaps equal) to unity. But the eigenvectors corresponding to these eigenvalues grow so slowly that, within the practical time limits—even much longer than a charge built-up time of a resonant double barrier—, no appreciable error was noticed because of this problem. Besides, simulations of physical geometries which require time-dependent solutions usually have some changes in the potential function, which in turn changes the matrix A and its eigenvalues. So in a realistic simulation, the eigenvalues change in time and the corresponding eigenvectors never have the time to grow up.

A.4 Breaking-up of the Exponential Term

For the sake of completeness, this chapter will be concluded by discussing the break-up of the exponential term given in Eq. (2.6). This approximation will be exact if the commutator of the operators K and v vanishes. Using the definition of the kinetic energy operator K stated in Eq. (2.3), we can express the commutation relation through the expression:

$$[K, v] \psi_l = (v_{l-1} - v_l) \psi_{l-1} + (v_{l+1} - v_l) \psi_{l+1}. \quad (\text{A.3})$$

The error in the break-up can be seen to be related to the size of the potential difference between two consecutive lattice points. Based on the above statement, some problems seem to appear if one tries to simulate a geometry having infinitely large potential walls. However, recalling the general updating mechanism described in Section 2.1.1, one may notice that the potential energy function v is only used in Eq. (2.7), and in this equation, it is on the complex exponential. This means that a very large potential may have the effect of a small one. Therefore, an infinite potential also should be expressed within the limits of the period of this exponential. It is concluded that, for small enough $\Delta\tau$, this break-up method is safe and it has been utilized extensively in solutions of time-dependent wave equations.

Bibliography

- [1] For an extensive discussion of theoretical work on this area and a more complete set of references, see E. Tekman, *Ballistic Transport and Tunneling in Small Systems*, Ph. D. thesis submitted to the Department of Physics and the Institute of Engineering and Sciences of Bilkent University, pp. 1-26, pp. 31-35, (1990).
- [2] R. Kubo, *Journal of the Physical Society of Japan* **12**, 570 (1957).
- [3] R. Landauer, *IBM Journal of Research and Development* **1**, 223 (1957).
- [4] R. Landauer, *Philos. Mag.* **21**, 863 (1970).
- [5] M. Büttiker, Y. Imry, R. Landauer, and S. Pinhas, *Physical Review B* **31**, 6207 (1985).
- [6] M. Büttiker, *Physical Review Letters* **57**, 1761 (1986).
- [7] M. Büttiker, *IBM Journal of Research and Development* **32**, 317 (1988).
- [8] W. R. Frensley, *Reviews of Modern Physics* **62**, 745 (1990).
- [9] A. D. Stone and A. Szafer, *IBM Journal of Research and Development* **32**, 384 (1988).
- [10] Y. Aharonov and D. Bohm, *Physical Review* **115**, 485 (1959).
- [11] Y. Aharonov and D. Bohm, *Physical Review* **123**, 1511 (1961).

- [12] R. A. Webb, S. Washburn, C. P. Umbach, and R. B. Laibowitz, *Physical Review Letters* **54**, 2696 (1985).
- [13] V. Chandrasekhar, M. J. Rooks, S. Wind, and D. E. Prober, *Physical Review Letters* **55**, 1610 (1985).
- [14] H. U. Baranger and A. D. Stone, *Physical Review B* **40**, 8169 (1989).
- [15] L. P. Kadanoff and G. Baym, *Quantum Statistical Mechanics*, W. A. Benjamin, New York, (1962).
- [16] L. V. Keldysh, *Soviet Physics-JETP* **20**, 1018 (1965).
- [17] For a wider description of nonequilibrium theory of quantum transport and a complete set of references, see E. Tekman, *Ballistic Transport and Tunneling in Small Systems*, Ph. D. thesis submitted to the Department of Physics and the Institute of Engineering and Sciences of Bilkent University, pp. 135-166, (1990).
- [18] S. Hershfield, *Physical Review Letters* **70**, 2134 (1992).
- [19] O. Heinonen and M. D. Johnson, *Physical Review Letters* **71**, 1447 (1993).
- [20] M. C. Yalabık, *Turkish Journal of Physics* **19**, 21 (1995).
- [21] C. S. Lent and D. J. Kirkner, *J. Appl. Phys.* **67**, 6357 (1990).
- [22] E. Wigner, *Physical Review* **40**, 749 (1932).
- [23] P. Carruthers and F. Zachariasen, *Reviews of Modern Physics* **55**, 245 (1983).
- [24] F. J. Narcowich and R. F. O'Connell, *Physical Review A* **34**, 1 (1986).
- [25] R. K. Mains and G. I. Haddad, *A New Formulation of the Wigner Function Method for Quantum Transport Modeling*, University of Michigan preprint, (1989).
- [26] M. Dyakonov and M. Shur, *Physical Review Letters* **71**, 2465 (1993).

- [27] L. D. Landau and E. M. Lifshitz, *Fluid Mechanics*, Pergamon, New York, (1966).
- [28] K. Stratford and J. L. Beeby, *Journal of Physics: Condensed Matter* **5**, L289 (1993).
- [29] J. Wang and H. Guo, *Physical Review B* **48**, 12072 (1993).
- [30] J. R. Hellums and W. R. Frensley, *Physical Review B* **49**, 2904 (1994).
- [31] J. Makhoul, *Proc. IEEE* **63**, 561 (1975).
- [32] R. Zwanzig, *Physica* **30**, 1109 (1964).
- [33] B. Engquist and A. Majda, *Mathematics of Computation* **31**, 629 (1977).
- [34] R. K. Mains and G. I. Haddad, *Journal of Applied Physics* **64**, 3564 (1988).
- [35] R. K. Mains and G. I. Haddad, *Journal of Applied Physics* **67**, 591 (1990).
- [36] M. C. Yalabik, G. Neofotistos, K. Diff, H. Guo, and J. D. Gunton, *IEEE Transactions on Electron Devices* **36**, 1009 (1989).
- [37] L. F. Register, U. Ravaioli, and K. Hess, *Journal of Applied Physics* **69**, 7153 (1991); **71**, 1555(E) (1992).
- [38] M. C. Yalabık, in *Negative Differential Resistance and Instabilities in 2-D Semiconductors*, N. Balkan, B. K. Ridley, and A. J. Vickers Eds. Plenum, pp. 171-178, (1993).
- [39] T. Shibata, *Physical Review B* **43**, 6760 (1991).
- [40] J.-P. Kuska, *Physical Review B* **46**, 5000 (1992).
- [41] M. C. Yalabık and M. İ. Ecemiş, *Physical Review B* **51**, 2082 (1995).
- [42] G. Dahlquist and A. Björck, *Numerical Methods*, Prentice Hall, Englewood Cliffs, NJ, p284, (1974).
- [43] *Ibid.*, p102.

- [44] M. C. Yalabık, "Some ad-hoc methods for introducing dissipation to the Schrödinger equation", in *Science and Engineering of One- and Zero-Dimensional Semiconductors*, edited by S. P. Beaumont and C. M. Sotomajor Torres, Plenum Press, New York, pp. 83-89, (1990).
- [45] U. Ravaioli, T. Kerkhoven, M. Raschke and A. T. Galick. *Superlattices and Microstructures* **11**, 343 (1992).
- [46] J. C. Wu, M. N. Wybourne, A. Weisshaar and S. M. Goodnick, *Journal of Applied Physics* **74**, 7 (1993).
- [47] B. W. Alphenaar, Z. A. K. Durrani, A. P. Heberle, and M. Wagner, *Applied Physics Letters* **66**, 1234 (1995).
- [48] V. J. Goldman, D. C. Tsui and J. E. Cunningham, *Physical Review Letters* **58**, 1256 (1987).
- [49] H. Chang, R. Grundbacher, T. Kawanura, J.-P. Leburton and I. Adesida, *Semiconductor Science Technology* **9**, 210 (1994).
- [50] For a set of important references concerning the work on resonant tunneling devices, see F. A. Buot and A. K. Rajagopal, *Physical Review B* **48**, 17217 (1993).
- [51] R. K. Mains and G. I. Haddad, *Journal of Applied Physics* **64**, 5041 (1988).
- [52] R. K. Mains, J. P. Sun and G. I. Haddad, *Applied Physics Letters* **55**, 371 (1989).
- [53] K. K. Gullapalli, D. R. Miller and D. P. Neikirk, *Physical Review B* **49**, 2622 (1994).
- [54] I. Zozulenko, *Journal of Physics: Condensed Matter* **6**, 5507 (1994).